

**ZERO-VALENT IRON DECOLORIZATION OF THE ANTHRAQUINONE DYE
REACTIVE BLUE 4 AND BIODEGRADATION ASSESSMENT
OF ITS DECOLORIZATION PRODUCTS**

A Thesis
Presented to
The Academic Faculty

By
Hanbae Yang

In Partial Fulfillment
of the Requirements for the Degree
Master of Science in Environmental Engineering in the
School of Civil and Environmental Engineering

Georgia Institute of Technology
May 2005

**ZERO-VALENT IRON DECOLORIZATION OF THE ANTHRAQUINONE DYE
REACTIVE BLUE 4 AND BIODEGRADATION ASSESSMENT
OF ITS DECOLORIZATION PRODUCTS**

Approved by:

Dr. Spyros G. Pavlostathis, Advisor
School of Civil and Environmental Engineering
Georgia Institute of Technology

Dr. Lawrence A. Bottomley
School of Chemistry and Biochemistry
Georgia Institute of Technology

Dr. Ching-Hua Huang
School of Civil and Environmental Engineering
Georgia Institute of Technology

Date Approved: April 15, 2005

Dedicated to

My Parents

for their endless love and support.

ACKNOWLEDGEMENTS

I would like to express my sincere gratitude and appreciation to my advisor, Dr. Spyros G. Pavlostathis for his support and invaluable advice with a continuous stream of suggestions, feedback, and encouragement that have guided me throughout the whole period of my MS research. I especially would like to thank him for always being accessible and making research his top priority.

I would also like to thank my committee members, Dr. Lawrence A. Bottomley and Dr. Ching-Hua Huang for their constructive comments, suggestions and salient advice.

The State of Georgia/Consortium on Competitiveness for the Apparel, Carpet, and Textile Industries (CCTI) and the National Science Foundation/Bioengineering & Environmental Systems Division are acknowledged for funding of this research.

I would like to thank the faculty and staff in the School of Civil and Environmental Engineering for their continuous support and high quality education. I would like to thank all past and present students of Dr. Pavlostathis' group, especially Didem Okutman Tas, A. Evren Tugtas, Ulas Tezel, Jennifer Ebner and Andrew Tartaglia for their friendship and contributions to my research. In particular, I want to give my special thanks to William J. Epolito for his detailed and thoughtful comments, tremendous help, analytical method development and friendship that made my introduction to laboratory life a wonderful experience.

Many thanks to all students in Environmental Engineering for creating a stimulating and supportive environment, and all my friends at the Georgia Institute of Technology, who have made another part of my life full of joy and excitement.

I would like to thank Sunjeong (Sunny) for her love and friendship while completing my thesis, and especially for embarking on my life's journey with me.

Finally, my sincere warmhearted gratitude goes to my parents for their endless love, understanding, patience and support. Without them, none of my accomplishments would have been possible. To them, I dedicate this thesis.

TABLE OF CONTENTS

ACKNOWLEDGEMENTS	iv
LIST OF TABLES	ix
LIST OF FIGURES	x
SUMMARY	xv
CHAPTER 1. INTRODUCTION	1
CHAPTER 2. BACKGROUND	4
2.1. Dyes	4
2.1.1. General Aspects	4
2.1.2. Decolorization processes	10
2.1.2.1. Physical processes	10
2.1.2.2. Chemical processes	13
2.1.2.3. Biological processes	15
2.2. Zero-Valent Iron Reductive Transformation	18
2.3. Problem Identification	24
2.4. Research Objectives	25
CHAPTER 3. MATERIALS AND ANALYTICAL METHODS	26
3.1. Analytical Methods	26
3.1.1. pH	26
3.1.2. Dissolved Oxygen (DO)	26
3.1.3. Volatile Suspended Solids (VSS)	27
3.1.4. Dissolved Organic Carbon (DOC)	28
3.1.5. Spectrophotometric Analysis	28

3.2. Dye	29
3.2.1. Dye Stock Solution Preparation	31
3.2.2. Physico-chemical Properties of RB4	32
3.2.3. Analysis of RB4	35
3.3. Iron	40
CHAPTER 4. PHASES OF STUDY	42
4.1. Effect of Mixing Intensity and Initial Dye Concentration on the Batch Zero-Valent Iron Decolorization of RB4	42
4.2. Decolorization of RB4 in a Continuous-Flow Zero-Valent Iron Column	43
4.3. Biodegradation Assessment of RB4 Decolorization Products	43
CHAPTER 5. ZERO-VALENT IRON BATCH DECOLORIZATION OF RB4	44
5.1. Introduction	44
5.2. Materials and Methods	45
5.2.1. Effect of Mixing Intensity	45
5.2.2. Effect of Initial Dye Concentration	46
5.2.3. Reaction Rate Analysis	47
5.3. Results and Discussion	49
5.3.1. Effect of Mixing Intensity	49
5.3.2. Effect of Initial Dye Concentration	53
5.4. Summary	63
CHAPTER 6. A CONTINUOUS-FLOW ZERO-VALENT IRON RB4 DECOLORIZATION	65
6.1. Introduction	65
6.2. Materials and Methods	66
6.2.1. Column Characterization	69

6.2.2. Continuous-flow ZVI RB4 decolorization	75
6.3. Results and Discussion	76
6.3.1. Column Characterization	76
6.3.2. Long-term ZVI RB4 Decolorization Kinetics	85
6.4. Summary	95
CHAPTER 7. BIODEGRADATION ASSESSMENT OF RB4 DECOLORIZATION PRODUCTS IN A MIXED, AEROBIC HALOPHILIC CULTURE	97
7.1. Introduction	97
7.2. Materials and Methods	98
7.2.1. ZVI Column	98
7.2.2. Halophilic Stock Culture	101
7.2.3. Batch Aerobic Biodegradation Assay	107
7.3. Results and Discussion	109
7.3.1. RB4 Decolorization by a Continuous-flow ZVI Column	109
7.3.2. Halophilic Culture Performance	114
7.3.3. Biodegradation Assessment of RB4 Decolorization Products	118
7.4. Summary	125
CHAPTER 8. CONCLUSIONS	129
APPENDIX A. CALIBRATION CURVES	132
REFERENCES	137

LIST OF TABLES

Table 2.1. Different techniques used for dye decolorization	11
Table 3.1. Experimental and estimated property values of unhydrolyzed RB4 at 25°C	34
Table 3.2. RB4 dye characterization data	38
Table 5.1. Kinetics of RB4 decolorization by ZVI as a function of mixing intensity	50
Table 5.2. Kinetics of RB4 decolorization by ZVI as a function of initial dye concentration	55
Table 6.1. Calculated Reynolds numbers for column A at 23°C as a function of flow rate	78
Table 6.2. Characteristics of the two iron/sand columns used in this study	79
Table 6.3. Experimental and estimated transport parameter values for column B at 23°C	83
Table 6.4. Operational conditions of column B used for the continuous-flow ZVI RB4 decolorization assay	86
Table 6.5. Results of the long-term, continuous-flow ZVI RB4 decolorization using column B at 23°C	90
Table 7.1. Composition of the halophilic stock culture media	102
Table 7.2. Composition of the trace metal stock solution used in the preparation of the halophilic culture media	103
Table 7.3. Composition of the vitamin stock solution used in the preparation of the halophilic culture media	104
Table 7.4. Batch biodegradation assay set-up	108
Table 7.5. Results of the OUR measurements with the halophilic culture kept under starvation conditions	116

LIST OF FIGURES

Figure 2.1. Structure of an azo (A) and an anthraquinone (B) chromophore	5
Figure 2.2. Reactive Blue 4 (RB4) reactive group reaction with fiber or water	6
Figure 2.3. Chemical structure of unhydrolyzed Reactive Blue 4 (RB4) (A) and Reactive Blue 19 (RB19) (B). Hydrolysis of the dichlorotriazinyl reactive group (RB4) (C) and vinyl sulfonic reactive group (RB19) (D)	8
Figure 2.4. A typical flow diagram for a textile cotton knit plant	9
Figure 2.5. General iron corrosion mechanism (3 and 4 only occur in the presence of oxygen)	19
Figure 2.6. General anaerobic/anoxic iron reductive transformation of an anthraquinone reactive dye (2 and 3 occur simultaneously competing for electrons)	20
Figure 2.7. Fe^{2+} and Fe^{3+} solubility diagrams at 25°C, infinite dilution and 0.1M ionic strength; A, Fe^{2+} and B, Fe^{3+}	23
Figure 3.1. Chemical structure of unhydrolyzed Reactive Blue 4 (RB4)	30
Figure 3.2. Chemical structure of monohydrolyzed (A) and dihydrolyzed (B) RB4	33
Figure 3.3. UV/Visible spectra of reacted and unreacted RB4 (100 mg/L)	36
Figure 3.4. HPLC analysis of reacted and unreacted RB4 (300 mg/L): total chromatograms at 598 nm (A), enlarged chromatograms from 27.0 to 28.5 min retention time (B), spectra of reacted RB4 components (C), and spectra of unreacted of RB4 components (D) (DH, dihydrolyzed; MH, monohydrolyzed; UH, unhydrolyzed)	37
Figure 3.5. LC/ESI-MS analysis of reacted RB4 (5000 mg/L) in negative-ion mode of operation; ESI-MS spectra for 28.6 min retention time peak (A), isotope model predicted mass peaks for unhydrolyzed RB4 (B); and isotope model predicted mass peaks for 1-amino-4-hydroxy-anthraquinone-2-sulfonic acid (C)	39
Figure 5.1. Effect of mixing intensity (rpm) on the ZVI decolorization of RB4 (All sets at 300 mg/L initial RB4; (A) experimental data based on absorbance at 598 nm; (B) lines are non-linear regression fits based on the pseudo first-order model)(Error bars represent \pm one standard error of the mean)	51

Figure 5.2. Effect of mixing intensity (rpm) on the ZVI pseudo first-order decolorization rate constant of reacted RB4 (Initial RB4 concentration equal to 300 mg/L); experimental data based on absorbance at 598 nm (A); non-linear regression fit based on the pseudo first-order model (B) (Error bars represent \pm one standard error of the mean)	52
Figure 5.3. UV/Visible spectra during the decolorization of reacted RB4 (Initial dye concentration 300 mg/L; 100 g/L NaCl, 3 g/L Na ₂ CO ₃ , and 1 g/L NaOH)(Mixing speed (rpm): A, 0; B, 200; and C, 400)	54
Figure 5.4. Effect of initial dye concentration on the ZVI decolorization of RB4 (All bottles mixed with the end-over-end tumbler at 4 rpm; (A) experimental data based on absorbance at 598 nm; and (B) non-linear regression fits based on the pseudo first-order model) (Error bars represent \pm one standard error of the mean)	56
Figure 5.5. Effect of initial dye concentration on the decolorization kinetics of reacted RB4 (Conditions: 100 g/L NaCl, 3 g/L Na ₂ CO ₃ , and 1 g/L NaOH; mixing with end-over-end tumbler at 4 rpm); A) experimental data based on absorbance at 598 nm; and B) non-linear regression fit based on the pseudo first-order model) (Error bars represent \pm one standard error of the mean)	58
Figure 5.6. Pseudo first-order regression fit to RB4 data over the initial decolorization time. Case A: C _o as variable; Case B: C _o at fixed value (Conditions: initial reacted RB4 concentration 1,500 mg/L; 100 g/L NaCl, 3 g/L Na ₂ CO ₃ , and 1 g/L NaOH; experimental data based on absorbance at 598 nm) (Error bars represent \pm one standard error of the mean)	59
Figure 5.7. UV/Visible spectra during the decolorization of reacted RB4 (Conditions: initial RB4 concentration equal to 1,500 mg/L; 100 g/L NaCl, 3 g/L Na ₂ CO ₃ , and 1 g/L NaOH; mixing with end-over-end tumbler at 4 rpm)	60
Figure 5.8. Non-linear fit of initial volumetric RB4 decolorization rate data to the site saturation model as a function of initial dye concentration (Conditions: mixing with an end-over-end tumbler at 4 rpm; 100 g/L NaCl, 3 g/L Na ₂ CO ₃ , and 1 g/L NaOH) (Error bars represent \pm one standard error of the mean)	62
Figure 6.1. Schematic of the ZVI column A used for the hydraulic conductivity test	67
Figure 6.2. Schematic of column B set up used for the long-term continuous-flow ZVI RB4 decolorization	68

Figure 6.3.	Grain size distribution of iron, sand, and iron/sand mixture (d_{10} = diameter where 10% is finer; d_{60} = diameter where 60% is finer)	77
Figure 6.4.	Darcy's velocity versus hydraulic gradient according to equation 6-7 for the determination of the hydraulic conductivity and intrinsic permeability of column A at 23°C (Error bars represent \pm one standard error)	81
Figure 6.5.	Experimental data and model fitted breakthrough curves for the KI and KBr tracers at a flow rate of 10 mL/min (Data fit based on the CXTFIT 2.0 program)	82
Figure 6.6.	Color change during the continuous-flow decolorization assay at each sampling port [port 0 (0cm), port 1 (2.8cm), port 3 (16.3cm), port 4 (23.3cm), port 5 (30.0cm) and port 6 (32 cm)]. (A) 1.0 pore volume (4.5 hours); (B) 5.0 pore volumes (22.5 hours); (C) 100 pore volumes (19 days); (D) 200 pore volumes (38 days)	87
Figure 6.7.	RB4 concentration as a function of pore volumes and column bed height (column B; 1.0 mL/min flow rate; 1000 mg/L influent RB4 concentration; 23°C ambient temperature)	88
Figure 6.8.	RB4 decolorization kinetics by a continuous-flow ZVI column (1.0 mL/min flow rate; 1,000 mg/L influent RB4 concentration; 23°C ambient temperature)	91
Figure 6.9.	Effect of long-term continuous-flow decolorization kinetics of reacted RB4 (1000 mg/L with salt and base solution) on the decolorization rate constant; A) experimental data based on absorbance at 598 nm, and B) data fit with non-linear regression fit based on a first-order model (Error bars represent \pm one standard error of the mean)	92
Figure 6.10.	Bed depth service time (BDST) at 50% breakthrough for the decolorization of 1000 mg/L RB4 with salt and base by the ZVI column B as a function of column bed depth	94
Figure 7.1.	Schematic of the ZVI column used for the preparation of the RB4 decolorization products for the biodegradation assays [section A (10 cm), iron filings passed through the 12-mesh sieve; section B (30 cm), iron filings retained on the 12-mesh sieve; and section C (10 cm), iron filings passed through the 12-mesh sieve]	99

Figure 7.2.	Influent and effluent concentration of RB4 during the first column run with recycle: (A) RB4 concentration profiles over the first 8 days at a flow rate of 1.0 mL/min; (B) RB4 concentration profiles after the increase of the flow rate to 5.0 mL/min (closed system with recycle of the column effluent to the dye reservoir)	110
Figure 7.3.	DOC profiles during the second ZVI column run with recycle of the column effluent to the dye reservoir (Influent RB4 equal to 1,000 mg/L) (Error bars represent \pm standard error of the mean)	112
Figure 7.4.	UV/Visible spectra during the continuous-flow decolorization of reacted RB4 using a ZVI column with effluent recycle to the dye reservoir (Initial dye concentration 1,000 mg/L; 100 g/L NaCl, 3 g/L Na ₂ CO ₃ , and 1 g/L NaOH): (A) first column run (14 days); (B) second column run (3 days)	113
Figure 7.5.	Comparison of RB4 decolorization kinetics by the ZVI continuous-flow column (with recycle of the column effluent to the dye reservoir) before and after regeneration (Initial dye concentration 1,000 mg/L; flow rate 1.0 mL/min)	115
Figure 7.6.	DO profiles (A) and OUR plots for the estimation of the specific death constant (B) of the halophilic culture incubated under starvation conditions	117
Figure 7.7.	Relative ratio of the DOC, VSS, OUR and SOUR profiles in the halophilic culture under starvation conditions	119
Figure 7.8.	DOC profiles in the batch halophilic cultures: (A) phase I – after first glucose addition; (B) phase II – after second glucose addition; (C) glucose-DOC profiles after each glucose addition	121
Figure 7.9.	VSS profiles in the batch halophilic cultures	122
Figure 7.10.	Non-linear fit of the Monod model to the biodegradable DOC (glucose) concentration profiles (A) control culture without any dye amendment; (B) RB4- amended culture; (C) and (D) cultures amended with RB4 decolorization products generated during ZVI column run 1 and 2, respectively	124
Figure 7.11.	UV/Visible spectra during the biodegradation assay in the halophilic culture as a function of incubation time: (A) abiotic control with RB4 products 1 (run 1); (B) RB4-amended culture; (C) culture amended with RB4 decolorization products 1; (D) culture amended with RB4 decolorization products 2	126

Figure 7.12. Absorbance profiles during the biodegradation assay: (A) culture amended with RB4; (B) abiotic control with RB4 product 1 (column run 1); (C) culture amended with RB4 products 1; (D) culture amended with RB4 products 2 (characteristic wavelength of RB4 is 598 nm and RB4 products is 485 nm)

127

SUMMARY

Anthraquinone dyes constitute the second largest class of textile dyes after azo dyes, and are used extensively in the textile industry, particularly for dyeing of cellulosic fabric (mainly cotton), wool and polyamide fibers. A high fraction of the initial reactive dye mass used in the dyeing process remains in the spent dyebath. Reactive dyes are not readily removed by typical wastewater treatment processes and the high salt concentration typical of reactive dyeing further complicates the management of spent reactive dyebaths. In contrast to significant research conducted on the reductive decolorization of azo dyes using zero-valent iron (ZVI), investigation of the reductive transformation (decolorization and mineralization) of reactive anthraquinone dyes and their decolorization products has been very limited. Additionally, very limited research has been conducted on the decolorization of spent reactive dyebaths containing high concentrations of both dye and salt, typically present in spent reactive dyebaths.

Research was conducted to investigate the key operational parameters of batch and continuous-flow ZVI decolorization of a reactive anthraquinone dye, Reactive Blue 4 (RB4), under anoxic conditions, as well as the potential for the biodegradation of its decolorization products in a halophilic culture under aerobic conditions. The effect of two operational parameters, such as mixing intensity and initial dye concentration, on the ZVI batch decolorization kinetics indicates that ZVI decolorization of RB4 is a surface-catalyzed, mass transfer-limited process. The high salt and base concentrations, typical of spent reactive dyebaths, enhanced the rate of RB4 decolorization. Based on parameters such as porosity, hydraulic conductivity, Reynolds number, pore water velocity, and

dispersion coefficient, non-ideal transport characteristics were observed in a continuous-flow ZVI column. The results of a long-term continuous-flow ZVI decolorization column demonstrated that continuous-flow ZVI decolorization is feasible. However, column porosity losses and a shift of reaction kinetics occur in long-term column operation, leading to a decrease in column decolorization efficiency. ZVI decolorization of RB4 was successfully described with a pseudo first-order or a site saturation model. Lastly, the RB4 decolorization products generated by ZVI treatment had no inhibitory effect on the halophilic, aerobic culture. However, biodegradation and/or mineralization of RB4 decolorization products was not observed after a long-term incubation of the culture.

This research demonstrated the feasibility of ZVI decolorization of reactive anthraquinone dyes, which will help in the development of a continuous-flow, dyebath decolorization process and the possible reuse of the renovated dyebath in the dyeing operation. Such a system could lead to substantial reduction of water usage, as well as a decrease of salt and dye discharges.

CHAPTER 1

INTRODUCTION

Anthraquinone dyes constitute the second largest class of textile dyes, after azo dyes and are used extensively in the textile industry due to their wide variety of color shades, ease of application, and minimal energy consumption (Baughman and Weber, 1994; Aspland, 1997). Normally, to obtain a desired fabric color shade, a mixture of dyes, especially red, yellow and blue, is used in textile dyebaths. These dyes consist of many different chromophores (dye groups) including azo, anthraquinone and phthalocyanine (Hao et al., 2000; Zollinger, 2003). Among the textile dyes, reactive dyes are an important class used not only to color cellulosic fabric (mainly cotton), but also wool and polyamide fibers. A steady increase in reactive dye usage has been observed as a result of the increase in cotton and wool use worldwide (Phillips, 1996).

Reactive dyes have environmental implications because up to 50% of the initial dye mass (up to or exceeding 800 mg/L) used in the dyeing process remains in the spent dyebath in its hydrolyzed form which no longer has an affinity for the fabric, and thus cannot be reused in the dyeing process (Rys and Zollinger, 1989; Steenken-Richter and Kermer, 1992; Laszlo, 1995;). Reactive dyes are not readily removed by typical wastewater treatment processes due to their inherent properties, such as stability and resistance towards light or oxidizing agents (Poots et al., 1976; McKay, 1979; Tincher and Robertson, 1982; Banat et al., 1996; Lee, 2003; Lee et al., 2005). In addition to the presence of dye, the high salt concentrations as well as high pH values under typical reactive dyeing conditions further complicate the management of spent reactive dyebaths

(Ryes and Zollinger, 1989; Lewis, 1999). Thus, the management of spent reactive dyebaths is a pressing environmental problem for the textile industry. Lastly, the long-term health effects of commercial dyes and their transformation (decolorization) products have important implications (Tincher and Robertson, 1982). Recent research shows that although the level of the anthraquinone dye Reactive Blue 4 in the environment is expected to be orders of magnitude lower than that found in commercial, spent reactive dyebaths, the effect of long-term, low-level dye exposure needs to be evaluated (Epolito et al., 2005).

Although significant research has been conducted on the reductive decolorization of azo dyes using zero-valent iron (ZVI) followed by biomineralization of their decolorization products (Perey et al., 2002; Tan et al., 1999), limited information exists on the reductive transformation (decolorization and mineralization) of reactive anthraquinone dyes and their decolorization products. Additionally, very limited research has been conducted on the decolorization of spent reactive dyebaths containing high concentrations of both dye and salt, typically present in spent reactive dyebaths (Epolito, 2004; Lee, 2003; Lee et al., 2005). Therefore, effective and efficient treatment methods for both the decolorization and mineralization of anthraquinone reactive dyes and their decolorization products are needed.

Reactive Blue 4 (RB4), an anthraquinone reactive dye was selected for this research based on several factors, including relatively slow biodecolorization kinetics (Lee, 2003; Lee et al., 2005), commercial use and previous research conducted. This research provides a better understanding of the kinetics and parameter effects on the reductive decolorization of RB4 by ZVI and an assessment of the feasibility

of a continuous-flow, decolorization process for anthraquinone dyebaths at relatively high salt and base concentration. Furthermore, the possible toxicity and biodegradation/mineralization potential of RB4 decolorization products formed by ZVI treatment were assessed using a mixed, aerobic halophilic culture.

CHAPTER 2

BACKGROUND

2.1 Dyes

2.1.1 General Aspects

Dye molecules consist of chromophores (color-bearing groups; e.g., an aromatic structure absorbing visible light). Among twelve different chromophore groups, azo and anthraquinone (Figure 2.1) are the major units (Ingamells, 1993; Hao et al., 2000). A second classification of dyes is based on their mode of application to textiles, such as: acid, basic, direct, disperse, reactive, mordant, sulfur, and vat dyes (Zollinger, 2003). Reactive dyes, which are the only textile colorants designed to bond covalently with cellulosic fibers (i.e., cotton), are used extensively due to their superior colorfastness, ease of application, and color properties (Aspland, 1997). Reactive dye production in 1996 was over 110,000 metric tons, and was expected to reach 50% of the market share by 2004 (Phillips, 1996). The property of reactive dyes that differs from other dyes is that they covalently bond to the cotton (cellulose) fiber resulting in a strong bond that resists fading. In the reactive dyeing of cotton, the pH and the equilibrium concentration of cellulosate ions (CellO^-), are increased in order to result in the formation of a covalent bond between the dye and fiber. The reactive nature of the dyes at high pH values also results in a large amount of unused hydrolyzed dye, which reacts with OH^- ions instead of the CellO^- ions on the fibers due to competition between the CellO^- and OH^- ions present in the dyebath (Figure 2.2). The hydrolyzed dye has the same color as the unhydrolyzed

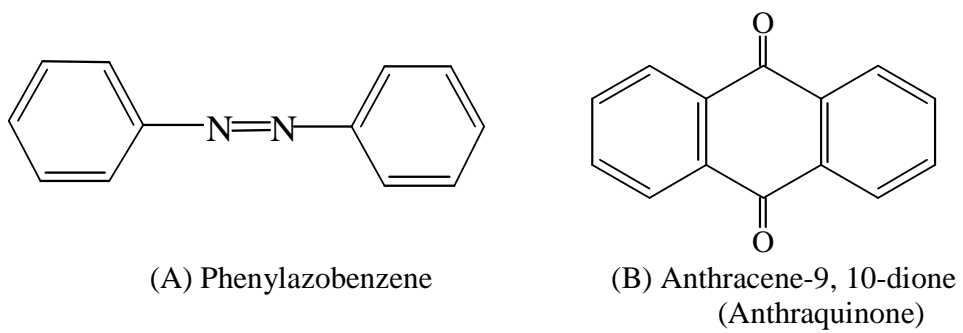


Figure 2.1. Structure of an azo (A) and an anthraquinone (B) chromophore.

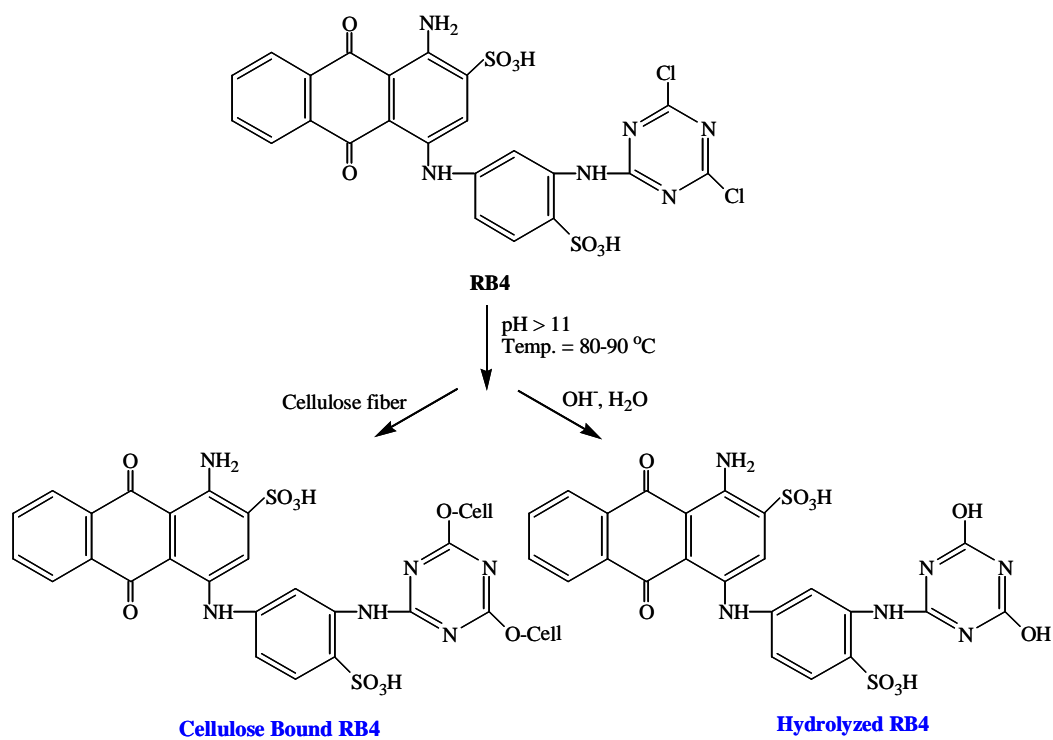
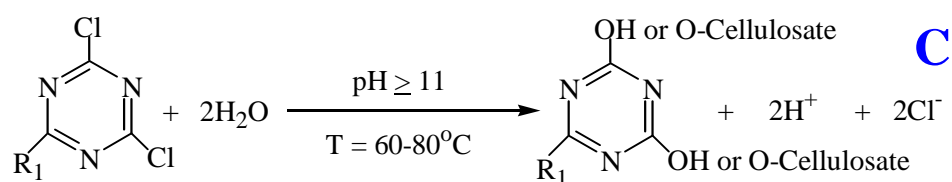
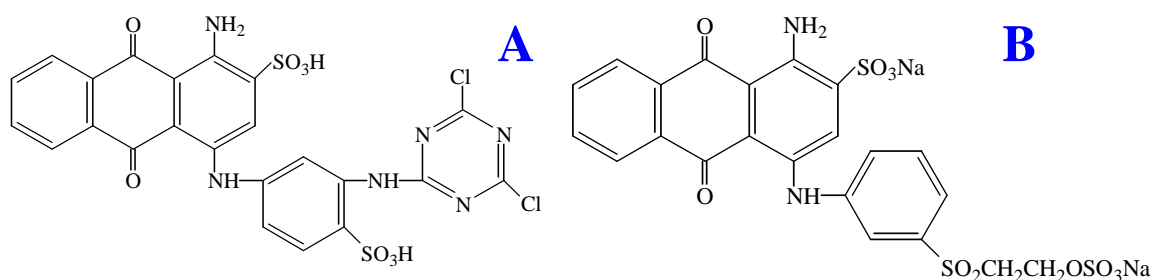


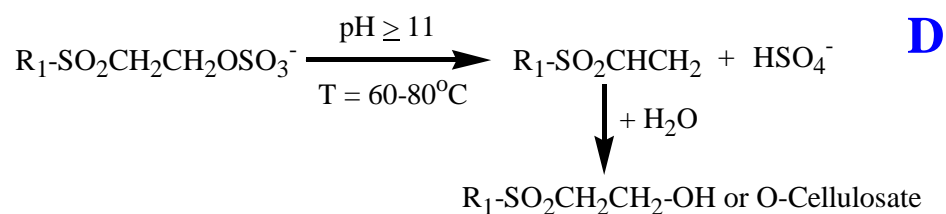
Figure 2.2. Reactive Blue 4 (RB4) reactive group reaction with fiber or water.

(unreacted) dye, but cannot react with the fiber and must be disposed of (Lee, 2003; Epolito et al., 2005). In terms of chemical structure, the main classes of reactive dyes are anthraquinone, azo, and phthalocyanine. Azo dyes account for up to 70% of all textile dyestuffs produced, and represent the most common chromophore within reactive dyes (Carliell et al., 1995; Zollinger, 2003). Another important chromophore group is the anthraquinone (Figure 2.1B). Anthraquinone has a pale yellow color, which is due to an $n \rightarrow \pi^*$ transition that produces a weak color band at 405 nm (Zollinger, 2003). Electron-withdrawing groups have little effect on the color of the compound, whereas electron-donating groups (e.g., OH^- and $-\text{NH}_2$) determine the compound's distinctive color (Zollinger, 2003). As mentioned, the reaction of the electrophilic anthraquinone reactive groups (i.e., a dichlorotriazinyl for Reactive Blue 4 and a vinyl sulfonic reactive group for Reactive Blue 19) with water under elevated pH and temperature conditions, typically encountered during reactive dyeing, results in hydrolyzed dyes (Figure 2.3).

In the textile industry, color is applied to finished products through dyeing, resulting in the generation of various waste streams as shown in Figure 2.4. The effluent (including sizing, desizing, scouring, bleaching, dyeing, rinsing, and finishing wastes) contains unfixed dyes with a high intensity of color (Babuna et al., 1998; Hao et al., 2000). It has been estimated that approximately 50% of applied reactive dyes is wasted because of dye hydrolysis in the alkaline dyebath. As a result, typical spent dyebaths contain dyes at a concentration up to or higher than 800 mg/L (Steenkeen-Richer and Kermer, 1992; Vandevivere et al., 1998). As state and federal environmental regulations become more stringent (requiring lower effluent color limits), reduction or elimination of discharge of colored wastewater is mandated (Hao et al., 2000; Epolito et al., 2005).



Dichlorotriazinyl reactive group (RB4)



Vinyl sulfonyl reactive group (RB19)

Figure 2.3. Chemical structure of unhydrolyzed Reactive Blue 4 (RB4) (A) and Reactive Blue 19 (RB19) (B). Hydrolysis of the dichlorotriazinyl reactive group (RB4) (C) and vinyl sulfonyl reactive group (RB19) (D).

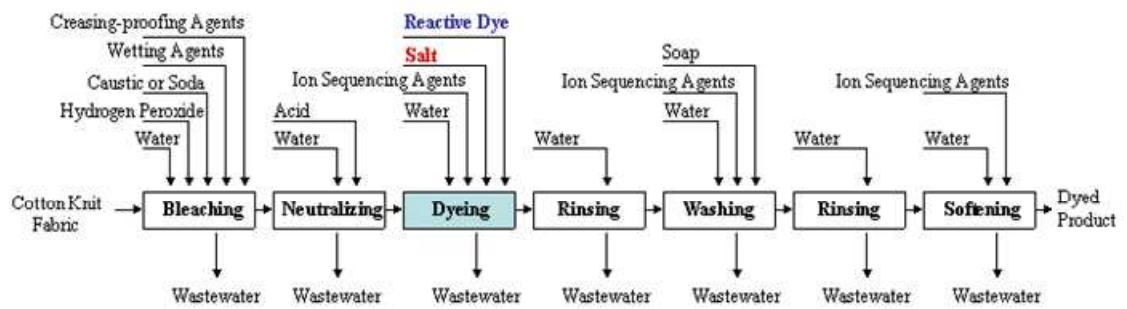


Figure 2.4. A typical flow diagram for a textile cotton knit plant (Babuna et al., 1998).

2.1.2 Decolorization Processes

Many processes have been used and/or researched for dye decolorization. A brief description of dye decolorization of each process compiled from literature is summarized in Table 2.1. However, not all processes work for all colored wastewaters (Hao et al., 2000; Robinson et al., 2001; Naim and Abd, 2002), which has driven research in this area. Some studies have reported successful decolorization using different treatment schemes, despite the fact that the treated wastewater still has a low color intensity. Only a few cases have been reported with complete decolorization and dye mineralization (Hao et al., 2000; Robinson et al., 2001; Naim and Abd, 2002).

2.1.2.1 Physical Processes

Activated carbon is the most used method of dye decolorization by adsorption, and is very effective for adsorbing cationic, mordant and acid dyes (Nasser and El-Geundi, 1991; Raghavacharya, 1997). Numerous other adsorbents, such as peat, wood chips, fly ash, and brown coal have been used as dye adsorbents (Nigam et al., 2000; Robinson et al., 2001). However, although adsorption can efficiently decolorize textile effluents, its application has been limited by the high cost of adsorbents and the large volume of wastewater normally involved (Robinson et al., 2001; Naim and Abd, 2002). Nanofiltration removed up to 99% of a variety of reactive dyes in laboratory studies (Wu et al., 1998) and has been successfully applied in a pilot-scale study (Chen et al., 1997). Rozzi and coworkers (1999) employed a microfiltration unit followed by a nanofiltration unit or a reverse osmosis membrane process for a potential textile wastewater reuse. Nonetheless, the use of membrane processes for large flow rates is prohibitively costly, in

Table 2.1. Different techniques used for dye decolorization

Process	Dye	Influent dye Conc. (color measurement)	Treatment Process	Comments
Adsorption	Orange Red, Crystal Violet and Methylene Blue	200 mg/L (respective λ_{\max})	Sorption capacity of different activated carbons	Equilibrium capacity various with dyes and carbons; correlated well with mesopore and large micropore volume ^a
Membrane	Various dyes to simulate textile waste	Integration of the area under $A_{400-700}$	Polysulfone nanofiltration membrane with total area of 10 m ²	99% color removal by a particular polyamide membrane at 20°C and 180 psi ^b
Fenton and photo-Fenton	Reactive Orange 4	100-400 mg/L (respective λ_{\max})	Varying pH, Fe ²⁺ , H ₂ O ₂ and UV light intensity	98% color removal; photo-Fenton process is more efficient ^c
Photocatalytic (TiO ₂)	Orange II	50 mg/L (respective λ_{\max})	TiO ₂ catalysts supported on three different absorbents	Over 95% color removal; TiO ₂ supported on absorbents is more efficient than that of bare TiO ₂ ^d
Ozonation and ultrasound- enhanced ozonation	Reactive Blue 19	30 mg/L (respective λ_{\max})	Varying ozone, ultrasound and ultrasound enhanced ozone operational conditions	First-order rate constants increased by 200% for ultrasonic power inputs compared to ozonation alone ^e
Sonication	Reactive Blue 7 and Reactive Blue 21 under spent dyebath conditions	70 to 500 mg/L (respective λ_{\max})	Varying dye concentration and effect of salt and base on sonochemical decolorization	Complete decolorization and increase rate of decolorization under spent dyebath conditions ^f
Reduction (ZVI)	Nine azo dyes	100 to 700 mg/L (respective λ_{\max})	Varying mixing intensity and dye concentration under batch conditions	Rapid decolorization rate (short half life); enhanced rates with mixing intensity (mass-transfer limited process) ^g

^a Krupa and Cannon, 1996^b Wu et al., 1998^c Muruganandham and Swaminathan, 2004^d Bhattacharyya et al., 2004^e Lall et al., 2003

Table 2.1. (continued)

Process	Dye	Influent dye Conc. (color measurement)	Treatment Process	Comments
Biological (fungi)	Acid Violet 7, Acid Green 27 and Indigo carmin	Up to 900 mg/L (respective λ_{\max})	Removal by fungus <i>T. versicolor</i>	Fast initial adsorption followed by slow biodegradation ^h
	Congo Red dye	50 mg/L (respective λ_{\max})	Degradation by <i>P.</i> <i>chrysosporium</i>	Rapid adsorption on both live and dead cells; biodegradation only in live cells ⁱ
Biological (bacteria)	Reactive Blue 2	100 mg/L (respective λ_{\max})	Pre-dried activated sludge culture by sorption	56% color removal by sorption ^j
	Acid Red 151	25 to 50 mg/L (respective λ_{\max})	Aerobic sequencing batch biofilter	73% of initial dye (as carbon) and 99% of color removal ^k
	Reactive Blue 4 and 19	50 to 300 mg/L (respective λ_{\max})	Removal by a methanogenic culture	73-90% for RB4 and 90-95% for RB19 color removal ^l
	Reactive Blue 19 and 21 and Reactive Red 198 under spent dyebath conditions	300 mg/L (respective λ_{\max})	Removal by a halophilic culture under sequential aerobic/anoxic coditions	Over 87% color removal under anoxic conditions ^m
	Direct Black 38 dye to simulate textile wastewater	3200 mg/L (respective λ_{\max})	Up-flow anaerobic sludge blanket reactor/aerobic continuous stirred tank reactor (UASB/CSTR)	Up to 94% color removal under anoxic conditions and 92% COD removal under aerobic conditions ⁿ
	Reactive Black 5	530 mg/L (respective λ_{\max})	Aerobic/anaerobic rotating disc reactors (RDR)	Up to 65% color removal and partial mineralization ^o
	Reactive Blue 5 and 19	23 to 115 mg/L (respective λ_{\max})	Removal by mesophilic and thermopilic anaerobic granular sludge	Higher decolorization rates (11 fold) at thermophilic conditions ^p

^h Wang and Yu, 1998ⁱ Tatarko and Bumpus, 1998^j Aksu, 2004^k Buitron et al., 2004^m Lee, 2003ⁿ Isik and Sponza, 2004^o Libra et al., 2004^p Santos et al., 2005

addition to the common problems of membrane processes with respect to flux decline, irreversible fouling, and required treatment and disposal of the concentrate (Van't Hul et al., 1997; Hao et al., 2000; Naim and Abd, 2002).

2.1.2.2 Chemical Processes

Chemical oxidation is the most frequently used decolorization process in research and applied in industry, partly due to the diversity of chemical processes that can be effective. Chemical oxidation removes the dye from the dye-containing effluent by oxidation resulting in aromatic ring cleavage of the dye molecules (Raghavacharya, 1997; Robinson et al., 2001). Recently, many advanced oxidation processes, such as the Fenton's reagent (H_2O_2 and Fe^{2+}), UV light with or without catalysis (e.g., TiO_2), H_2O_2 , and ozone (O_3), have been evaluated for the decolorization of textile wastewater (Hao et al., 2000; Robinson et al., 2001; Naim and Abd, 2002). The advanced oxidation processes are essentially based on the generation of highly reactive radical species, specially the hydroxyl radical ($\bullet\text{OH}$) which reacts with the dye molecules (Hao et al., 2000). Muruganandham and Swaminathan (2004) reported that Fenton and photo-Fenton processes achieved 98% decolorization of Reactive Orange 4. Photocatalytic degradation of an azo dye, Orange II by TiO_2 catalysts supported on adsorbents was also compared with that of bare TiO_2 produced by the acid catalyzed sol-gel formation method (Bhattacharyya et al., 2004). The supported catalysts effectively removed Orange II from solution, and the rate of degradation was significantly better than that of bare TiO_2 . Semiconductor-mediated photocatalyzed degradation of an azo dye, Chrysoidine Y (1), was investigated in aqueous suspensions of TiO_2 and ZnO (Qamar et al., 2004). It was observed that the dye degraded more efficiently in the presence of TiO_2 as compared to

ZnO. Ozonation, ultrasound, and ultrasound-enhanced ozonation were investigated for the oxidation of Reactive Blue 19 (RB19, an anthraquinone dye), under various operating conditions by Lall and co-workers (2003). Ozonation and ultrasound-enhanced ozonation were both effective for the decolorization of 30 mg/L RB19. Compared to ozonation alone, the apparent first-order rate constants increased by 35 and 200 % for ultrasonic power inputs of 40 and 120 W/L, respectively. Matthews (2003) also investigated sonication of two phthalocyanine dyes, Reactive Blue 21 (RB21) and Reactive Blue 7 (RB7) under typical spent reactive dyebath conditions. RB7 and RB21 were completely decolorized and an increased rate of decolorization was observed under spent dyebath conditions.

Reduction processes are also widely used for the decolorization of dyes. Decolorization of reactive phthalocyanine dyes was investigated with palladium (Pd) catalyzed H₂ reduction (Matthews, 2003). It was demonstrated that Pd-catalyzed H₂ reduction was capable of completely decolorizing phthalocyanine dyes and a phthalocyanine-based dyebath. One of the most popular technologies for reductive decolorization of dye-bearing wastewater is zero-valent iron (ZVI). ZVI has been mainly used for *in situ* groundwater treatment of subsurface contaminants, but its use for wastewater decolorization is growing because of its abundance, low toxicity, low cost, and effectiveness as a reducing agent (Bigg and Judd, 2000). The use of ZVI has been shown to be successful in decolorization of dye wastewaters (Weber, 1996; Cao et al., 1999; Nam and Tratnyek, 2000). Nam and Tratnyek (2000) investigated the effect of mixing rate on the reduction of nine azo dyes in batch experiments and founded that these

reactions were mass-transfer limited. Further discussion on the zero-valent iron (ZVI) process and its applications can be found in Section 2.2, below.

2.1.2.3 Biological Processes

Many researchers have demonstrated the biological decolorization of dyes by pure and mixed cultures of fungi and bacteria. The use of ligninolytic fungi is one of the possible alternatives studied for the biodegradation of dyes. Fungi can mineralize xenobiotic compounds to CO₂ and H₂O through their highly oxidative and non-specific ligninolytic system, which is also responsible for the decolorization and degradation of a wide range of dyes (Fu and Viraraghavan 2001; McMullan et al., 2001; Wesenberg et al., 2003; Pinheiro et al., 2004). Since degradation of dyes by the white-rot fungi was first reported by Glenn and Gold (1983), white-rot fungi have been the most widely studied, dye-decolorizing microorganisms. Fungi such as *Phanerochaete chrysosporium*, *Pleurotus*, *Bjerkandera*, *Trametes*, *Poyporus*, *Phelinus*, *Iperx lacteus*, *Funalia trogii*, and *Thelephora* sp., have been investigated for the decolorization and mineralization of various dyes (Fu and Viraraghavan 2001; Selvam et al., 2003; Wesenberg et al., 2003; Yesilada et al., 2003). Santos and co-workers (2004) have recently evaluated the ability of 19 isolates of filamentous fungi for the decolorization of the commercial reactive dye Blue-BF-R on solid and in liquid media. Although these fungi have been shown to decolorize dyes, different decolorizing ability of these fungi was observed and attributed to their growth and enzyme production requirements. As textile wastewater is not the natural environment of white-rot fungi, enzyme production may be unreliable and thus

the decolorizing ability of fungi may also be affected (Robinson et al., 2001; Santos et al., 2004;).

Conventional biological treatment processes are ineffective against dyes (Tan et al., 1999; Hao et al., 2000; Perey et al., 2002). The major color removal mechanism is adsorption to the sludge, but reactive dyes in particular adsorb poorly due to their high aqueous solubility (Pagga and Taeger, 1994; Delee et al., 1998). A few bacterial species have shown to decolorize dye wastewater aerobically, either in activated sludge or in fixed film systems (Jiang and Bishop, 1994; Hao et al., 2000). Churchley and co-workers (2000) reported that 19.7% of RB4 dye was biologically eliminated due to sorption on an aerobic, activated sludge culture. Aksu (2001) investigated the biosorption of RB2 (an anthraquinone dye with a monochlorotriazinyl reactive group), onto pre-dried activated sludge, and observed that 56% of 100 mg/L dye was removed by sorption onto 500 mg/L biomass at 25°C. Buitron and co-workers (2004) also reported that the Acid Red 151 dye was aerobically biodegraded in a sequencing batch biofilter. It showed that 73% (as carbon) of the initial dye and up to 99% of the initial color were removed. To effectively decolorize dyes that pass through biological treatment plants, pre- or post-treatment processes must be incorporated. For example, using zero-valent iron (ZVI) decolorization for azo dyes before biological treatment reduces the dye into products (e.g., aniline) that can be degraded by conventional, aerobic biological treatment processes (Tan et al., 1999; Perey et al., 2002). Anaerobic systems can decrease the color intensity more satisfactorily than aerobic processes (Hao et al., 2000; Beydilli et al., 2000; Robinson et al., 2001; Naim and Abd, 2002). For example, reductive cleavage of the azo bond results in the decolorization of azo dyes under anaerobic conditions (Nigam et al., 1996; Beydilli

et al., 2000; Stolz, 2001; McMullan et al., 2001; van der Zee et al., 2001; van der Zee et al., 2003). However, the decolorization (or intermediate) products need to be further degraded by an aerobic treatment (Panswad and Luangdilok, 2000). Decolorization of two anthraquinone reactive dyes (Reactive Blue 4 (RB4) and Reactive Blue 19 (RB19)) was investigated using a mixed, methanogenic culture (Fontenot, 1998; Lee, 2003; Lee and Pavlostathis, 2004). The extent of color removal was in the range of 73-90% for RB4, and 90-95% for RB19. However, biological decolorization of full-strength reactive spent dyebaths using a methanogenic culture was not feasible because of culture inhibition to the anthraquinone dyes and further inhibitory effects from the high salt content of the industrial reactive dyebaths. For this reason, a mixed halophilic culture was developed and over 87% of decolorization under anoxic conditions was achieved under spent dyebath conditions (Lee, 2003). Recently, several high rate anaerobic/aerobic reactors have been evaluated to get high decolorization rates and mineralization of dyes, such as anaerobic/aerobic sequencing batch reactor (SBR) (Panswad and Luangdilok, 2000), up-flow anaerobic sludge blanket reactor/aerobic continuous stirred tank reactor (UASB/CSTR) (Isik and Sponza, 2004), and anaerobic/aerobic rotating disc reactors (RDR) (Libra et al., 2004). Another approach is the use of thermotolerant or thermophilic microorganisms in decolorization systems (Banat et al., 1996). Recently, Santos and co-workers (2005) investigated the transformation and toxicity of anthraquinone dyes during mesophilic (30°C) and thermophilic (55°C) anaerobic treatment. Compared with mesophilic conditions, distinctly higher decolorization rates at thermophilic conditions were observed with anthraquinone dyes. Thermophilic decolorization may be

advantageous as many textile and other dye effluents are produced at relatively high temperature (40-70°C).

2.2 Zero-Valent Iron Reductive Transformation

Zero-valent iron (ZVI) has recently become the most common metallic reducing agent (reductant) for environmental applications due to its abundance, low toxicity, low cost and effectiveness as a reductant (Bigg and Judd, 2000; Tratnyek et al., 2003). While most studies have used purified ZVI, it has been reported that many types of scrap steel can be substituted for ZVI with little change in reaction efficiency (Gould, 1982; Gillham and O'Hannesin 1994; Bigg and Judd, 2000), which is important in maintaining low cost. ZVI has been widely used to reduce the following contaminants (Bigg and Judd, 2000; Tratnyek et al., 2003; Miehr et al., 2004): 1) halogenated aliphatic and aromatic organic compounds (e.g., solvents and pesticides); 2) nitro-aromatic compounds; 3) high-valence toxic metals (including oxy-anions); and 4) textile dyes (e.g., reactive dyes).

The reductive transformation of these contaminants involves (1) direct electron transfer from ZVI at the surface of the iron metal (surface mediated process); and (2) reaction with dissolved Fe^{2+} or H_2 , which are products of oxidative iron corrosion as shown in Figure 2.5. The two electrons produced, with ZVI serving as the electron donor, can be used to reduce relatively oxidized contaminants. The general reduction mechanism for dyes shown in Figure 2.6 occurs in several reaction steps as follows: (Matheson and Tratnyek, 1994; Chen et al., 2001).

- (1) Diffusion of contaminant through the solution to the metal surface
- (2) Adsorption to the metal surface

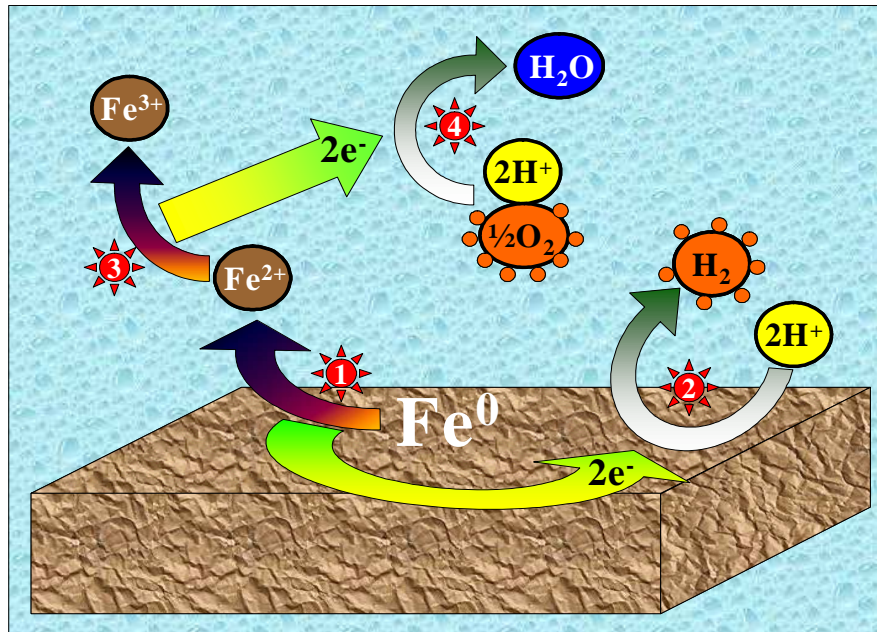


Figure 2.5. General iron corrosion mechanism (3 and 4 only occur in the presence of oxygen)(Epolito, 2005b).

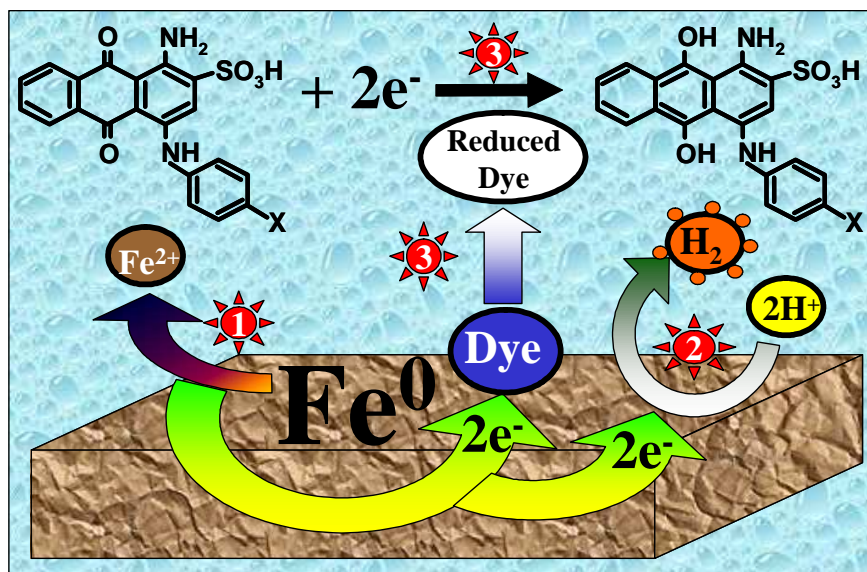
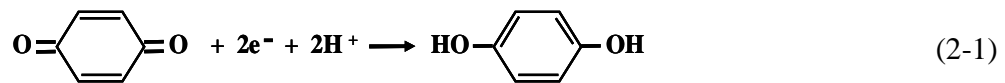


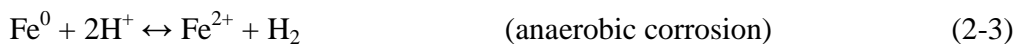
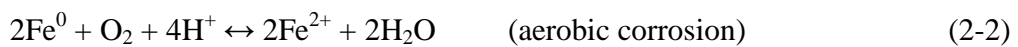
Figure 2.6. General anaerobic/anoxic iron reductive transformation of an anthraquinone reactive dye (2 and 3 occur simultaneously competing for electrons) (Epolito, 2005b).

- (3) Electrons transferred from ZVI to contaminant resulting in a chemical reaction
- (4) Production of intermediate (reduced) products
- (5) Desorption of the product(s) and diffusion to the solution

The reduction of anthraquinone reactive dyes can be written as Reaction 2-1.



The quinone reduction is widely believed to be the reduction reaction for anthraquinone reactive dyes. As can be seen in Figures 2.5 and 2.6, both the reduction of the dye and production of H_2 occur simultaneously, thus competing for electrons (Reaction 2-2). It should also be noted that if oxygen is present, another iron dissolution reaction could compete with Reaction 2-1. The overall aerobic and anaerobic corrosions which can compete with Reaction 2-1 are described by the following reactions (Helland et al., 1995; Agrawal and Tratnyek, 1996):



Both reactions (2-2 and 2-3) will increase pH in an unbuffered system, as can be seen by the consumption of H^+ in these reactions and produce potential reductants for reduction of the dye (i.e., Fe^{2+} and H_2). However, H_2 is not an effective reductant without a catalyst (House, 1972; Matheson and Tratnyek, 1994), and Fe^{2+} -mediated reduction is relatively

slow (Klecka and Gonsior, 1984; Doong and Wu, 1992). Nevertheless, iron dissolution has a potential beneficial effect: it increases the reactive surface area due to pitting of the iron surface (Snoeyink and Jenkins, 1980). Aerobic corrosion, however, could also adversely affect reduction of the dye. Dissolved oxygen (DO) would accelerate the oxidation of dissolved Fe^{2+} to Fe^{3+} , which could readily precipitate as iron oxides at neutral and basic pH values. Such rust could eventually form a surface layer on the metal surface that would inhibit surface-mediated reactions (Helland et al., 1995). In theory, oxygen could also inhibit the reduction rate by binding to the iron surface and reducing the availability of reactive surface sites (Helland et al., 1995). Conflicting reports of whether aerobic or anaerobic conditions produce the fastest reduction have been reported. Helland (1995), Siantar (1996), Bigg (2000), Judd (2000), and their co-workers have shown that the rate of reaction is faster without O_2 . However, Lavine et al. (2001) determined that the rate for nitrobenzene reduction was faster with O_2 , which may be attributed to an increased corrosion rate in the presence of O_2 (Bowers, 1986; Lavine et al., 2001) and release of more electrons that can participate in the dye reduction. It appears that experimental conditions and the contaminant involved significantly affect the effect of O_2 . Figure 2.7 shows representative solubility diagrams for Fe^{2+} and Fe^{3+} , respectively. Generally, as pH increases above neutral, the solubility of aqueous iron is reduced until basic conditions are reached. Fe^{2+} is much more soluble than Fe^{3+} . Fe^{2+} is the dominant aqueous iron species in anaerobic/anoxic conditions and Fe^{3+} is the dominant species in aerobic conditions. As the pH increases, solid precipitates begin to dominate and form layers on the ZVI, which can inhibit further reduction of Fe^0 to Fe^{2+} or Fe^{3+} .

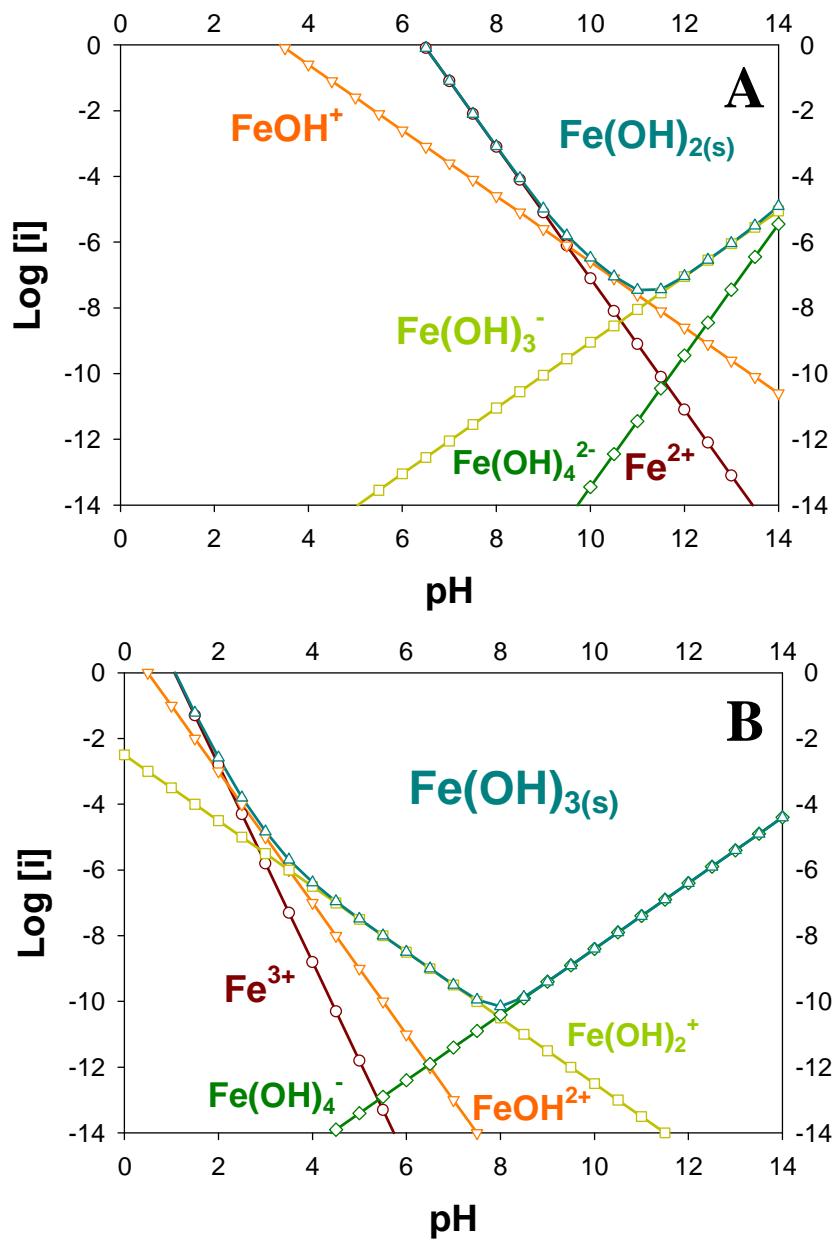


Figure 2.7. Fe²⁺ and Fe³⁺ solubility diagrams at 25°C, infinite dilution and 0.1M ionic strength; A, Fe²⁺ and B, Fe³⁺ (Epolito, 2005b).

2.3 Problem Identification

Although considerable research has been conducted on the reductive decolorization of azo dyes using zero-valent iron (ZVI) and mineralization of their decolorization products (Tan et al., 1999; Nam and Tratnyek, 2000; Perey et al., 2002), limited information exists on the reductive transformation (decolorization and mineralization) of reactive dyes and their decolorization products. Additionally, only little research has been conducted on the decolorization of spent reactive dyebaths containing high concentrations of both dye and salt, typically present in spent reactive dyebaths (Lee, 2003; Matthews, 2003; Epolito, 2004). Most of previous reports regarding the ZVI and biotransformation of reactive dyes have not addressed the issue of high concentrations of dye and salt present in commercial reactive spent dyebaths. Under typical commercial reactive dyeing conditions, up to 50% of the initial amount (up to or above 800 mg/L) of dye remains in the spent dyebath. In addition to the high concentration of hydrolyzed reactive dye, which no longer has affinity for the fiber, spent reactive dyebaths contain very high concentrations of salt (up to 100 g/L NaCl). Therefore, effective and efficient treatment methods for both the decolorization and mineralization of anthraquinone reactive dyes and their decolorization products are needed. To this end, this study may help in the development of a continuous-flow, dyebath decolorization process and the possible reuse of the renovated dyebath in the dyeing operation, which will result in the minimization of water consumption, as well as wastewater volume and concentration of textile pollutants such as dyes and salt.

2.4 Research Objectives

Based on the above-presented literature review, information about the ZVI reductive decolorization of anthraquinone reactive dyes and assessment of the biodegradation of their decolorization products has been relatively limited. More importantly, the decolorization and possible mineralization of reactive dyes by ZVI followed by a biological process under both high dye and salt concentration conditions have not been sufficiently investigated. Therefore, the main focus of the research reported here was to investigate the feasibility, kinetics and key parameter effects of reductive decolorization of the anthraquinone dye Reactive Blue 4 (RB4) by zero-valent iron and the biodegradation assessment of its decolorization products by a mixed, aerobic halophilic culture.

The specific objectives of this research were to:

- 1) Assess the effect of operational parameters (i.e., mixing speed and initial dye concentration) on the batch decolorization kinetics of RB4 by ZVI.
- 2) Determine the feasibility and decolorization kinetics of RB4 in a continuous-flow, ZVI column at typical dybath conditions.
- 3) Assess any inhibitory effect and possible mineralization of RB4 decolorization products resulting from the ZVI process on a mixed, aerobic halophilic culture.

CHAPTER 3

MATERIALS AND ANALYTICAL METHODS

3.1 Analytical Methods

3.1.1 pH

All pH measurements were performed using the potentiometric method with a digital pH meter (Orion Digital pH/millivolt Meter, Model 611) and a gel-filled combination pH electrode (Fisher Scientific). For each pH measurement, a sample was transferred into a 10 ml vial and the pH was then immediately measured to minimize any atmospheric oxidation effect. Between samples, the electrode was rinsed with deionized water and stored in an electrode storage solution (Fisher Scientific). The pH meter was calibrated weekly with pH 4.0, 7.0, 10.0 standard buffer solutions (Fisher Scientific). Although the sensitivity of the meter display was 0.01 units, the limit of accuracy was taken to be only 0.1 pH units (APHA, 1998).

3.1.2 Dissolved Oxygen (DO)

The dissolved oxygen (DO) concentration of the cultures used in this study was measured *in situ* using the polarographic method with a Yellow Springs Instrument (YSI) Model 58 oxygen meter in conjunction with a YSI 5750 oxygen probe. The instrument was calibrated to air saturated solutions with known DO concentrations (at a given temperature) before each use and the probe electrolytic solution and membrane were changed periodically. The meter was calibrated to measure DO in the halophilic culture, which contained 100 g/L NaCl. The DO saturation concentration in a solution containing

100 g/L NaCl, at 22°C and 760 mm Hg was estimated as 4.50 mg/L using the equations given in *Standard Methods* (APHA, 1998). A solution containing 100 g/L NaCl in deionized water was prepared in a temperature-controlled room at 22 °C. Then, the solution was saturated with air by purging with compressed air using a microporous diffuser while mixing on a magnetic stir plate. After performing the zero adjustment on the meter, the oxygen probe was immersed in the air-saturated, saline solution and the meter reading was adjusted to 4.50 mg/L.

3.1.3 Volatile Suspended Solids (VSS)

Volatile suspended solids (VSS) were determined according to procedures described in *Standard Methods* (APHA, 1998). Filters were washed with deionized water and ignited at 550°C for 20 min in a Fisher Isotemp Model 550-126 muffle furnace before use. The filters were then cooled in a desiccator and weighed using an Ohaus AP250D analytical balance. Culture samples of known volume (typically 5-10 mL) were filtered through 21-mm diameter Whatman GF/C glass fiber filters (1.2 µm nominal pore size, Whatman, Springfield Mill, England), which were placed in Gooch crucibles while applying vacuum. The filters were then rinsed with equal volumes of deionized (DI) water to remove dissolved organic carbon, residual inorganic carbon and salt. The filters containing the samples were dried at 105°C for at least 1.5 h in a Fisher Isotemp Model 750G oven. After cooling down in a desiccator, the dry weight was recorded and the filters containing dry samples were transferred to a Fisher Isotemp Model 550-126 muffle furnace and ignited at 550°C for 20 min. After ignition, the samples were cooled in a

desiccator. The residual solids weight was measured, and then the VSS concentration was calculated.

3.1.4 Dissolved Organic Carbon (DOC)

DOC measurements were performed using a Shimadzu TOC-5050A Total Organic Carbon Analyzer (Shimadzu Scientific Instruments, Inc., Columbia, MD) equipped with a Non-Dispersive Infrared (NDIR) detector for the analysis of total, organic, and inorganic carbon of liquid samples. Autosampler tubes were washed with weak bleach solution, rinsed with DI water and baked at 500°C before use to ensure absence of any residual carbon. In order to measure dissolved organic carbon, liquid samples were filtered through 0.22 µm membrane syringe filters (National Scientific Company) and acidified (pH < 2.0) using a 0.2 N HCl solution. Then, 4 mL of acidified samples (3.6 mL 0.2N HCl solution + 0.4 mL sample) were transferred to autosampler tubes. Duplicate measurements were performed for each sample. The injection volume was 25 µL. Carbon analysis was based on catalytic combustion of the sample at 680°C. A calibration curve was prepared using standard solutions of potassium hydrogen phthalate (KHP).

3.1.5 Spectrophotometric Analysis

Quantification of RB4 was performed using a UV-Visible, diode array spectrophotometer (Hewlett Packard Model 8453, Hewlett Packard Co., Palo Alto, CA) equipped with a diode array detector, deuterium and tungsten lamps and a 1-cm path length. Samples analyzed with the spectrophotometer were first centrifuged at 14,000

rpm for 5 min using a microcentrifuge (Eppendorf Centrifuge 5415C) in 2 mL, polypropylene microcentrifuge tubes (Fisher Scientific). Supernatants were diluted if needed with deionized water or salt/base solution (100 g/L NaCl + 3 g/L Na₂CO₃ + 1 g/L NaOH) in 1.5 mL or 2.0 ml cuvettes before absorbance measurements with the spectrophotometer. The dye concentration was calculated using the measured absorbance and prepared standard curves (Appendix A).

3.2 Dye

Commercial Reactive Blue 4 (RB4, Procion Blue MX-R; Color Index 61205; CAS no. 13324-20-4) was obtained from DyStar LP, Charlotte NC and used without any further purification. RB4, an anthraquinone dye with a dichlorotriazinyl reactive group, was selected for this research based on the following factors: previous biodecolorization research conducted and feasibility of ZVI decolorization determined by preliminary decolorization tests in our laboratory. The molecular structure of RB4 is shown in Figure 3.1. The color of anthraquinone dyes is partially associated with the anthraquinone nucleus and is modified by the type, number, and position of the substituents (Zollinger, 2003). Unsubstituted anthraquinone has a pale yellow color, which is due to an $n \rightarrow \pi^*$ transition that produces a weak color band at 405 nm (Zollinger, 2003). Electron-withdrawing substituents have little effect on the color of the compound, whereas electron-donating substituents (e.g., OH⁻ and -NH₂) give compounds their distinctive colors due to a charge transfer band involving the electron lone pair of hydroxyl or amino groups (Zollinger, 2003). RB4 has two amino groups in the 1, 4- α -positions, and a

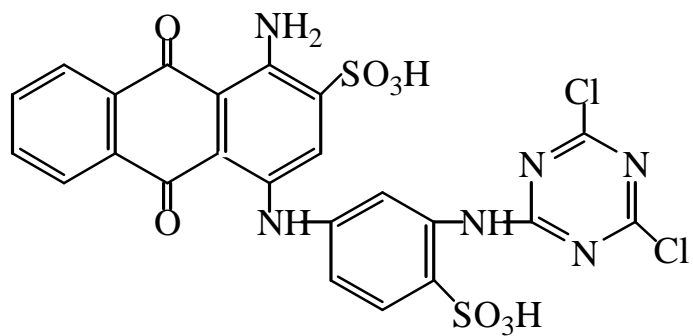


Figure 3.1. Chemical structure of unhydrolyzed Reactive Blue 4 (RB4).

sulfonic acid group in the 2-position (Figure 3.1). The sulfonic acid groups result in high aqueous dye solubility (Zollinger, 2003).

RB4 was used as received to prepare reacted 5 g/L and 20 g/L dye stock solutions. Dye stock solutions were prepared according to procedures outlined below (see section 3.2.1). Details on estimated and measured values of physico-chemical properties of RB4 are also provided in section 3.2.2.

3.2.1 Dye Stock Solution Preparation

Reacted RB4 dye stock solutions (5g/L and 20 g/L) were prepared in 1-L quantities. Preparation of reacted dye stock solution simulated conditions encountered in textile plant dyebaths. Spent reactive dyebaths after dyeing mainly contain the hydrolyzed (reacted) form of dyes due to the addition of both NaOH and Na₂CO₃ to the dyebath, which results in elevated pH values (above 11) under high temperature conditions (above 60°C). Because the research presented in this thesis was part of a research project on the abiotic/biotic decolorization and reuse of spent reactive dyebaths, all of the experiments were performed using reacted RB4 dye solutions. The NaOH reacted (hydrolyzed) dye stock solution method used in this research is identical to that used by Matthews (2003) and Lee (2003) and is as follows: (1) dye powder was dried in a 105°C oven overnight to remove excess moisture; (2) dried dye powder was cooled in a desiccator overnight; (3) 5 g (or 20 g) dried dye powder was added to 800 mL deionized water and mixed thoroughly; (4) 5 mL 10 N NaOH (0.1 M) were added; (5) solution was heated to 80 ~ 90°C for 1 h; (6) after cooling down, the solution pH was adjusted to 7.0 with 0.1 M HCl; (7) the dye solution was poured into 1 L flask and deionized water was

added up to 1 L level; (8) the pH was adjusted to 7.0 with 0.1 M NaOH; (9) the flask was sealed with parafilm and turned end-over-end for 1 min; (10) the dye solution was dispensed in a 1-L bottle, sealed with a screw-cup, covered with aluminum foil and stored in 4°C refrigerator.

For typical spent dyebath conditions, salt- and base-containing reacted dye solutions were prepared by adding 100 g/L NaCl, 3 g/L Na₂CO₃ and 1 g/L NaOH to the reacted dye stock solution and adjusting the pH to 7.0.

3.2.2 Physico-chemical Properties of RB4

As a result of hydrolysis, two OH-substituted compounds form, monohydrolyzed and dihydrolyzed RB4 as shown in Figure 3.2. Table 3.1 shows experimentally measured and estimated property values of unhydrolyzed RB4 (Lee and Pavlostathis, 2003; Epolito, 2004; Epolito et al, 2005). Although any conclusions cannot be drawn as to the accuracy of these estimates due to the lack of experimental data, they do help evaluating the overall environmental fate of RB4. Based on these estimates, RB4 is expected to partition strongly to the aqueous phase due to its high water solubility, low K_{ow} and very low vapor pressure. Based on estimated pKa values, the speciation of RB4 at different pH values, which is important in assessing its environmental fate and impact, was determined. Epolito and co-workers (2005) found three predominant, deprotonated, unhydrolyzed RB4 species between the pH values of 4 and 14 based on the estimated pKa values. Based on these data, pH effects of RB4 were also evaluated. There was no significant shift, but the absorbance in the region at the maximum wavelength generally increased as the pH increased (Epolito, 2004; Epolito et al., 2005). The effect of salt and base on

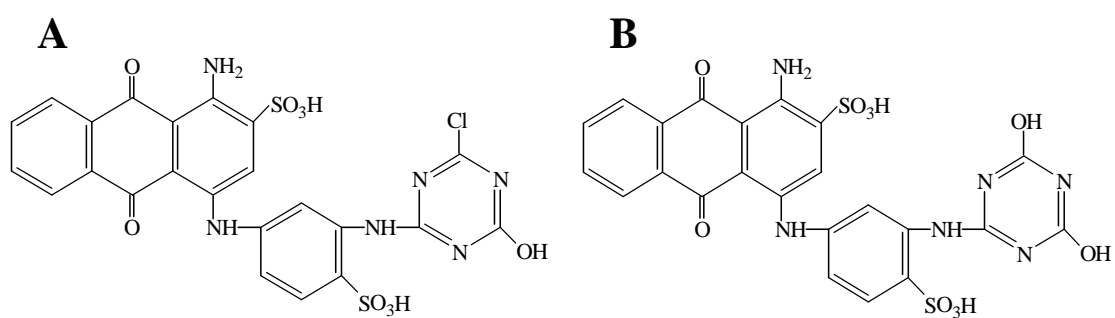


Figure 3.2. Chemical structure of monohydrolyzed (A) and dihydrolyzed (B) RB4.

Table 3.1. Experimental and estimated property values of unhydrolyzed RB4 at 25°C (Epolito, 2004; Epolito et al., 2005)

Parameter	Experimental value ^d	Estimated value ^f
Molecular weight (g/mol) ^a		637.4
λ_{\max} (nm)	598	
pH (units) ^b	6.6 ± 0.1	
COD (mg/L) ^c	390 ± 2	
Carbon content (% dry weight)	29.6 ± 0.2 ^e	43.3 ^a
Melting Point (°C)		349.84 ^g
Boiling Point (°C)		939.92 ^g 872.88 ^h
Vapor pressure (atm)		2.38E-32 ^g 1.42E-33 ^h
Water solubility (mol/L)	1.57E-1	3.77E-9 ^g 5.27E-2 ^g 2.64E-8 ^h
Henry's Law Constant		1.66E-31 ^g 2.58E-25 ^g 2.19E-27 ^h
log K_{ow}		1.72 ^g , 4.20 ^h
pKa		0.80, 1.44, 7.83, 12.05 ^h

^a Average mass based on the molecular formula $C_{23}H_{14}O_8N_6S_2Cl_2$

^b 50 mg/L unreacted dye solution

^c Chemical oxygen demand value of a 500 mg/L unreacted dye solution

^d Mean ± standard deviation ($n = 3$)

^e Measured experimentally as DOC of a 100 mg/L unreacted dye solution

^f Value at 25 °C

^g Values estimated by EPI SuiteTM using two separate methods

^h Values estimated by SPARC On-line

spectrophotometry of RB4 was evaluated due to the fact that salt and base are used in the reactive dyeing process to increase the ionic strength, decrease the electronic double layer thickness and favor the transfer of dye aggregates from the aqueous solution to the fiber (Hamlin et al., 1994). Dye aggregation was observed and the UV/Vis absorbance of a 100 mg/L RB4 solution at 598 nm decreased by 19.7, 11.4, and 20.1% after the addition of salt, base, or both salt and base, respectively, and centrifugation (Epolito, 2004; Epolito et al., 2005). Despite of these effects, RB4 dye solutions containing salt and base can still be quantified with spectrophotometry if separate calibration curves are developed taking into account the effect of salt and base.

3.2.3 Analysis of RB4

In order to determine different RB4 species, UV/Visible spectrophotometry, High Performance Liquid Chromatography (HPLC), and Liquid Chromatography/Electrospray Ionization-Mass Spectrometry (LC/ESI-MS) were used (Lee et al., 2003; Epolito et al., 2005). Figure 3.3 shows that UV/Vis spectrophotometric analysis cannot distinguish between the unhydrolyzed (or unreacted) and hydrolyzed (or reacted) form of RB4. Thus, HPLC was used to separate and identify dye components due to different reactivity of each species, which may affect the effectiveness of various decolorization processes and their optimal condition. Several dye components, especially the unhydrolyzed and hydrolyzed RB4 species, were identified using HPLC analysis (Figure 3.4 and Table 3.2). One major impurity in reacted RB4 dye solutions was also identified as 1-amino-4-hydroxyanthraquinone-2-sulfonic acid using LC/ESI-MS (Figure 3.5).

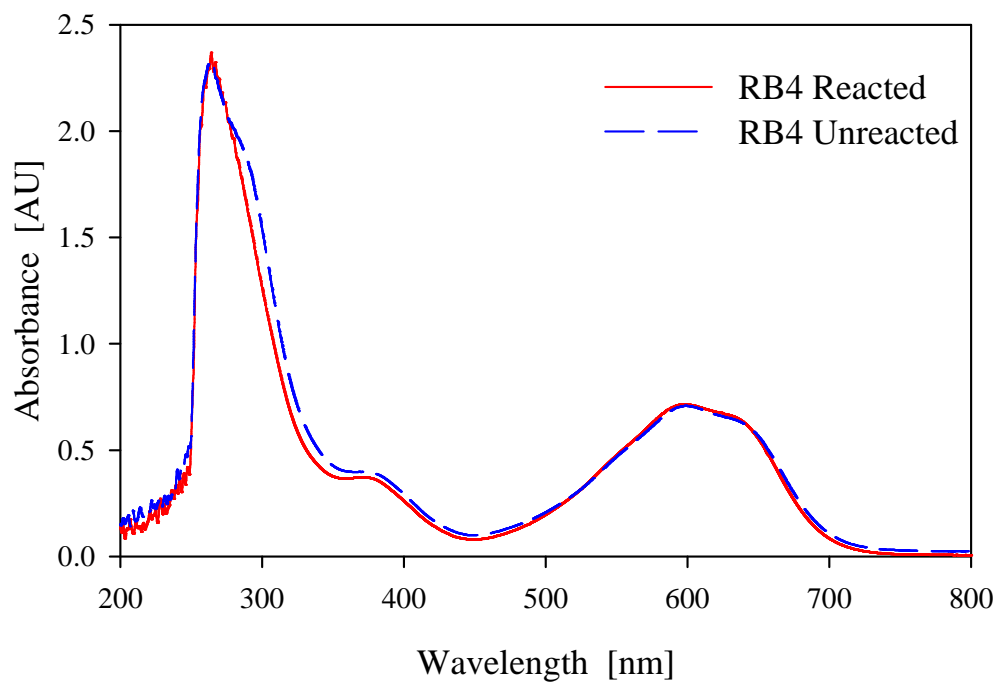


Figure 3.3. UV/Visible spectra of reacted and unreacted RB4 (100 mg/L) (Epolito, 2004; Epolito et al., 2005).

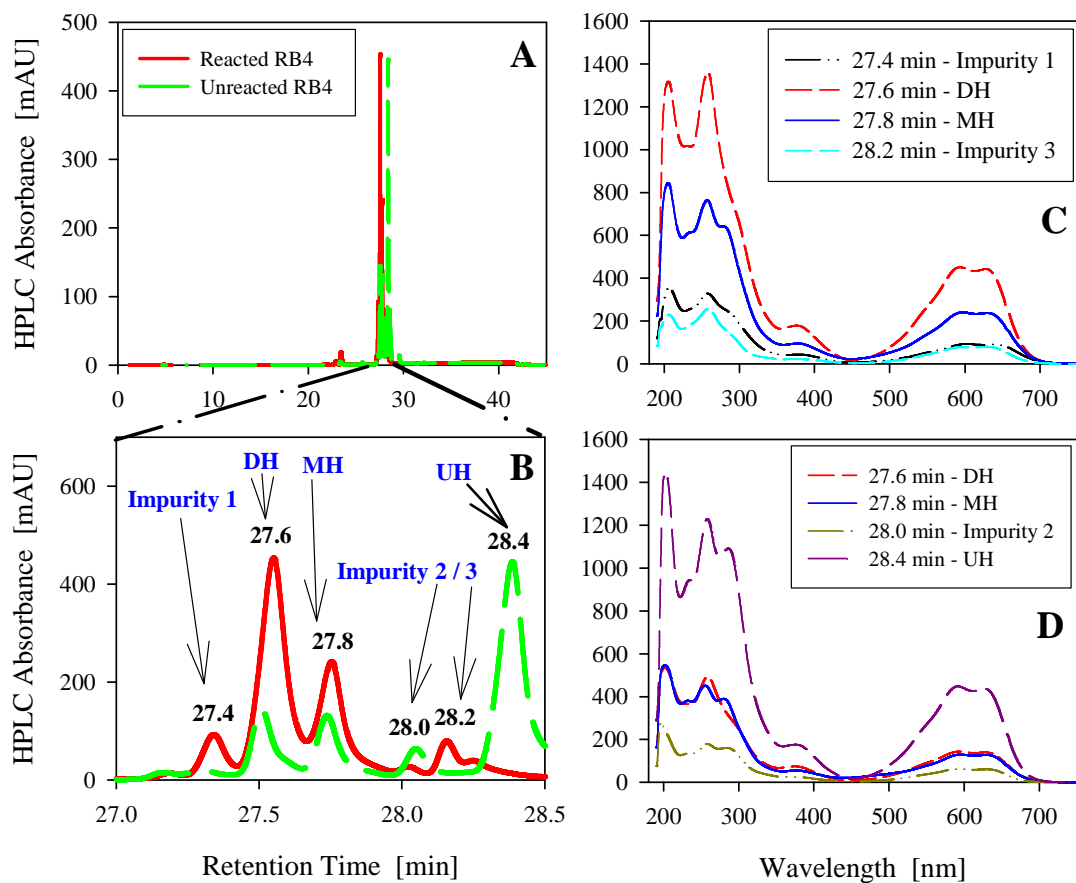


Figure 3.4. HPLC analysis of reacted and unreacted RB4 (300 mg/L): total chromatograms at 598 nm (A), enlarged chromatograms from 27.0 to 28.5 min retention time (B), spectra of reacted RB4 components (C), and spectra of unreacted of RB4 components (D) (DH, dihydrolyzed; MH, monohydrolyzed; UH, unhydrolyzed)(Epolito, 2004; Epolito et al., 2005).

Table 3.2. RB4 dye^a characterization data

Dye	Composition ^b	Molecular Formula	Molecular Weight (g/mol)	λ_{max} (nm)
Unreacted RB4	~65% UH	$\text{C}_{23}\text{H}_{14}\text{Cl}_2\text{N}_6\text{O}_8\text{S}_2$	637.4	598
	~14% MH	$\text{C}_{23}\text{H}_{15}\text{ClN}_6\text{O}_9\text{S}_2$	619.0	
	~15% DH	$\text{C}_{23}\text{H}_{16}\text{N}_6\text{O}_{10}\text{S}_2$	600.5	
	~6% MI			
Reacted RB4	~23.5% MH	$\text{C}_{23}\text{H}_{15}\text{ClN}_6\text{O}_9\text{S}_2$	619.0	598
	~58.5% DH	$\text{C}_{23}\text{H}_{16}\text{N}_6\text{O}_{10}\text{S}_2$	600.5	
	~18% MI			

^a Based on RB4 dye received from DyStar LP (Color Index 61205; CAS no. 13324-20-4)

^b Based on HPLC analysis (Epolito, 2004); minor impurities (< 5% of total 598 nm HPLC peak area) are ignored; UH = unhydrolyzed; MH = monohydrolyzed; DH = dihydrolyzed; MI = major impurities

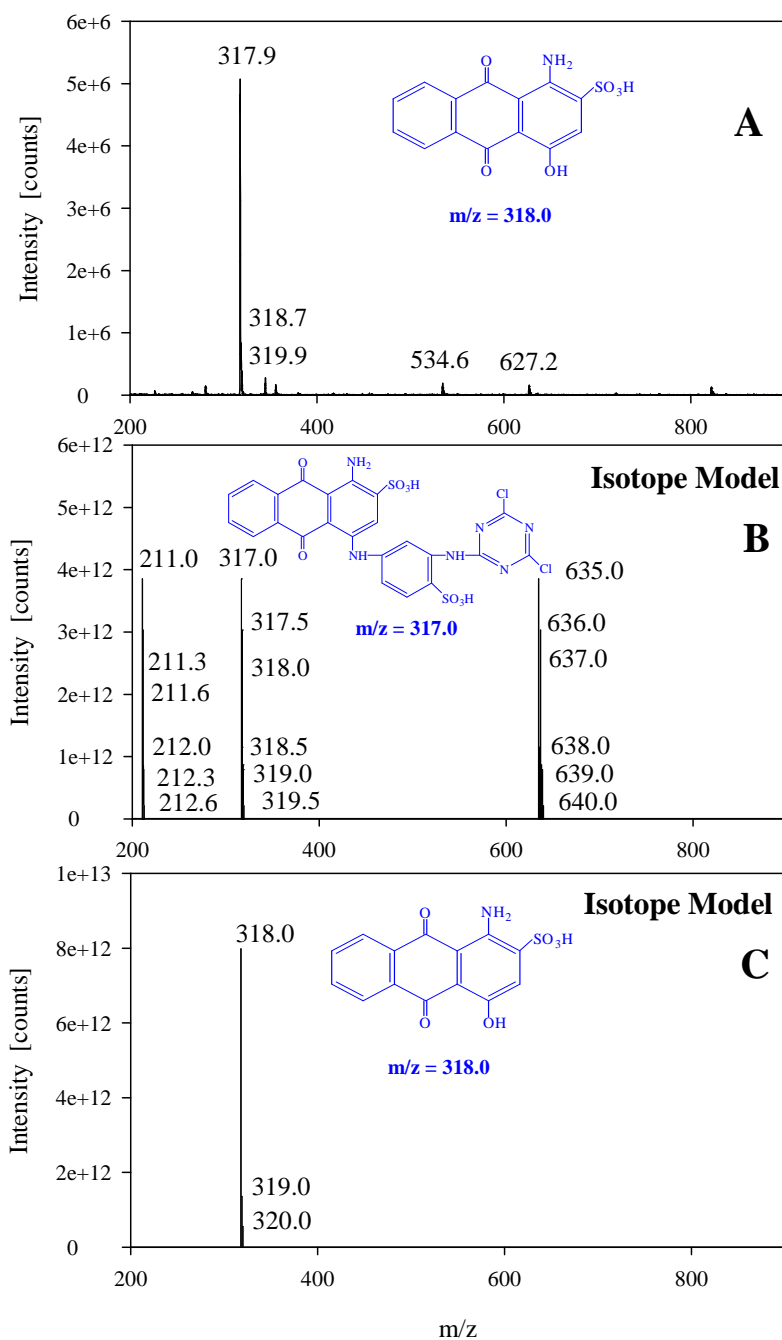


Figure 3.5. LC/ESI-MS analysis of reacted RB4 (5000 mg/L) in negative-ion mode of operation; ESI-MS spectra for 28.6 min retention time peak (A), isotope model predicted mass peaks for unhydrolyzed RB4 (B); and isotope model predicted mass peaks for 1-amino-4-hydroxyanthraquinone-2-sulfonic acid (C) (Epolito, 2004; Epolito et al, 2005).

Although UV/Visible spectrophotometric analysis cannot distinguish different dye species of RB4 (e.g., reacted and unreacted form), UV/Visible spectrophotometric analysis was mainly used in this research due to time limitations and the seemingly adequate monitoring of RB4 and its decolorization products by UV/Visible spectrophotometry. Selected samples were also analyzed by HPLC.

3.3 Iron

Connelly-GPM iron filings were used for batch and continuous-flow decolorization assays (Connelly, Chicago, IL) (Chapters 5, 6 and 7, respectively). Methanol-treated iron filings were used in all experiments and were prepared as follows:

Based on the method used by Bigg and Judd (2001), who used methylated spirits for 1 min and ethanol for 1 min, iron was treated using methanol (Epolito, 2004). To obtain uniform iron particles, the iron filings were passed through an ASTM NO.14 (Tyler 12-mesh, 1.4 mm) stainless-steel sieve to remove larger filings and then through an ASTM NO.35 (Tyler 32-mesh, 0.5 mm) sieve to remove smaller filings. The iron filings retained between the two sieves were then placed in a 2-port, 1-L glass bottle. The upper port was used to add rinsing solutions and the lower port was used to drain the rinsing solutions after mixing and treatment. The iron filings were first rinsed with deionized water five times or until the water was clear using a sonicating bath. After the deionized water rinse, the iron filings were rinsed with methanol five times or until the wasted solution was clear. The methanol evaporated faster than water and therefore significantly reduced oxidation of the iron surface by the rinsing solution while drying. Each rinse consisted of adding the rinsing solution to approximately three times the

volume of the iron filings, vigorously shaking the bottle for 15 s, and pouring out the rinsing solution. The reactor's headspace was then immediately purged with He gas until the iron filings were dry. The iron filings were then transferred to a storage glass bottle and sealed with a rubber stopper and aluminum crimp. The bottle was purged with He gas for 5 min and equilibrated at 15 psig. The bottle was then wrapped in aluminum foil and stored at room temperature ($\sim 23^{\circ}\text{C}$).

CHAPTER 4

PHASES OF STUDY

The zero-valent iron (ZVI) reductive decolorization of the anthraquinone dye Reactive Blue 4 (RB4) and biodegradation assessment of its decolorization products was conducted in three phases. Phase I involved the assessment of the effect of mixing intensity and initial dye concentration on the batch ZVI decolorization of RB4 as well as reaction rate analysis. Phase II involved the decolorization of RB4 in a continuous-flow ZVI column at typical textile reactive dyebath conditions. Finally, during Phase III, the potential for biodegradation of RB4 decolorization products resulting from a ZVI column treatment was investigated with a mixed, aerobic, halophilic culture.

4.1 Phase I – Effect of Mixing Intensity and Initial Dye Concentration on the Batch Zero-Valent Iron Decolorization of RB4

RB4, a commercially important anthraquinone dye, was selected and its reductive decolorization with zero-valent iron was investigated at different mixing speeds and initial dye concentrations under typical textile dyebath conditions in a series of batch assays. Based on the experimentally observed RB4 decolorization kinetics, a reaction rate analysis was performed (Chapter 5).

4.2 Phase II – Decolorization of RB4 in a Continuous-Flow Zero-Valent Iron Column

RB4 decolorization was performed with a continuous-flow, ZVI column at typical textile reactive dyebath conditions (1 g/L dye, 4 g/L base and 100 g/L salt) in order to determine the feasibility of a continuous-flow, ZVI dyebath decolorization process. Key column properties, such as porosity, pore volume and hydraulic conductivity were measured and a tracer test was conducted. The long-term decolorization kinetics of RB4 were investigated and quantified (Chapter 6).

4.3 Phase III – Biodegradation Assessment of RB4 Decolorization Products

Aerobic batch assays were conducted with a mixed, aerobic halophilic culture to assess possible inhibitory effects and biodegradation/mineralization of the RB4 decolorization products. The halophilic culture was maintained under fully aerobic conditions and its growth kinetics were determined. RB4 decolorization products were prepared using a ZVI column under anoxic conditions and were then fed to a batch halophilic culture (Chapter 7).

CHAPTER 5

ZERO-VALENT IRON BATCH DECOLORIZATION OF RB4

5.1 Introduction

The batch decolorization of RB4 with ZVI under anoxic conditions was investigated at different mixing intensity and initial dye concentration. Other parameters affecting ZVI RB4 decolorization, such as oxygen, pH and temperature were periodically evaluated by Epolito (2004). RB4 stock solutions simulated conditions encountered in textile reactive dyebaths. Spent reactive dyebaths mainly contain the hydrolyzed form of reactive dyes due to the high pH conditions achieved by the addition of both NaOH and Na₂CO₃ to the dyebath. All of the experiments reported in this chapter were performed using hydrolyzed (i.e., reacted) RB4 solutions in order to be consistent with the main objective of the broader research project, which is the renovation and reuse of spent reactive dyebaths. Therefore, high salt and base dyebath conditions were used in all experiments, except the one which tested the mixing intensity of the ZVI RB4 decolorization kinetics. Two alternative models were used to describe the experimentally obtained RB4 decolorization kinetics and compared.

The objectives of the work presented in this chapter were: (1) to investigate the effect of mixing intensity on the ZVI RB4 decolorization kinetics; and (2) to evaluate the effect of the initial dye concentration on the ZVI decolorization kinetics at high salt and base dyebath conditions.

5.2 Materials and Methods

The general procedure for the batch decolorization assays was as follows. Triplicate, 160-ml serum bottles were used in all assays. Controls (i.e., iron-free) were set up with D.I. water or a salt and base solution (100 g/L NaCl, 3 g/L Na₂CO₃ and 1 g/L NaOH). The iron concentration in each serum bottle was 1 M (5.59 g/100 mL) and was achieved by the addition of methanol treated iron filings. All serum bottles were sealed with rubber stoppers and aluminum crimps and then purged with He gas to achieve anoxic conditions. He was bubbled through the liquid sample in each serum bottle using two needles. He gas was added through the longer needle submerged in the liquid sample, whereas the second needle served as the gas outlet. The liquid was purged for 5 min with the gas cylinder regulator set at 10 psig. The headspace was then purged for another 5 min. Then, the outlet needle was removed and the headspace was allowed to equilibrate at 10 psig headspace pressure (for approximately 3 s). Finally, the inlet needle was removed while He gas was still flowing. For each assay, a reacted RB4 dye stock solution was also purged with He gas to achieve anoxic conditions before the dye was added to each bottle. All assays were initiated at pH 7 by adjusting it using 1 N NaOH and HCl solutions. Details on specific batch assays are listed below.

5.2.1 Effect of Mixing Intensity

Iron filings (1 M) and 96 mL of D.I. water were added to each bottle, which was then purged with He gas as mentioned above. Then, 4 mL of the dye stock solution (5 g/L reacted RB4) were added by syringe to each bottle bringing the final liquid volume to 100 ml, thus leaving a headspace of 60 ml of He gas. The bottle headspace pressure was

adjusted to 10 psig with He gas, thus leaving the bottle under a positive pressure in order to avoid introduction of air, as well as to allow frequent removal of liquid samples. The initial dye concentration for this assay was 300 mg/L. The bottles were then placed on an orbital shaker and mixed at speeds of 1, 25, 50, 100, 200, 300 and 400 rpm in a 22°C constant temperature room. In addition, another set of serum bottles were mixed using an end-over-end tumbler which rotated at 4 rpm. At each sampling time, liquid samples were removed by syringe, centrifuged at 14,000 rpm for 5 min and then the UV/Visible absorbance and pH were measured. Test bottles filled last were sampled first to minimize time errors caused by the bottle preparation.

5.2.2 Effect of Initial Dye Concentration

For effect of initial dye concentration on the ZVI decolorization kinetics at typical salt and base textile dyebath conditions was evaluated at initial dye concentrations of 100, 300, 500, 700, 1000 and 1500 mg/L. Each RB4 dyebath solution contained 100 g/L NaCl, 3 g/L Na₂CO₃ and 1 g/L NaOH and was purged with He gas. Then, an appropriate volume of dyebath solution was added by syringe to each bottle to a final liquid volume of 100 ml and a headspace of 60 ml of He gas. The bottles were then placed on an end-over-end tumbler at fixed mixing speed (4 rpm) in the 22°C constant temperature room. The end-over end tumbler was used for these assays because it provided better mixing and thus a much greater mass transfer rate than the orbital mixer. At each sampling time, liquid samples were removed by syringe, centrifuged at 14,000 rpm for 5 min and then the UV/Visible absorbance and pH were measured. Each sample was diluted if needed

with a salt and base solution (100 g/L NaCl, 3 g/L Na₂CO₃, and 1 g/L NaOH) in 2.0 ml cuvettes before absorbance measurements.

5.2.3 Reaction Rate Analysis

Dye concentrations based on UV/Visible absorbance measurements were used to determine decolorization rates using the pseudo first-order rate equation:

$$-\frac{dC}{dt} = k_{obs} [C] \quad (5-1)$$

where: C = RB4 dye concentration (mg/L); and k_{obs} = reaction rate constant (h⁻¹).

This reaction rate equation is a simplified version of equation (5-2) with assumptions such as (Epolito et al., 2005b): (1) all dye components have the same rate constant (i.e., i = 1); (2) the iron reactive sites (ρ_{Fe}) and pH are constant during the experiment; and (3) the reaction order is 1 (i.e., b = 1).

$$-\frac{dC_i}{dt} = k \rho_{Fe} [\text{pH}]^a [C_i]^b \quad (5-2)$$

$$r = -\sum_i \frac{dC_i}{dt} \quad (5-3)$$

where: C_i = concentration of RB4 dye component i (mg/L); i = 1, 2 ... # of individual RB4 dye components; k = rate constant (L/mg-h); ρ_{Fe} = iron reactive sites (usually equated to iron surface area)(mg/L); a = reaction order of pH; b = reaction order of RB4 dye concentration; and r = overall reaction rate (mg/L-h).

The following initial volumetric decolorization rate (r, mg/L-h) was also used to determine decolorization kinetics at relatively high initial dye concentrations:

$$r = \frac{(C_o - C)}{t} \quad (5-4)$$

where: C_0 = initial dye concentration (mg/L); C = dye concentration at time t (mg/L); and t = time (h).

Several studies have shown that the ZVI-mediated reaction rate is actually of shifting order, depending on the initial contaminant concentration. This type of behavior has been usually observed at relatively high initial contaminant concentrations and has been attributed to a saturation effect of ZVI surface reactive sites, which is common in heterogeneous reactions (Johnson et al., 1996; Johnson et al., 1998; Nam and Tratnyek, 2000; Agrawal et al., 2002). In such cases, the site saturation model (similar to the Michaelis-Menten enzyme kinetics model) has been used to describe the reaction kinetics, as follows:

$$-\frac{dC}{dt} = \frac{V_m C}{K + C} \quad (5-5)$$

First-order range: $-\frac{dC}{dt} = \left(\frac{V_m}{K}\right) C \quad (5-6)$

Zero-order range: $-\frac{dC}{dt} = V_m \quad (5-7)$

where: V_m = maximum reaction rate (mg/L-h); C = contaminant concentration (mg/L); K = C at $V_m/2$ (reflects the affinity of the metal surface for the contaminant)(mg/L).

K is approximately constant for a particular contaminant, but V_m varies with both the type/grade of ZVI and the experimental conditions (mixing, temperature, etc.) (Johnson et al., 1998; Nam and Tratnyek, 2000). In order to evaluate the effect of the initial RB4 concentration, this model (equation 5-5) was also used in the present study and was compared with the pseudo first-order rate equation (5-1).

5.3 Results and Discussion

5.3.1 Effect of Mixing Intensity

The effect of mixing intensity on the ZVI decolorization of 300 mg/L RB4 was assessed at a range of mixing speed from 0 to 400 rpm under anoxic conditions. This assay lasted from 12 to 500 h, depending on the mixing speed. The pH values increased throughout the experiment as shown in Table 5.1. Dye concentrations based on UV/Visible absorbance measurements were used to determine decolorization rates based on the pseudo first-order rate equation (equation 5-1) by non-linear regression. The nonlinear regression procedure based on the Marquardt-Levenberg algorithm was used to fit equation 5-1 to the dye concentration data by minimizing the residual standard error; an estimate of k_{obs} was obtained. Dye concentration data, as well as non-linear regression fits to the pseudo first-order rate equation are shown in Figure 5.1 and Table 5.1. All regression fits resulted in R^2 values greater than 0.96. Figures 5.1 and 5.2 show that as the mixing speed increased the observed decolorization rate constant (k_{obs}) increased as expected. However, the data fit was non-linear with respect to the square root of the mixing speed, contrary to previous reports (Agrawal, 1996; Nam, 2000; Bigg, 2001). A second observation is that different types of mixing regimes (orbital versus tumbler) resulted in different decolorization rates. The decolorization rate achieved with the tumbler at 4 rpm was almost as fast as that obtained with the orbital mixer at 300 rpm. This difference can be explained by the fact that orbital mixing moved the liquid over the stationary iron fillings on the bottom of the bottles, whereas the tumbler provided end-over-end mixing, resulting in a much greater mass transfer rate because the iron fillings were constantly moving through the liquid phase. This observation demonstrates that

Table 5.1. Kinetics of RB4 decolorization by ZVI as a function of mixing intensity^a

Mixer	Mixing Speed [rpm]	pH ^b	k_{obs} [h^{-1}] ^c	Data Points (#)	R ² Value	$t_{1/2\text{obs}}$ [h]
Orbital	0	7.3-9.7	0.010 ± 0.001	10	0.956	51.4
Orbital	25	7.5-8.4	0.015 ± 0.001	10	0.978	34.8
Orbital	50	7.2-8.8	0.016 ± 0.001	10	0.970	32.6
Orbital	100	7.2-9.1	0.039 ± 0.003	10	0.988	14.6
Orbital	200	7.2-9.5	0.087 ± 0.005	10	0.986	6.6
Orbital	300	7.2-9.3	0.166 ± 0.013	10	0.975	3.5
Orbital	400	7.2-8.7	0.279 ± 0.026	10	0.981	2.1
Tumbler	4	7.2-9.8	0.147 ± 0.016	10	0.983	4.1

^a All sets had 1 M iron fillings and an initial RB4 concentration of 300 mg/L

^b Denotes initial and final pH values

^c Pseudo first-order decolorization rate constant (mean \pm standard error)

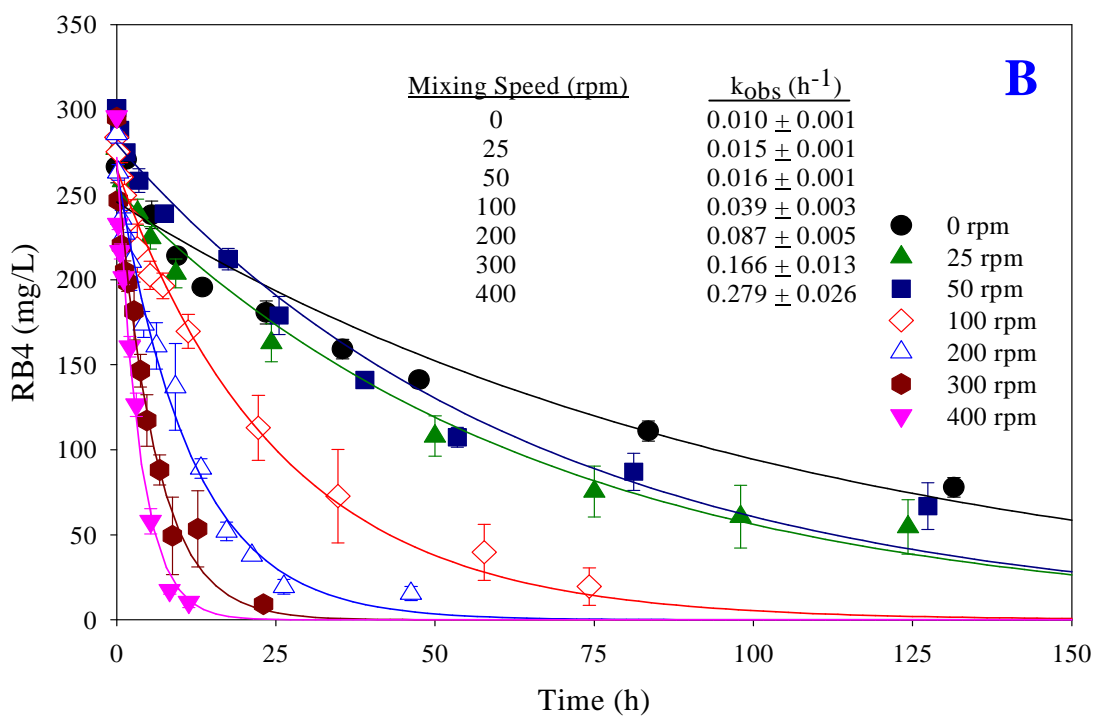
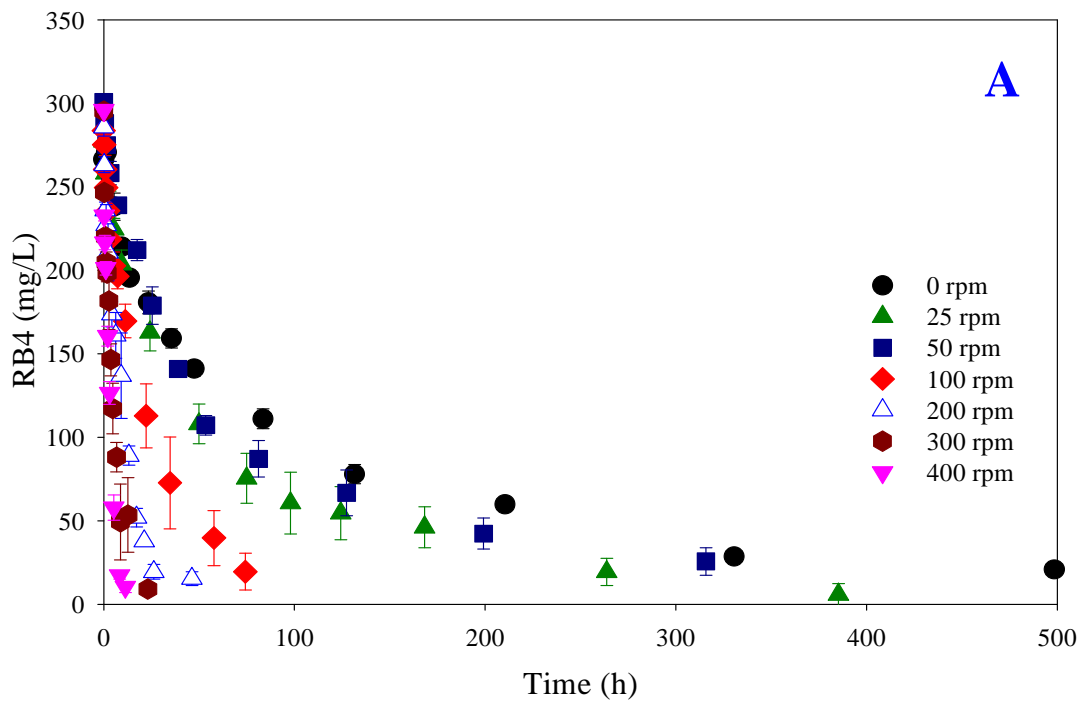


Figure 5.1. Effect of mixing intensity (rpm) on the ZVI decolorization of RB4 (All sets at 300 mg/L initial RB4; (A) experimental data based on absorbance at 598 nm; (B) lines are non-linear regression fits based on the pseudo first-order model)(Error bars represent \pm one standard error of the mean).

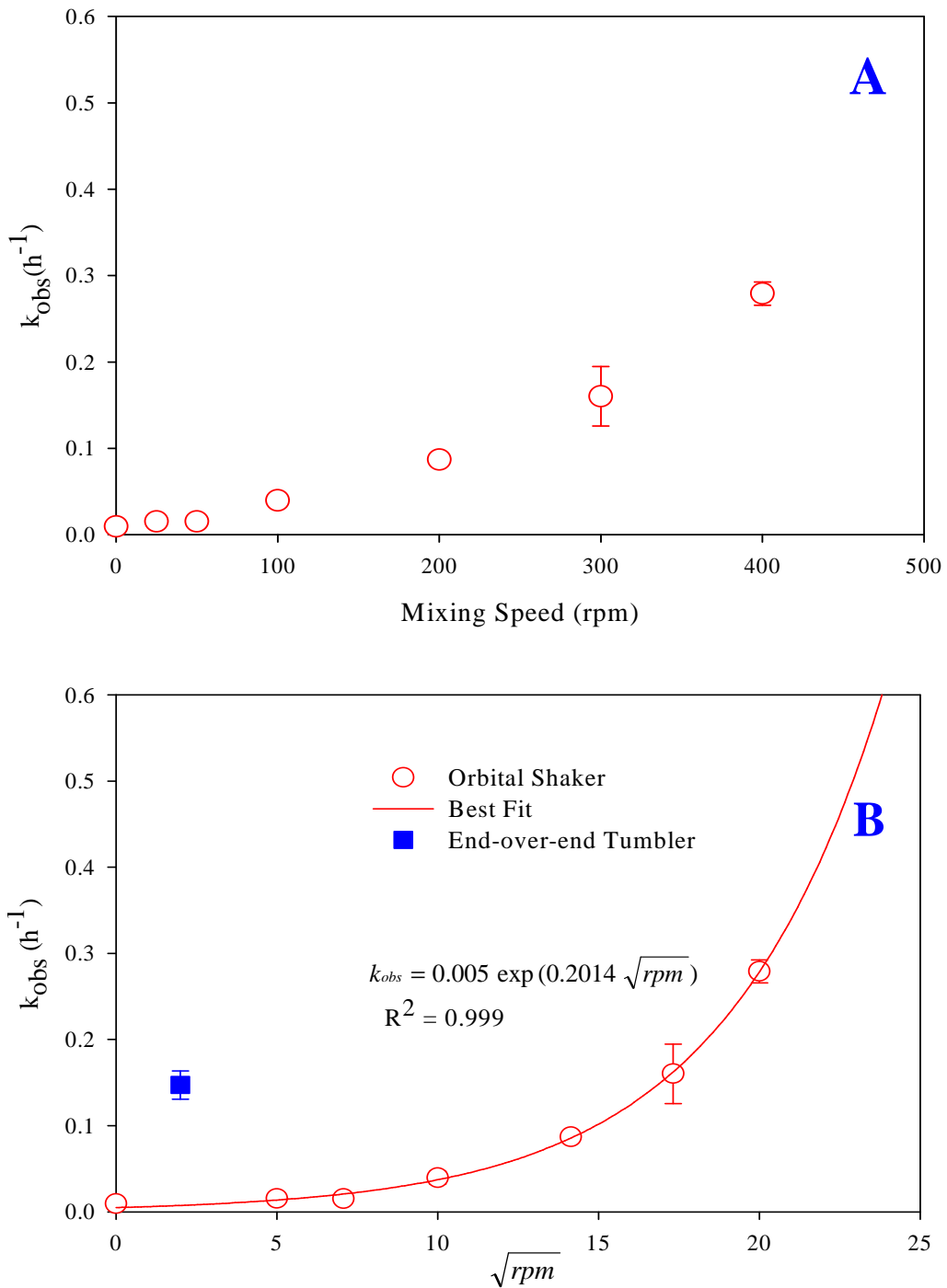


Figure 5.2. Effect of mixing intensity (rpm) on the ZVI pseudo first-order decolorization rate constant of reacted RB4 (Initial RB4 concentration equal to 300 mg/L); experimental data based on absorbance at 598 nm (A); non-linear regression fit based on the pseudo first-order model (B) (Error bars represent \pm one standard error of the mean).

mixing characteristics are more important than mixing speed and that ZVI RB4 decolorization is mass transfer limited.

Although all pseudo first-order fits resulted in R^2 values greater than 0.96, Figure 5.1 shows that residual color remained at prolonged incubation times. Figure 5.3 shows that there is some residual absorbance (at 598 nm) remaining after dye transformation. HPLC analyses conducted by both Lee (2003) and Epolito (2004) confirmed that such decolorization products have significant absorbance at 485 nm. In addition, a portion of this residual absorbance is most likely due to impurities. As mentioned in Chapter 3, Epolito and co-workers (2005) using advanced analytical techniques (HPLC and LC/ESI-MS) identified some of the impurities in reacted RB4 solutions. Based on the foregoing analysis, all non-linear regressions were conducted based on relatively early experimental data.

5.3.2 Effect of Initial Dye Concentration

The effect of initial dye concentration on the ZVI decolorization kinetics of RB4 was evaluated at an initial dye concentration from 100 to 1500 mg/L and at typical reactive textile dyebath conditions (100 g/L NaCl, 3 g/L Na₂CO₃ and 1 g/L NaOH). This assay was conducted under anoxic conditions and lasted from 47 to 337 h, depending on the initial dye concentration. The end-over-end tumbler at 4 rpm was used for this assay. The pH values increased throughout the experiment and their ranges are listed in Table 5.2. Decolorization rates were determined using the pseudo first-order equation and non-linear regression (equation 5-1). Dye concentration data, as well as non-linear regression fits to the pseudo first-order rate equation are shown in Figure 5.4 and Table 5.2. All

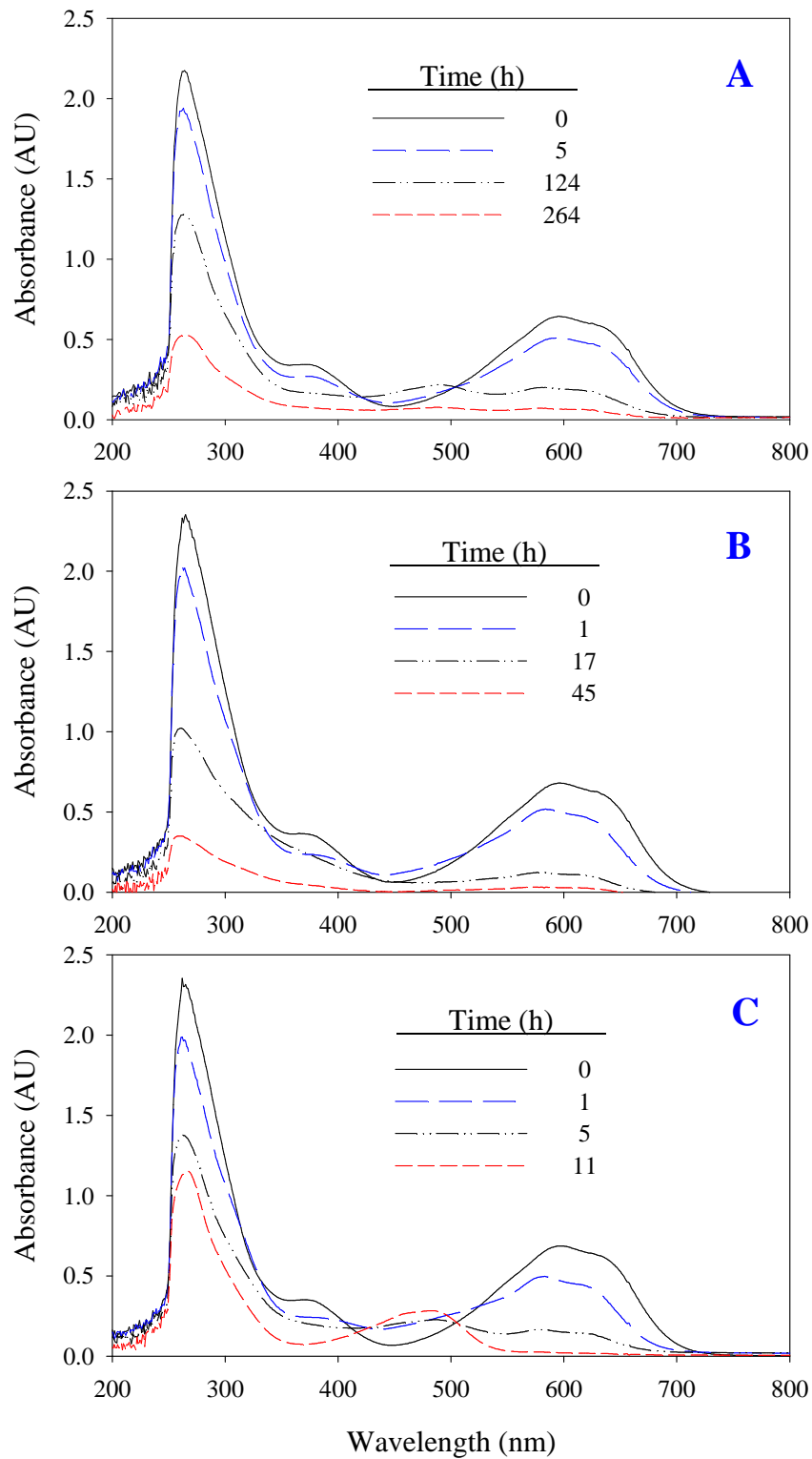


Figure 5.3. UV/Visible spectra during the decolorization of reacted RB4 (Initial dye concentration 300 mg/L; 100 g/L NaCl, 3 g/L Na₂CO₃, and 1 g/L NaOH)(Mixing speed (rpm): A, 0; B, 200; and C, 400).

Table 5.2. Kinetics of RB4 decolorization by ZVI as a function of initial dye concentration^a

Initial Dye Conc. [mg/L]	pH ^b	k_{obs} [h ⁻¹] ^c	Data Points (#) ^c	R ² Value ^c	k_{obs} [h ⁻¹] ^d	Data Points (#) ^d	R ² Value ^d	Initial Decolorization Rate [mg/L-h] ^e
100	7.9-8.1	1.520 ± 0.209	7	0.950	1.539 ± 0.180	8	0.950	80.3 ± 14.8
300	7.9-8.1	0.397 ± 0.058	7	0.961	0.519 ± 0.061	8	0.937	135.8 ± 39.0
500	7.9-8.0	0.145 ± 0.033	6	0.917	0.293 ± 0.057	7	0.817	190.6 ± 66.1
700	7.9-8.5	0.160 ± 0.038	6	0.930	0.302 ± 0.052	7	0.857	246.8 ± 78.2
1000	7.9-8.5	0.069 ± 0.016	6	0.922	0.190 ± 0.042	7	0.803	313.0 ± 103.3
1500	7.8-8.4	0.041 ± 0.008	6	0.946	0.107 ± 0.028	7	0.749	389.7 ± 105.0
300 ^f	7.2-9.8	0.147 ± 0.016	9	0.983	0.180 ± 0.018	10	0.971	72.6 ± 11.4

^a The end-over-end tumbler at 4 rpm was used (Conditions: 1 M iron fillings; 100 g/L NaCl, 3 g/L Na₂CO₃ and 1 g/L NaOH).

^b Denotes initial and final pH values

^c Non-linear regression without fixed C_o (mean ± standard error)

^d Non-linear regression with fixed C_o (mean ± standard error)

^e Mean ± standard error

^f Reacted RB4 (300 mg/L) in DI water, instead of the salt and base solution

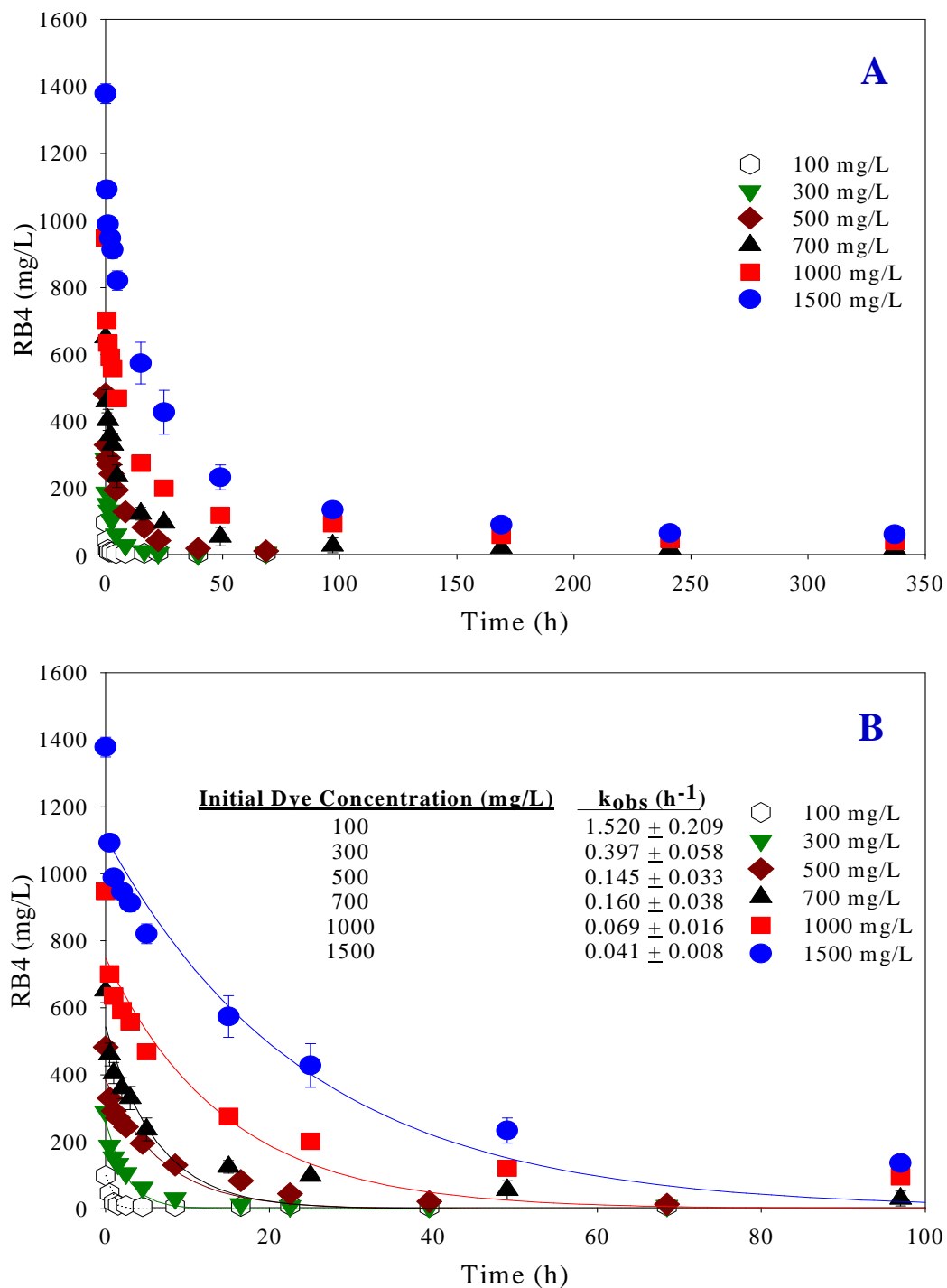


Figure 5.4. Effect of initial dye concentration on the ZVI decolorization of RB4 (All bottles mixed with the end-over-end tumbler at 4 rpm; (A) experimental data based on absorbance at 598 nm; and (B) non-linear regression fits based on the pseudo first-order model)(Error bars represent \pm one standard error of the mean).

regression fits resulted in R^2 values greater than 0.92. The relationship between rate constant (k_{obs}) and initial concentration appears to be non-linear even when plotted against the square root of concentration and are best fit by an exponential function (Figure 5.5A and B). However, as shown in Figure 5.6 and Table 5.2, the initial concentration of RB4 was underestimated by the pseudo first-order fit. When the initial RB4 concentration was fixed, the value of the reaction rate constant increased but such regression fits resulted in lower R^2 values compared to the case where the initial dye concentration was taken as a variable. This observation shows that pseudo first-order kinetics do not accurately represent the reaction mechanism (dye decolorization). The previously presented assumptions for this kinetic model - such as all dye components have the same rate constant; the iron reactive sites and pH are constant during the decolorization assay; and the reaction rate order is unity may not be entirely valid. Epolito (2005b) found that under a relatively constant pH, each dye component has a different rate constant. Figure 5.7 shows the UV/Visible spectra during the ZVI decolorization of RB4 at an initial dye concentration of 1,500 mg/L. As the dye decolorization proceeded, the absorbance at 598 nm gradually decreased and the absorbance at 485 nm increased due to the formation of RB4 decolorization products. With prolonged incubation, the absorbance at 485 nm decreased. It is noteworthy that a residual absorbance at 598 nm was always present, which, as discussed above, based on previous analyses (Lee, 2003; Epolito, 2004; Epolito et al., 2005a) is attributed to the RB4 decolorization products and not the parent dye. Epolito (2005b) used multiple pseudo first-order kinetics based on each dye component, which fit the data better than a single pseudo first-order rate. It is also possible that the reaction rate is not truly first-

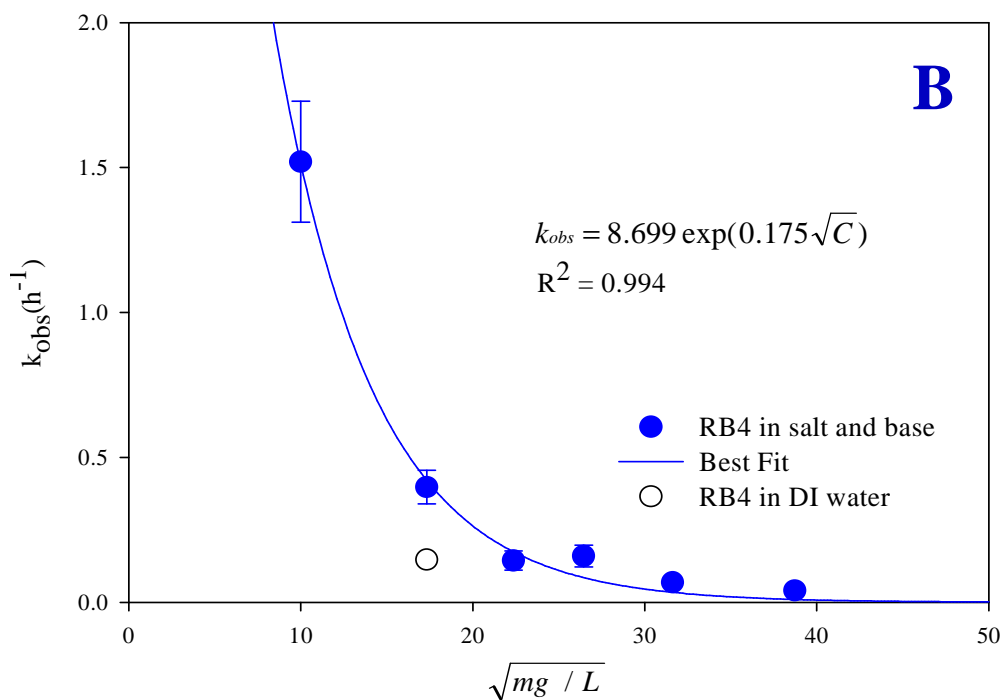
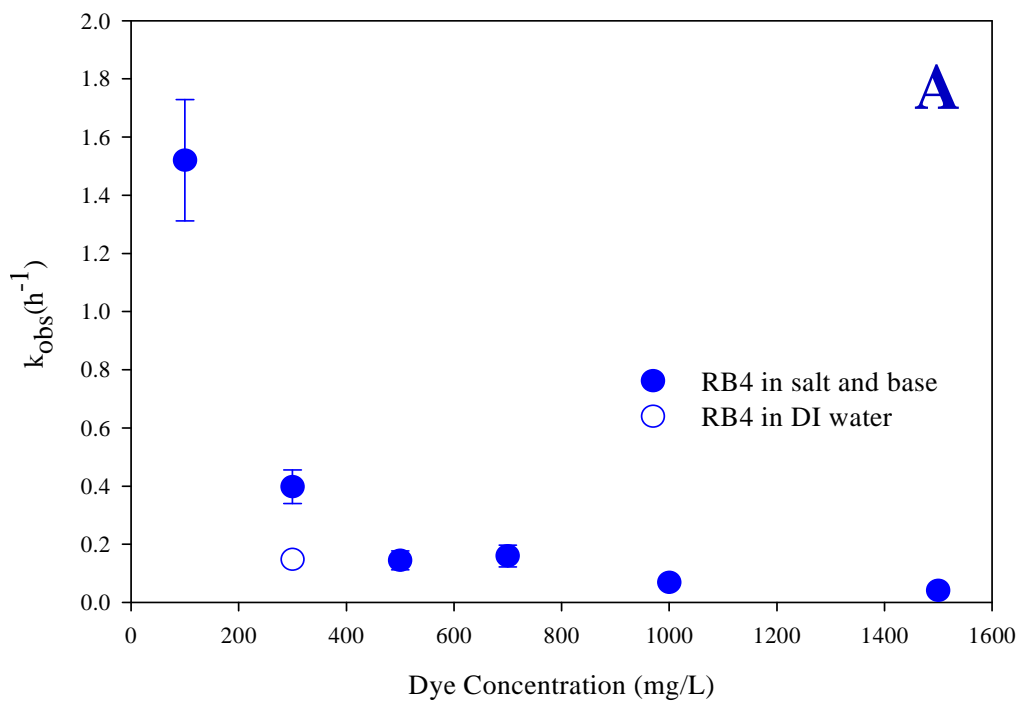


Figure 5.5. Effect of initial dye concentration on the decolorization kinetics of reacted RB4 (Conditions: 100 g/L NaCl, 3 g/L Na₂CO₃, and 1 g/L NaOH; mixing with end-over-end tumbler at 4 rpm); A) experimental data based on absorbance at 598 nm; and B) non-linear regression fit based on the pseudo first-order model) (Error bars represent \pm one standard error of the mean).

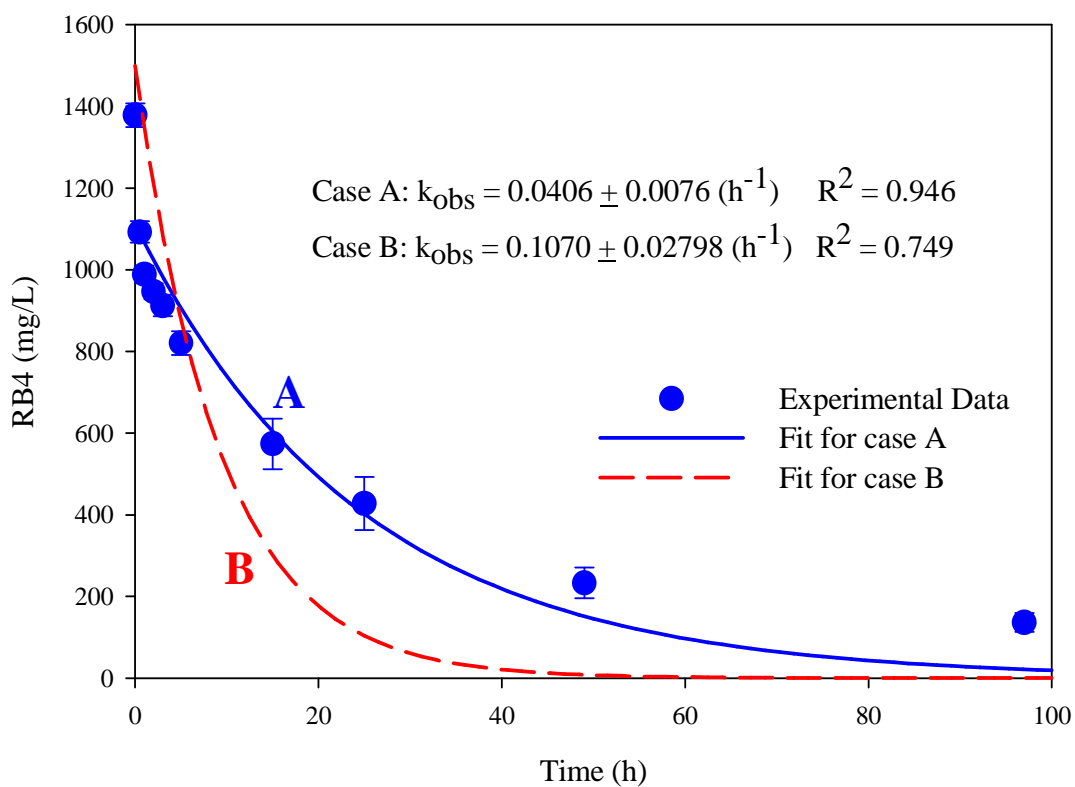


Figure 5.6. Pseudo first-order regression fit to RB4 data over the initial decolorization time. Case A: C_0 as variable; Case B: C_0 at fixed value (Conditions: initial reacted RB4 concentration 1,500 mg/L; 100 g/L NaCl, 3 g/L Na_2CO_3 , and 1 g/L NaOH; experimental data based on absorbance at 598 nm) (Error bars represent \pm one standard error of the mean).

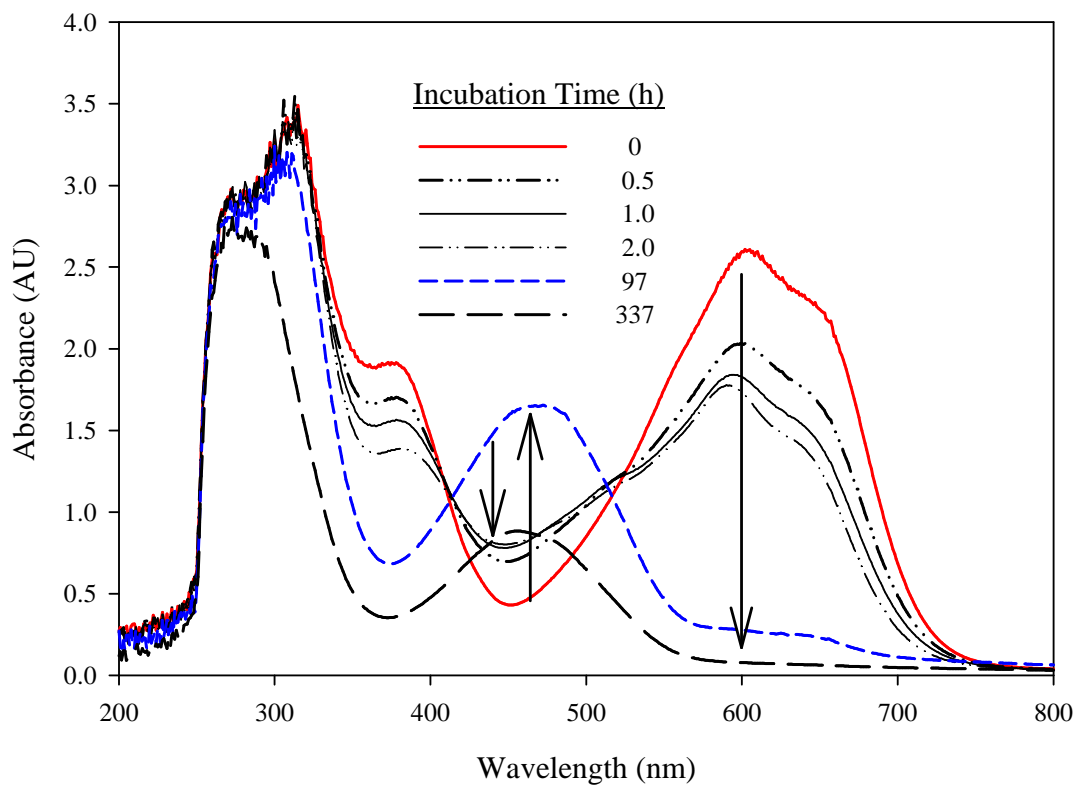


Figure 5.7. UV/Visible spectra during the decolorization of reacted RB4 (Conditions: initial RB4 concentration equal to 1,500 mg/L; 100 g/L NaCl, 3 g/L Na₂CO₃, and 1 g/L NaOH; mixing with end-over-end tumbler at 4 rpm).

order, but of a shifting order (first- to zero-order). Several studies which used ZVI have shown that the reaction rate can actually shift order depending on the initial contaminant concentration. At relatively high initial contaminant concentrations saturation of the ZVI surface sites is common in heterogeneous reactions (Johnson et al., 1996; Johnson et al., 1998; Nam and Tratnyek, 2000; Agrawal et al., 2002). Several studies have concluded that ZVI transformation reactions are either transport limited (Agrawal and Tratnyek, 1996; Nam and Tratnyek, 2000; Zhang et al., 2002) or reaction limited (Scherer et al., 1997; Su and Puls, 1999).

The initial volumetric RB4 decolorization rate data [r , mg/L-h; equation 5-4] and the previously discussed site saturation model (equation 5-5) were used to evaluate the RB4 decolorization kinetics. The initial volumetric decolorization rate (r) increased monotonically but non-linearly with increasing initial RB4 concentration (Table 5.2 and Figure 5.8). This behavior may be explained by the saturation of reactive sites of iron. Based on the non-linear regression of the experimental data based on the site saturation model (equation 5-5), the following parameter values were obtained: $K = 1299 \pm 273$ mg/L (mean \pm standard error) and $V_m = 720 \pm 88$ mg/L-h. (mean \pm standard error) ($R^2 = 0.991$; $n = 7$).

In order to assess the effect of salt and base on the ZVI RB4 decolorization kinetics, a set of triplicate serum bottles with an initial RB4 concentration of 300 mg/L in DI water was also evaluated and the results are shown in Table 5.2 and Figure 5.2. For the same initial dye concentration (300 mg/L), the RB4 decolorization rate increased from 0.147 ± 0.016 h⁻¹ to 0.397 ± 0.058 h⁻¹ for the case of DI water and salt plus base, respectively. Several researchers have observed higher decolorization rates in the

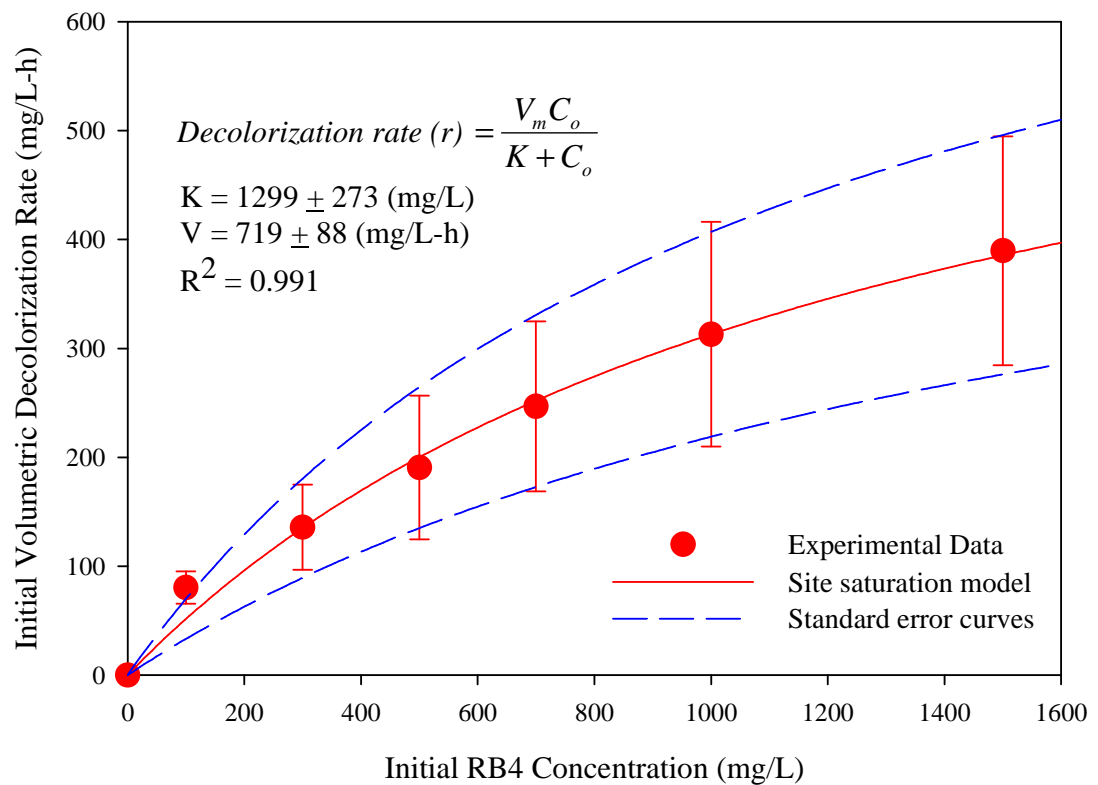


Figure 5.8. Non-linear fit of initial volumetric RB4 decolorization rate data to the site saturation model as a function of initial dye concentration (Conditions: mixing with an end-over-end tumbler at 4 rpm; 100 g/L NaCl, 3 g/L Na₂CO₃, and 1 g/L NaOH) (Error bars represent \pm one standard error of the mean).

presence of high salt and base concentrations and have been attributed to the positive effect of ionic strength of the solution to the decolorization rate (Matthews, 2003; Epolito, 2004; Johnson et al., 1998). Therefore, the high salt and base concentrations typically encountered in reactive dyebaths enhance the ZVI decolorization rates.

5.4 Summary

ZVI batch decolorization of RB4 was performed. The effect of operational parameters, such as mixing intensity and initial dye concentration, on the dye decolorization kinetics was evaluated. Dye concentrations were based on UV/Visible absorbance measurements and were used to determine decolorization rates using the pseudo first-order rate equation. As the mixing speed increased, the observed decolorization rate constant (k_{obs}) increased. However, at the same initial dye concentration, different types of mixing regimes (orbital versus tumbler) resulted in significantly different decolorization rates. Taking all together, these observations demonstrate that the ZVI decolorization process is a surface-catalyzed, mass transfer-limited process. The decolorization rate decreased as the initial dye concentration increased. The site saturation model was used to fit initial, volumetric dye decolorization data, and successfully depicted the experimental data. Two operational parameters (mixing and initial dye concentration) showed that decolorization of RB4 is mass transfer limited. Although the multiple pseudo first-order and the site saturation models accurately represent the RB4 decolorization process, the single pseudo first-order rate model was used for the remainder of this research project due to time constraints and the seemingly adequate overall data fit obtained. ZVI treatment appears to be promising for

the decolorization of commercial, anthraquinone-bearing, spent reactive dyebaths, which upon renovation can then be reused as process water in the dyeing process.

CHAPTER 6

CONTINUOUS-FLOW ZERO-VALENT IRON RB4 DECOLORIZATION

6.1 Introduction

Zero-valent iron (ZVI) reductive transformation has primarily focused on in-situ remediation in permeable reactive barriers (PRBs) to reduce halogenated organic compounds. Many studies have been conducted with this technology for the reduction/degradation of dyes, halogenated organic compounds, azo- and nitro-aromatics, arsenate, TNT, RDX, mercury, nitrate, and copper (Wragg and Bravo de Nahui, 1992; Shirakashi et al., 1993; Hao, R. et al., 2000; Westerhoff and Johnson, 2001; Loraine et al., 2002; Lubenow et al., 2002; Melitas et al., 2002; Oh et al., 2003; Oh and Alvarez, 2004). ZVI iron packed beds are flexible and scaleable to meet different wastewater loads of different industries and have been pilot-tested (Melitas et al., 2002) and field-tested (Westerhoff and Johnson, 2001). While key parameters affecting the reduction process, such as contact time (or residence time), flow rate, iron loading, iron type and composition, dissolved oxygen, pH, water composition, and contaminant loading, are relatively well understood, limited data exist on long-term iron column operation.

The objectives of the work presented here were (1) to design and characterize a ZVI column; (2) to investigate continuous-flow decolorization kinetics of RB4 under textile reactive dyebath conditions; and (3) to conduct a long-term continuous-flow RB4 decolorization kinetic study.

6.2 Materials and Methods

For the research reported here, two ZVI columns were constructed. A small, glass column (column A; Kimble/Kontes chromatography column) 15 cm long \times 4.8 cm inner diameter (I.D.) was constructed for the evaluation of the column characteristics (i.e., porosity, hydraulic conductivity, Reynolds number, pore water velocity, and dispersion coefficient). A continuous-flow RB4 decolorization assay was performed using a 32 cm long \times 4.8 cm I.D. glass column with adjustable column length adapters (column B; Kimble/Kontes). Column end caps, valves, and tubing were made of polypropylene and a variable speed (1 to 100 rpm) peristaltic pump (MasterFlex) was used to pump the solution through the columns in an up-flow mode to prevent gas entrainment. Figures 6.1 and 6.2 show schematic representations of the two columns used in this study. Column B was equipped with 5 lateral ports (capped with Mininert valves) at 2.8, 8.5, 16.3, 23.3 and 30.0 cm from the inlet. A stainless steel needle (19 inch; Popper & Sons) was placed in each sampling port, pushed till the center of the column and was connected to a 3-way stopcock with luer.

Sand (ASTM 20/30 Ottawa, IL) was first sterilized and then 2000 g were placed into a 5-L Pyrex glass drying dish and covered with 1M HCl solution for 30 min. The sand was then rinsed with D.I. water several times. Small amounts of sand were then placed in a 20/30/100-mesh sieve stack and D.I. water was run over sand until the wasted water had the same pH value as the D.I. water. The sand was placed back into the drying dish, covered with D.I. water and rinsed several times. After the excess water was drained, the sand was placed in an oven at 130°C for 3 h, then at 200°C for 2 h and then at 100°C for 3 h. The sand was autoclaved in a drying Pyrex dish for 30 min (15 psi, 121°C) and

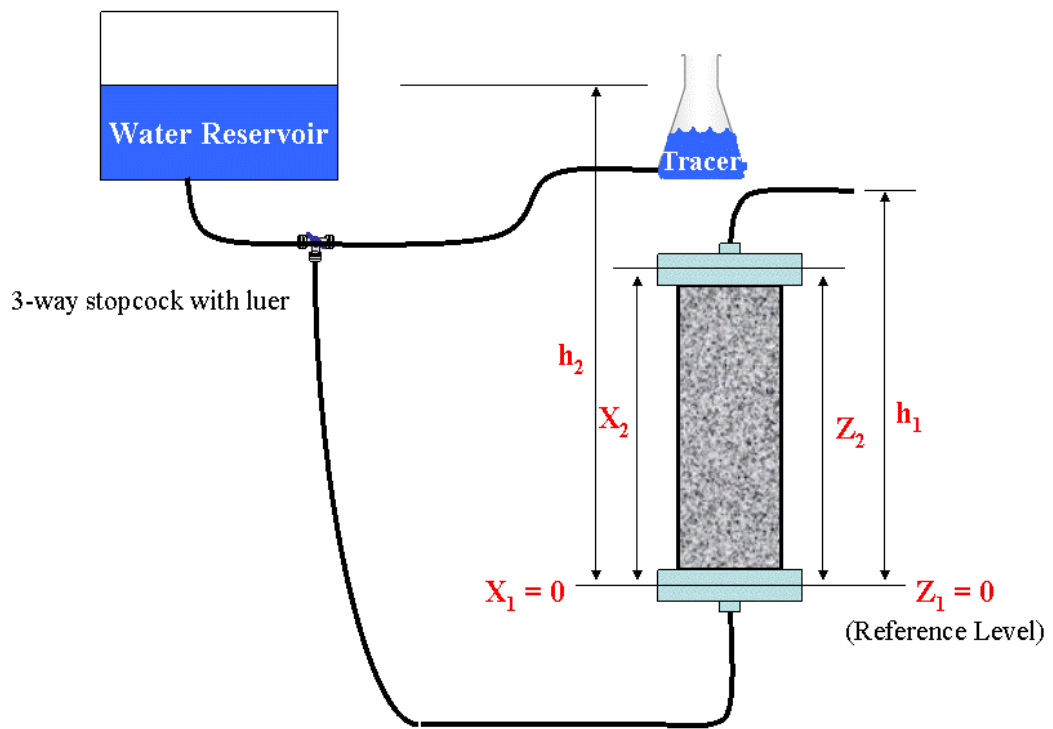


Figure 6.1. Schematic of the ZVI column A used for the hydraulic conductivity test.

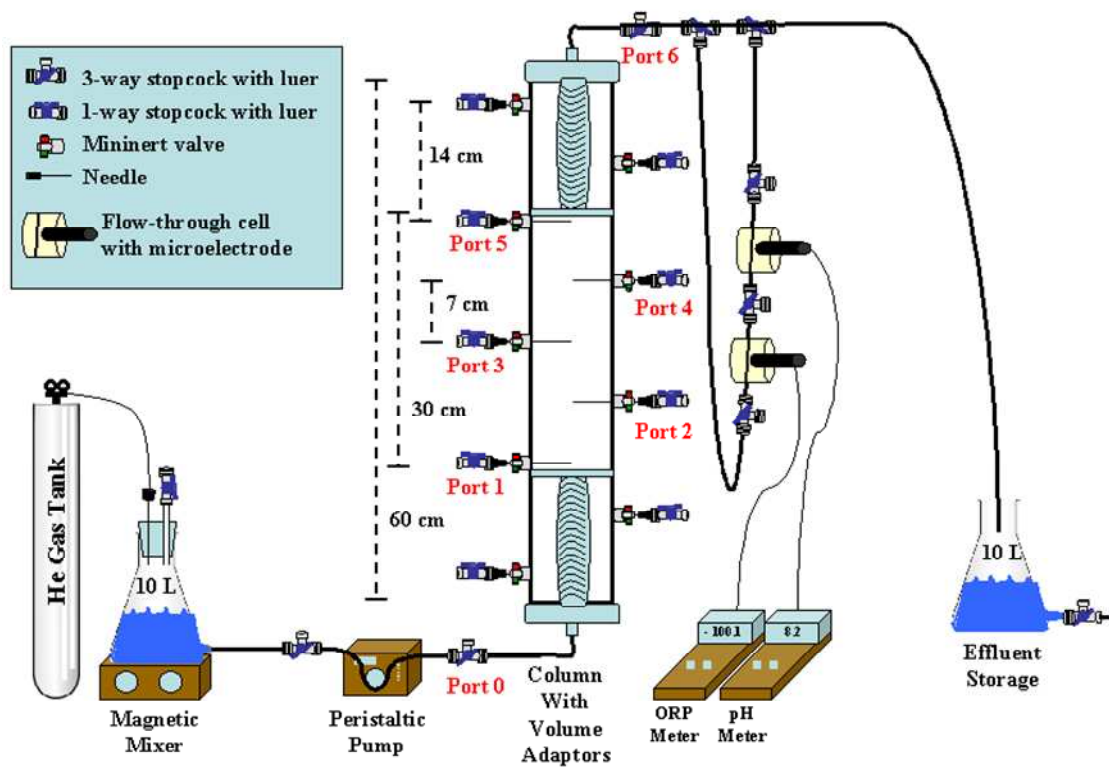


Figure 6.2. Schematic of column B set up used for the long-term continuous-flow ZVI RB4 decolorization (Epolito, 2005b).

kept in an oven at 100°C overnight. After cooled to room temperature, the sand was covered with an aluminum foil and stored until used (within 2 weeks).

Both columns were packed with sonicated/methanol treated iron fillings (Connelly, Chicago, IL) and treated sand (ASTM 20/30) at a ratio of 50:50 (by weight) to improve column longevity and permeability. Samples of 50 g of iron and 50 g sand were mixed thoroughly, the mixture was poured into the columns and tapped gently to form uniform layers until a predetermined column depth was reached. The total weight of iron/sand mixture was 542.2 and 1151.0 g respectively (271.5 and 575.5 g of iron) for column A and B. All experiments were performed under anoxic conditions at 23°C. Details on each column assay are described below.

6.2.1 Column Characterization

Sieve analysis of both iron and sand was first undertaken and then the following column parameters were determined: porosity (n), hydraulic conductivity (K), and intrinsic permeability (k). Tracer tests were performed using KI and KBr in order to determine seepage velocity (or pore water velocity, v) and dispersion coefficient (D) of the column. These experiments were conducted based on procedures described in the AEESP laboratory manual (Stapleton and Mihelcic, 2001).

The sieve analysis was carried out separately for iron and sand, and then the data were combined for further analysis. Each sieve (ASTM #10, #14, #20, #30, #40, #60, #100, and pan) was weighed and then 300.0 g of either iron or sand were applied to the sieve stack. Each sieve was shaken by hand for at least 10 min. The amount of iron or sand retained on each sieve was gravimetrically determined. The d_{10} (diameter where

10% is finer) and d_{60} (diameter where 60% is finer) were determined by plotting the semi-log grain size distribution curve (log grain size versus % finer). The uniformity coefficient (C_u) was calculated according to the following equation:

$$C_u = \frac{d_{60}}{d_{10}} \quad (6-1)$$

where: C_u = uniformity coefficient (or coefficient of uniformity); d_{10} = diameter where 10% is finer (mm); d_{60} = diameter where 60% is finer (mm).

The column porosity was calculated by two different methods: (1) dry method, and (2) wet method. For the dry method, the iron/sand density was calculated using the following equation:

$$n = 1 - \frac{\rho_b}{\rho_s} \quad (6-2)$$

where: n = porosity; ρ_b = bulk density (g/cm^3); ρ_s = solids density (g/cm^3).

The dry weight of each empty column and tubing was measured (W). After packing with iron/sand, the dry weight of each filled column plus the tubing was measured (W_s), and then the bulk density of iron/sand (ρ_b) was calculated using the following equation:

$$\rho_b = \frac{W_s - W}{V_t} \quad (6-3)$$

where: ρ_b = bulk density (g/cm^3); W_s = dry weight of filled column and tubing (g); W = dry weight of empty column and tubing (g); V_t = internal column bed volume (cm^3).

Based on the bulk density of the iron/sand mixture ($\rho_s = 3.833 \text{ g/cm}^3$) and equation 6-2, the column porosity was determined. The pore volume (V_{PV}) of each column was also determined by the following equation:

$$V_{PV} = n V_t \quad (6-4)$$

where: V_{PV} = pore volume (cm^3); n = porosity; V_t = internal column bed volume (cm^3).

The wet method for the determination of porosity was also used and compared to the dry method. After packing with iron/sand, the columns were weighed and autoclaved/deoxygenated D.I. water was pumped through the columns at a flow rate of 1 ml/min. In order to remove any air bubbles, each column was shaken using an electric vibrator and the water flow continued for at least 40 pore volumes (based on the dry method porosity). After the column bed was fully water saturated, the weight of each column was measured and the pore volume was determined through the weight of water in the columns. The porosity and pore volume of each column based on these two methods were compared and the pore volume based on the wet method was used for further data analysis.

Column A was used to determine the hydraulic conductivity (K) and the intrinsic permeability (k) of the iron/sand bed. Figure 6.1 shows the overall hydraulic conductivity test cell (column A). Each water head (H) was determined according to:

$$H = h + Z \quad (6-5)$$

where: H = water head (cm); h = water height outside the column; Z = elevation above a reference level (Figure 6.1)

The hydrostatic pressure acting on the iron/sand in the column was determined as the difference between the two water heads, as follows:

$$\Delta H = H_2 - H_1 \quad (6-6)$$

The hydraulic conductivity (K , cm/min) was calculated using the following equation:

$$Q = -K A \frac{\Delta H}{\Delta X} \quad (6-7)$$

where: A = column cross-section area (cm^2); ΔH = difference between the two water heads (cm); ΔX = column length (cm); Q = water flow rate (cm^3/min) ($\Delta H/\Delta X$ = hydraulic gradient).

Before conducting this experiment, the column was fully saturated with autoclaved/deoxygenated D.I. water. Then, 1 L of 0.33 mM CaCl_2 deoxygenated solution was prepared and let flow through the column at a fixed ΔX (15 cm) for at least 20 pore volumes or until consecutive flow rates were within 0.5 mL/min. At selected ΔH (3, 6, 10, 12, and 15 cm), the flow rates were measured based on water weight (volume was more than 30 mL) 5 times after flow rates were allowed to stabilize. The discharge rates ($q = Q/A$) were determined and then the hydraulic conductivity was calculated. Also, the Reynolds number (R_e) was calculated at each flow rate using the following expression:

$$R_e = \frac{\rho q d_{50}}{\mu} \quad (6-8)$$

where: μ = water viscosity (poise = g/s-cm); ρ = water density (g/cm^3); q = Darcy's velocity or discharge velocity ($= Q/A$, cm^3/s); d_{50} = mean iron/sand diameter (cm). The water density (ρ) and viscosity (μ) at 23°C used to determine the Reynolds number in this experiment are 0.997542 (g/cm^3) and 0.009316 (g/s-cm), respectively (Stapleton and Mihelcic, 2001).

The intrinsic permeability (k , cm^2) of iron/sand column was also calculated using the following equation:

$$k = \frac{K \mu}{\rho g} \quad (6-9)$$

where: μ = water viscosity (poise = g/s-cm); ρ = water density (g/cm^3); g = gravitation constant (981 cm/s^2).

Two of the most important transport parameters of the column, the pore water velocity (v) and dispersion coefficient (D) were determined by KI and KBr conservative tracer tests and use of the CXTFIT 2.0 program which provides analytical solutions for one-dimensional transport models based on the convection-dispersion equation (CDE) (Toride et al., 1995). Assuming steady-state flow in a homogeneous iron/sand mixture and first-order reaction kinetics, the CDE equation can be written as follows:

$$\frac{\partial C}{\partial t} + \frac{\rho}{\theta} \frac{\partial S}{\partial t} = D \frac{\partial^2 C}{\partial x^2} - v \frac{\partial C}{\partial x} - k_r C \quad (6-10)$$

where: t = time (min); x = depth (cm); ρ = bulk density (g/cm^3); θ = volumetric water content (cm^3/cm^3); C = the concentration of the liquid phase (mg/L); S = the concentration of the adsorbed phase (mg/kg); v = the average pore velocity (cm/min); D = the hydrodynamic dispersion coefficient (cm^2/min); and k_r = the first-order decay coefficient for degradation in the liquid phase (min^{-1}).

Based on equilibrium assumptions about S , the convection-dispersion equilibrium model assumes local equilibrium (LEA) for solute adsorption and that sorption can be described by a single linear isotherm:

$$S = K_d C \quad (6-11)$$

where: S and C are the concentrations in adsorbed and liquid phases at equilibrium; and K_d is the equilibrium partition coefficient (L/kg). Substituting equation 6-11 into equation 6-10, the CDE can be expressed as

$$R \frac{\partial C}{\partial t} = D \frac{\partial^2 C}{\partial x^2} - v \frac{\partial C}{\partial x} - k_r C \quad (6-12)$$

where: R = retardation factor = $1 + (\rho/\theta)K_d$

In the case of sorption-related transport, R is greater than 1.0. In the absence of any sorption, R is set equal to 1.0. The column transport parameters were evaluated based on the above equation without decay (i.e., $k_r = 0$) and the breakthrough curves (BTCs) constructed based on the data of the two tracers (KI and KBr). Column B was selected for the tracer tests, because this column was also used in a subsequent RB4 decolorization assay. For the KI tracer test, 2 L of 0.33 mM CaCl_2 deoxygenated solution and 2 L of 0.2 mM KI deoxygenated solution were prepared and used as the blank and tracer solution, respectively. The initial concentration of the KI solution and the CaCl_2 blank solution were measured at 225 nm using quartz cuvettes. Also, 50 marked 20-mL scintillation vials were prepared and weighed empty. First, the CaCl_2 blank solution was pumped through the column at a flow rate of 10 ml/min for 10 min, and then the solution was switched to the KI tracer solution which was pumped at the same flow rate for 1.5 pore volumes. At the same time, column effluent samples were collected in scintillation vials, and their weight and time were recorded in order to verify the solution flow rate. After 1.5 pore volumes of tracer solution had been pumped through the column, the CaCl_2 blank solution was fed to the column for at least 5 pore volumes and the sample absorbance was measured. For the KBr tracer test, 2 L of 0.2 mM KBr deoxygenated solution was prepared. This tracer test was performed as the above described KI tracer test, and the collected samples were analyzed using ion chromatography (IC). Based on the data, breakthrough curves were constructed, and the pore water velocity (v) and the dispersion coefficient (D) were determined using the CXTFIT 2.0 program. The retardation factor (R) was also estimated. The mass balance of bromide was also evaluated in order to determine whether a chemical reaction occurred or not.

6.2.2 Continuous-flow ZVI RB4 Decolorization

For the continuous ZVI RB4 decolorization, column B was set up and operated (Figure 6.2). The concentration and conditions of the RB4 stock solution for this experiment represented typical reactive dyebath conditions. The salt and base solution (100 g/L NaCl, 3 g/L Na₂CO₃ and 1 g/L NaOH) was prepared with autoclaved D.I. water and its pH was adjusted to 7.0. The dye concentration in the stock solution was 1000 mg/L and was prepared by the addition of reacted RB4 in the salt and base solution which was previously purged with He gas to remove all dissolved oxygen (DO < 1.0 mg/L). The dye stock solution reservoir was kept under a He gas atmosphere at 5 psig in order to maintain a constant head pressure and anoxic conditions. The column and dye stock solution reservoir were wrapped with black plastic to prevent any light exposure. Flow-through pH and oxidation-reduction potential (ORP) electrodes were connected at the column effluent line and both the pH and ORP values were recorded periodically.

Before the decolorization assay, the column was slowly purged with He gas to remove any oxygen from the column bed, and then was slowly saturated with autoclaved/deoxygenated D.I. water at a flow rate of 1.0 ml/min for 10 pore volumes. After full saturation, the column was fed with the dye stock solution (1,000 mg/L RB4). The flow rate of the stock solution was set at 1.0 ml/min, was periodically measured by collecting the effluent (port 6: 32 cm) of the column and, if necessary, the pump speed was adjusted to maintain the 1.0 mL/min flow rate. The RB4 concentration was measured periodically at each column sampling port. At each sampling time, 1-ml samples were collected from each column port using a syringe and the UV/Visible absorbance, pH, and ORP were measured and recorded. All samples were collected at rates not exceeding that

of column flow rate (i.e., 1-mL samples were collected for more than 1 min). Each sample was diluted if needed with a salt and base solution (100 g/L NaCl, 3 g/L Na₂CO₃, and 1 g/L NaOH) in 1.5 ml cuvettes. Samples used for absorbance measurements were first centrifuged at 14,000 rpm for 15 min.

6.3 Results and Discussion

6.3.1 Column Characterization

Two columns (A and B) were set up (Figure 6.1 and 6.2). Figure 6.3 shows the grain size distribution of iron, sand, and iron/sand mixture based on the sieve analysis. Based on the semi-log grain size distribution curve as shown in Figure 6.3 and equation 6-1, the following estimates were obtained: $d_{60} = 1.04$ mm, $d_{10} = 0.51$ mm and $C_u = 2.04$ for iron; $d_{60} = 0.76$ mm, $d_{10} = 0.62$ mm and $C_u = 0.82$ for sand; and $d_{60} = 0.80$ mm, $d_{10} = 0.60$ mm and $C_u = 1.33$ for the iron/sand mixture. The uniformity coefficient (C_u) of sand was much smaller than that of iron. Based on the d_{50} value of the iron/sand mixture, the Reynolds number (R_e) was evaluated using column A and equation 6-8 at each flow rate and data are shown in Table 6.1. At flow rates less than 2.2 cm³/min, relatively low Reynolds numbers ($R_e < 1.0$) were observed. Thus, at these flow rates, the flow was laminar. For the long-term decolorization assay, the column flow rate was set at 1mL/min (see Section 6.3.2).

The results of column characterization are shown in Table 6.2. The column porosity (n) was practically the same for both the dry and wet method. Pore volumes were calculated, but the wet pore volume estimate (136.6 and 270.5 cm³ for column A and B, respectively) was used for further data analysis. The hydraulic conductivity (K) of

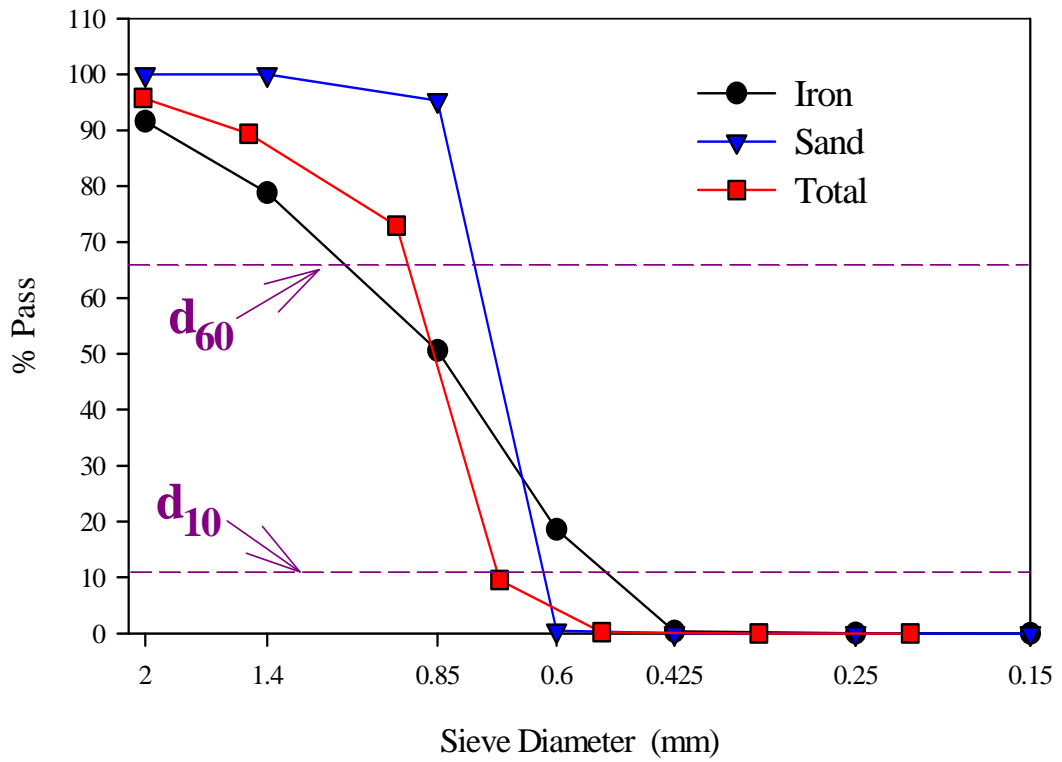


Figure 6.3. Grain size distribution of iron, sand, and iron/sand mixture (d_{10} = diameter where 10% is finer; d_{60} = diameter where 60% is finer).

Table 6.1. Calculated Reynolds numbers for column A at 23°C as a function of flow rate^a

Flow rate (cm ³ /min)	Discharge Velocity (q = Q/V, cm/sec)	Reynolds number (Re)
1.15 ± 0.03 ^b	0.063 ± 0.002	0.505 ± 0.014
2.17 ± 0.08	0.120 ± 0.004	0.954 ± 0.035
4.10 ± 0.09	0.226 ± 0.005	1.799 ± 0.039
5.54 ± 0.17	0.306 ± 0.009	2.435 ± 0.073
8.02 ± 0.18	0.443 ± 0.010	3.525 ± 0.081

^a Density of water (ρ) = 0.99754 (g/cm³); d_{50} = 0.076 cm; Viscosity of water (μ) = 0.009532 (g/sec-cm)

^b Mean ± standard deviation

Table 6.2. Characteristics of the two iron/sand columns used in this study

Parameters	Column A	Column B	
Bed Length (L, cm)	15	32	
Inner Diameter (I.D., cm)	4.8	4.8	
Cross-section Area (A, cm ²)	18.1	18.1	
Bed Volume (V _t , cm ³)	271.4	583.0	
Total weight of packed iron/sand (g)	542.2 ^a	1151.0 ^a	
Porosity (n)	Dry method	0.479	0.485
	Wet method	0.496	0.464
Pore Volume (cm ³)	Dry method	130.0	282.8
	Wet method	136.6	270.5
Hydraulic Conductivity (K, cm/min) ^b	0.468 ± 0.048 ^c		
Intrinsic permeability (k, cm ²) ^b	7.60E-8 ± 7.8E-9 ^c		

^a A ratio of 50:50 iron/sand mixture by weight

^b Measured for only column A, and assumed to be the same for column B

^c Mean ± standard deviation

column B was determined from the slope value of a line obtained by linear regression based on Darcy's law (see equation 6-7 and Figure 6.4). The intrinsic permeability was then calculated using equation 6-9. The hydraulic conductivity and intrinsic permeability of column B were 0.468 ± 0.048 cm/min (mean \pm standard error) and $7.60\text{E-}8 \pm 7.80\text{E-}9$ cm² (mean \pm standard error), respectively. These values were assumed to be the same for column B because the same ratio of iron/sand and the same column preparation procedure was used, except column B was longer than column A.

As discussed above, the CXTFIT 2.0 program was used to fit KI and KBr measured normalized concentrations (i.e., C/C_0) versus cumulative pore volume data. Figure 6.5 shows the curve fitting results of BTCs based on the tracer analysis. Both tracer tests conducted at a flow rate of 10 mL/min had asymmetric shapes and extended tailing, indicating non-ideal transport (Hu and Brusseau, 1995; Zhang et al., 2004). Each data fit based on the CXTFIT 2.0 program correctly described the extended tailing, but it failed to describe the asymmetric tracer concentration peak. Each fit resulted in R^2 values greater than 0.89. Estimates of the pore water velocity (v) and dispersion coefficient (D) are listed in Table 6.3. The pore water velocities were underestimated compared to the measured velocities, which is due to the asymmetric tracer concentration peak. Relatively high estimated D values were observed at 10 mL/min. Several studies have shown that D is directly proportional to v (Hu and Brusseau, 1995; Beigel and Pietro, 1999). Although these tracers are conservative, the effluent tracer peak concentration was lower than the expected concentration of $C/C_0 = 1.0$). Concentration peaks at a lower value of $C/C_0 = 0.6$ were obtained after the elution of 2.2 pore volumes. Observations such as asymmetric shapes, extended tailings, and low tracer concentration peaks, can be possibly explained

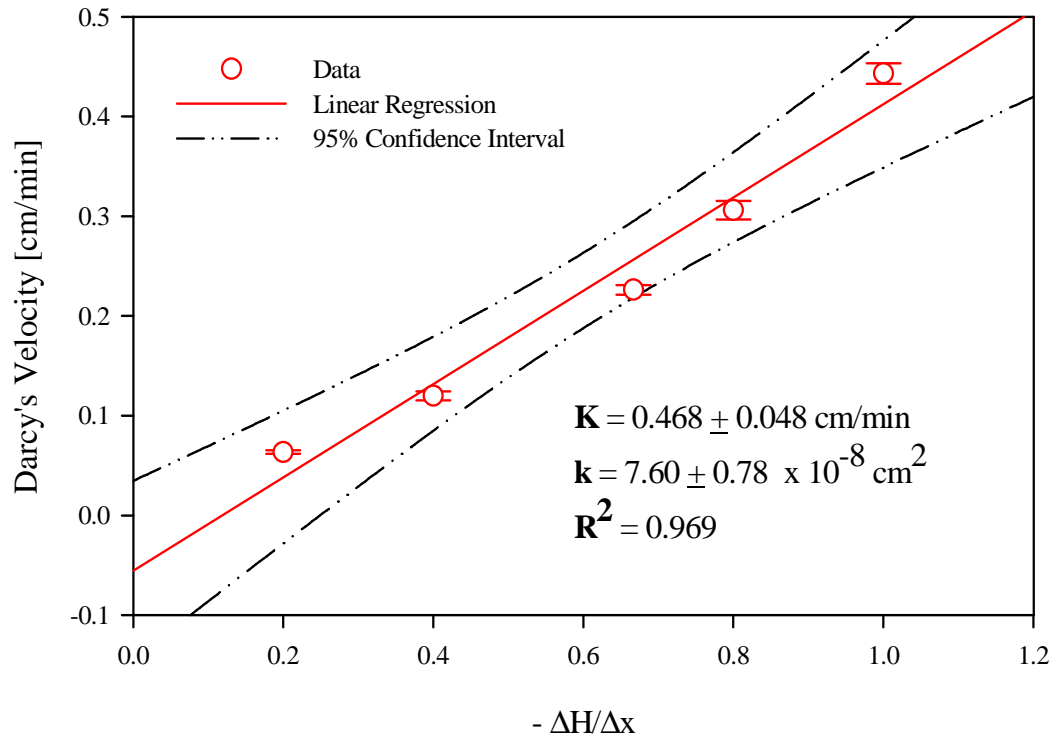


Figure 6.4. Darcy's velocity versus hydraulic gradient according to equation 6-7 for the determination of the hydraulic conductivity and intrinsic permeability of column A at 23°C (Error bars represent \pm one standard error).

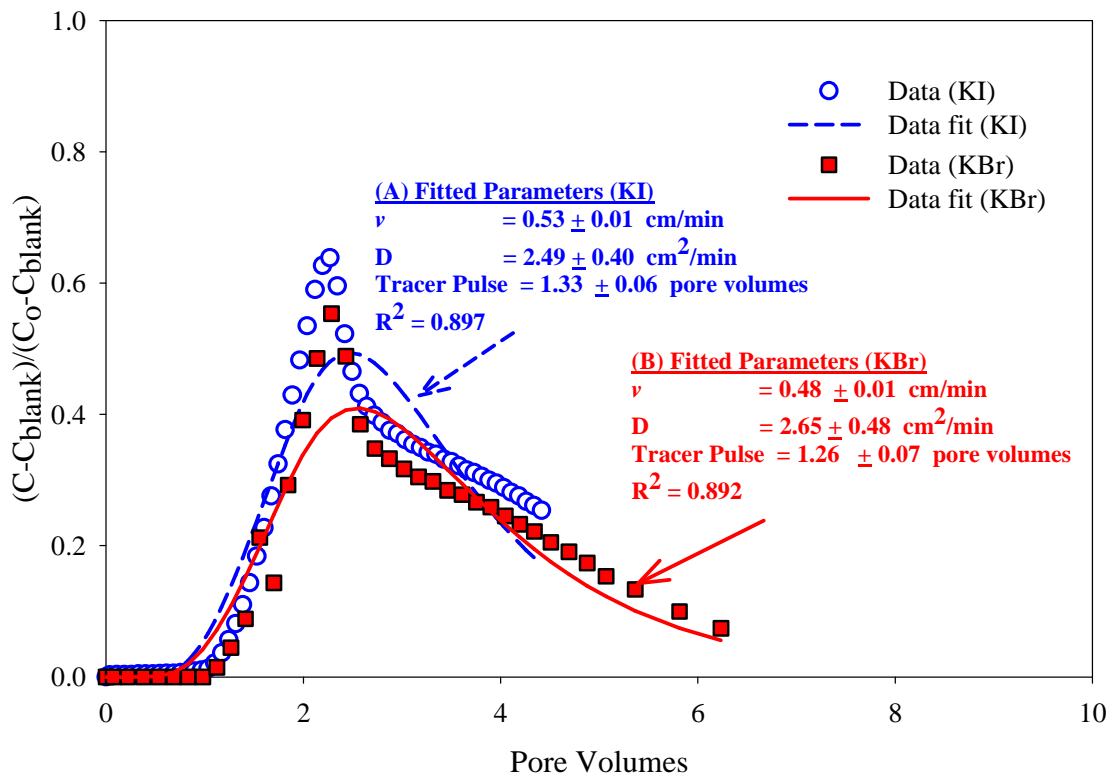


Figure 6.5. Experimental data and model fitted breakthrough curves for the KI and KBr tracers at a flow rate of 10 mL/min (Data fit based on the CXTFIT 2.0 program).

Table 6.3. Experimental and estimated transport parameter values for column B at 23°C

Tracers	Experimental values	Estimated values ^a		
	Water pore velocity (v , cm/min) ^b	Water pore velocity (v , cm/min)	Dispersion coefficient (D , cm ² /min)	R^2
KI	1.15	0.53 ± 0.01^c	2.49 ± 0.40^c	0.897
KBr	1.12	0.48 ± 0.01^c	2.65 ± 0.48^c	0.892

^a Based on tracer tests and simulation using the CXTFIT 2.0 program (flow rate = 10 ml/min and $R = 1.0$)

^b Water pore velocity (cm/min) according to $v = Q/(n A)$

^c Estimated value \pm standard deviation

by (1) high dispersion coefficients due to relatively large size grain of the iron/sand mixture in the column, (2) non-homogeneous iron/sand mixture packing, and (3) sorption-related non-equilibrium transport. The grain size of iron/sand mixture was relatively larger than that of sand. Therefore, higher dispersion coefficients can be expected in the case of the iron/sand mixture. Also, the distribution of iron and sand in the column was not completely homogeneous due to density difference, which may explain the asymmetric shapes. The extended tailing suggests that it is primarily sorption related. Similar sorption/desorption-related non-equilibrium transport characteristics have been reported in homogeneous soil columns (Lee et al., 1988; Gaber et al., 1995; Beigel and Pietro 1999). The tracers can be adsorbed on the surface of iron/sand and result in extended tailing of the BTCs. In order to evaluate sorption-related transport, the retardation factor (R) was estimated using the CXTFIT 2.0 program. Based on the KI tracer BTC, the CXTFIT 2.0 program was unable to estimate an R value due to the termination of the experiment at 6.3 pore volumes prior to the observed extended tailing area. Similar results were observed with the KBr tracer BTC, in which case the R value was estimated as equal to 1.14. However, this estimate was not satisfactory as the standard deviation was much higher than the R value because of limited data points at the extended tailing area. To determine whether or not any chemical reaction (e.g., reduction of tracers) occurred in the column, bromide mass recovery, determined by trapezoidal integration of the areas under the BTC, resulted in 91.4% bromide recovery. The less than 100% bromide mass recovery is due to the fact that the tracer test was terminated at 6.3 pore volumes when the effluent bromide concentration was still around 7% of the input concentration. Based on the bromide mass recovery, it can be concluded that only

adsorption/desorption of tracers took place in the column, thus excluding the possibility of other chemical reactions.

The tracer analysis indicates non-ideal transport characteristics of column B. Many studies have shown that the CXTFIT 2.0 program provides a complete toolbox for fitting transport parameters, though it fails to give an exact solution for finite columns. As a result, systematic deviations between the measured and fitted breakthrough curves (BTCs) often occur (Toride et al., 1995; Beigel and Pietro 1999; Mojid et al., 2004). The fitted BTCs based on the CXTFIT 2.0 program were fairly reasonable, although they failed to predict the tracer concentration peak and underestimated the pore water velocity.

6.3.2 Long-term ZVI RB4 Decolorization Kinetics

This assay was conducted under anoxic conditions using column B, lasted for 85 days and used 122 L of reacted 1000 mg/L RB4 solution. The RB4 solution contained salt and base to simulate commercial spent reactive dyebaths and was pumped through the column at a flow rate of 1.0 mL/min. The initial dye solution pH was adjusted to 7.0. Table 6.4 shows the operational conditions of column B. Based on the pore volume (270.5 cm^3), the number of pore volumes (PV) was used for data analysis. Figure 6.6 shows the color changes during the continuous-flow decolorization of RB4. As can be seen the color starts as dark blue at the influent (port 0), then changes to light blue, then bluish-green and finally pale-yellow at the effluent (port 6), respectively. The column effluent pH values increased throughout the assay and the ORP values were almost constant around -550mV (see Table 6.5). Figure 6.7 shows the absorbance-based RB4 concentration at each sampling port as a function of pore volumes. The RB4

Table 6.4. Operational conditions of column B used for the continuous-flow ZVI RB4 decolorization assay^a

Operational conditions	Sampling Port						
	X0	X1	X2	X3	X4	X5	X6
Height (cm)	0	2.8	8.5	16.3	23.3	30.0	32.0
Residence time (min) ^b	0	23.5	71.4	136.9	195.7	252.0	268.7
Flow rate (mL/min)	1.0						
Pore volume (cm ³) ^c	270.5						
Influent RB4 concentration (mg/L) ^d	1000						
Initial pH ^e	7.0						

^a At 23°C room temperature

^b Based on a flow rate of 1.0 mL/min

^c Conversions: 1 pore volume (PV) = 270.5 cm³ = 4.5 hours (based on 1.0 mL/min flow rate)

^d Reacted RB4 with salt and base solution

^e Influent RB4 stock solution reservoir



Figure 6.6. Color change during the continuous-flow decolorization assay at each sampling port [port 0 (0cm), port 1 (2.8cm), port 3 (16.3cm), port 4 (23.3cm), port 5 (30.0cm) and port 6 (32 cm)]. (A) 1.0 pore volume (4.5 hours); (B) 5.0 pore volumes (22.5 hours); (C) 100 pore volumes (19 days); (D) 200 pore volumes (38 days).

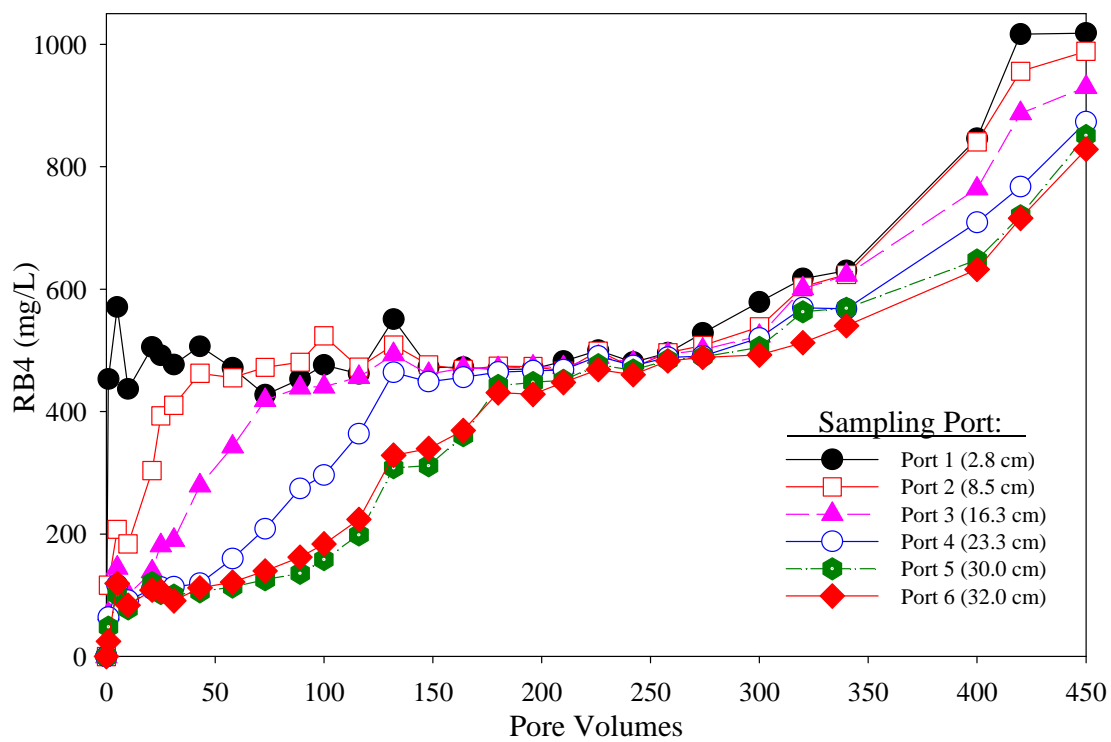


Figure 6.7. RB4 concentration as a function of pore volumes and column bed height (column B; 1.0 mL/min flow rate; 1000 mg/L influent RB4 concentration; 23°C ambient temperature).

concentration at each sampling port gradually increased, and then relatively constant concentrations (around 500 mg/L) were observed between 200 and 300 pore volumes (38 and 56 days). After that time, the RB4 concentration in all six sampling ports increased significantly and the column effluent RB4 concentration reached 800 mg/L after 450 pore volumes (84 days). Such breakthrough curves may be the result of porosity losses due to (1) RB4 aggregation and deposition on the ZVI surface, and/or (2) formation of iron precipitates in the column. Similar trends have been observed with several column experiments (MacKenzie et al., 1999; Gu et al., 1999; Yausaki et al., 2001; Westerhoff and Janmes, 2003). MacKenzie and co-workers (1999) suggested that $\text{Fe}(\text{OH})_2$, FeCO_3 , and CaCO_3 in highly carbonated waters would contribute to porosity losses. Formation of precipitates can then lead to significant changes in the pore water velocity, which in turn affects reaction kinetics during the long-term column operation. Decolorization rates were calculated based on the RB4 concentration data at each sampling port using either a pseudo first-order rate equation (for 1 and 100 pore volumes) or a zero-order equation (for 400 and 450 pore volumes)(Table 6.5). Based on these results, it appears that the RB4 decolorization transitioned from pseudo first-order to zero-order kinetics during the long-term column operation (Figure 6.8). Such shift in reaction rate order can be explained by the saturation of reactive ZVI surface sites. Several studies on ZVI treatment have used a site saturation model to describe the shift of rate order at higher solute concentration (Johnson et al., 1996; Nam and Tratnyek, 2000; Agrawal et al, 2002). However, the data fit based on the site saturation model (equation 5-5) was very poor because of limited data points. Figure 6.9 shows that as the pore volumes increased the observed decolorization rate constants (k_{obs} , h^{-1}) decreased as expected. However, the

Table 6.5. Results of the long-term, continuous-flow ZVI RB4 decolorization using column B at 23°C

Pore Volumes ^a	pH ^b	ORP (mV)	k _{obs} ^c		R ² Value	Extent of Decolorization (%) ^d
			First-order (h ⁻¹)	Zero-order (mg/L-h)		
1.0	9.3	-154	1.892 ± 0.223		0.987	97.5
5.0	7.7	-538	1.127 ± 0.238		0.942	88.1
25.0	8.1	-562	0.836 ± 0.195		0.918	89.4
58.0	8.2	-548	0.506 ± 0.130		0.863	87.9
100.0	8.2	-535	0.351 ± 0.097		0.801	81.6
200.0	8.1	-572		N/A ^e	N/A ^e	55.3
300.0	8.2	-583		N/A ^e	N/A ^e	50.7
400.0	7.9	-554		0.069 ± 0.009	0.917	36.8
450.0	7.9	-565		0.042 ± 0.003	0.968	17.1

^a Conversions: 1 Pore Volume = 270.5 cm³ = 4.5 hours based on 1.0 mL/min

^b Measured in column effluent samples

^c Mean ± standard error

^d Based on the column effluent RB4 concentration (measured at sampling port X6)

^e Not available

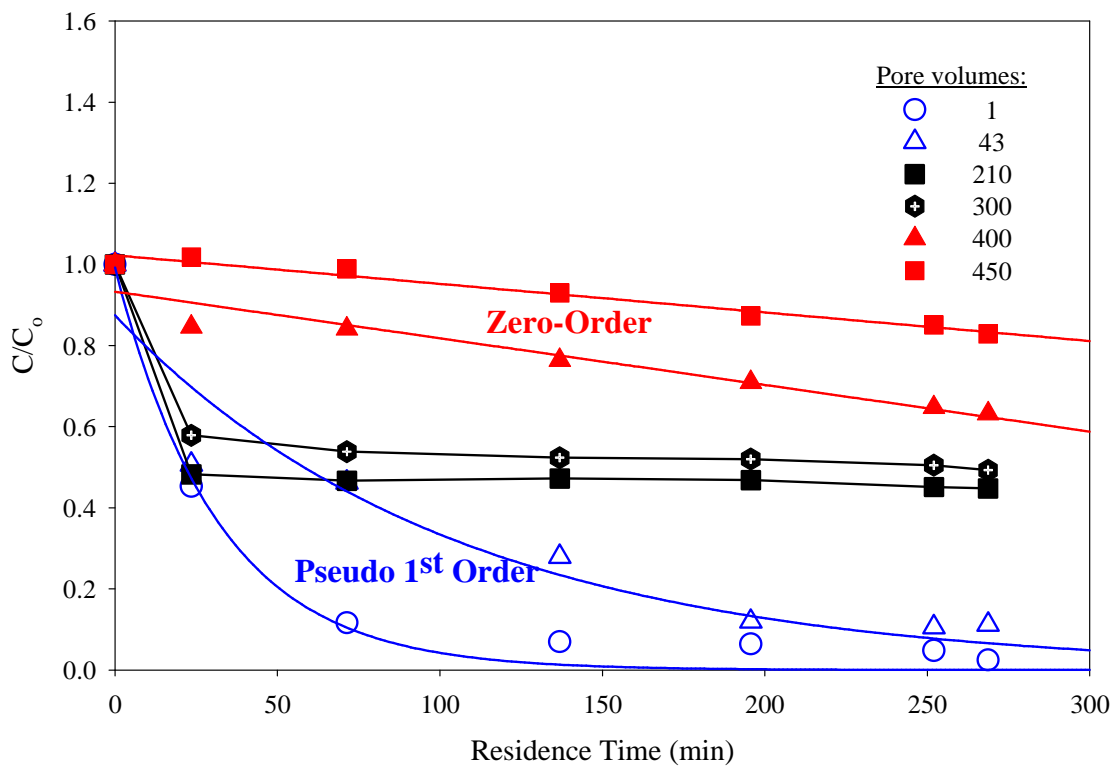


Figure 6.8. RB4 decolorization kinetics by a continuous-flow ZVI column (1.0 mL/min flow rate; 1000 mg/L influent RB4 concentration; 23°C ambient temperature).

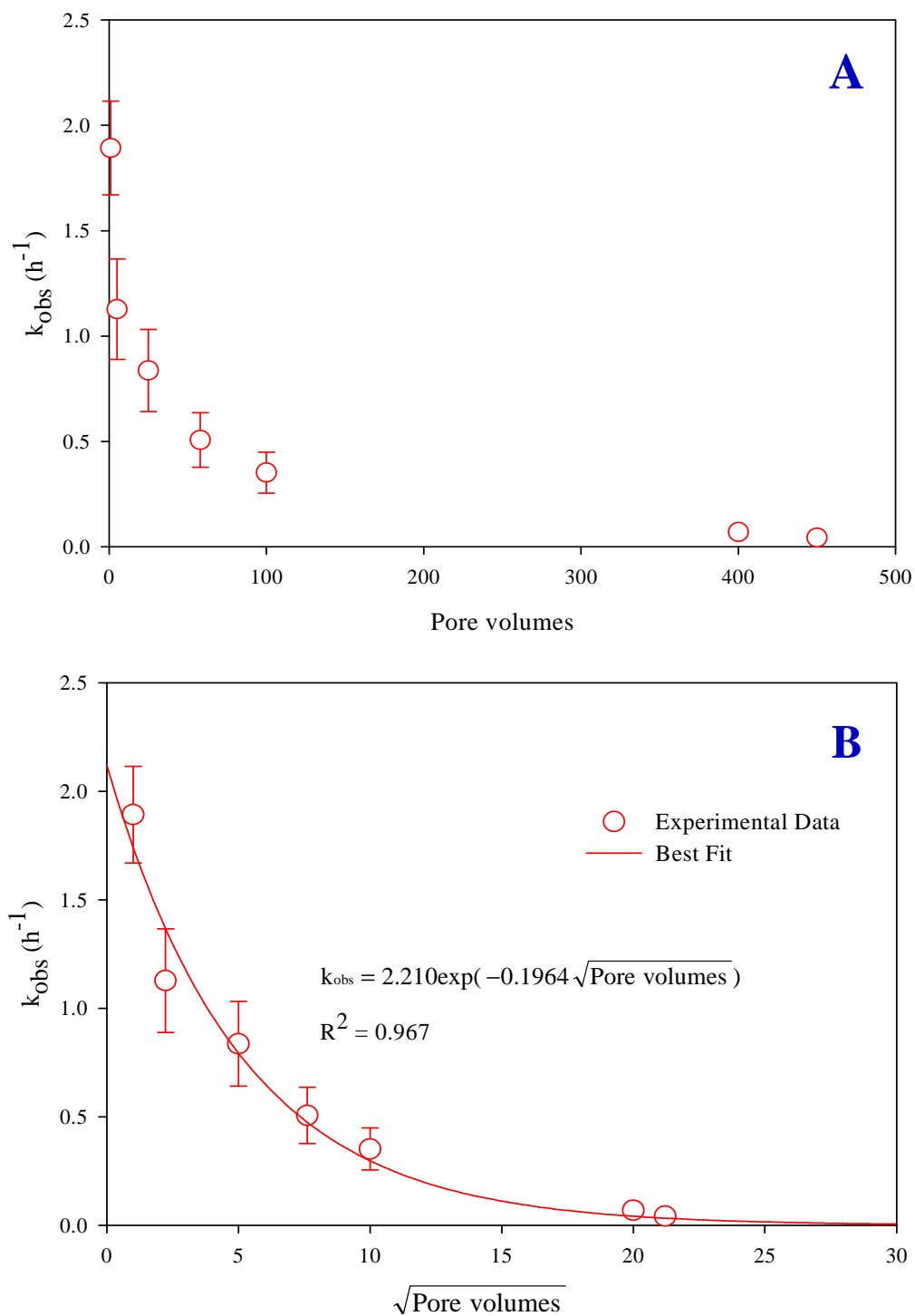


Figure 6.9. Effect of long-term continuous-flow decolorization kinetics of reacted RB4 (1000 mg/L with salt and base solution) on the decolorization rate constant; A) experimental data based on absorbance at 598 nm, and B) data fit with non-linear regression fit based on a first-order model (Error bars represent \pm one standard error of the mean).

data were non-linear with respect to the square root of the pore volumes, and appear to be best fit by an exponential function. This observation can be explained due to the fact that each component of RB4 has a different rate constant and due to ZVI surface sites were heterogeneously saturated due to non-ideal transport characteristics of the column.

To determine the decolorization capacity of column B, the following bed depth service time (BDST) model was used (Hutchins, 1973; Faust and Aly 1987):

$$T_b = \frac{N_o Z}{C_o v} - \frac{1}{k_r C_o} \ln \left(\frac{C_o}{C_b} - 1 \right) \quad (6-11)$$

where: T_b = time required for the effluent to reach the breakthrough concentration (h); N_o = average decolorization capacity per volume of column bed (mg dye/cm³); Z = bed depth (cm); C_o = column influent dye concentration (mg/L); v = linear flow rate through the bed = Q/A (cm/h); k_r = decolorization rate constant (L/mg-h); C_b = allowable effluent dye concentration at breakthrough point (mg/L).

The BDST model has been successfully used in describing and predicting the performance of columns (McKay et al., 1984; Walker et al., 1997; Marlovska et al., 2001; Netpradit et al., 2003). At 50% breakthrough or $C/C_o = 0.5$, $C_o/C_b = 2$, the logarithmic term in equation 6-11 becomes zero, reducing the BDST equation to the following relationship:

$$T_{50} = \frac{N_o Z}{C_o v} \quad (6-12)$$

where: T_{50} = time required for the effluent concentration to reach 50% (i.e., $C/C_o = 0.50$) breakthrough (h). A plot of the 50% breakthrough (T_{50}) data versus the column bed depth (Z) is shown in Figure 6.10. T_{50} increased with increasing column bed depth as expected. According to equation 6-12, and based on the slope value, the 50% decolorization

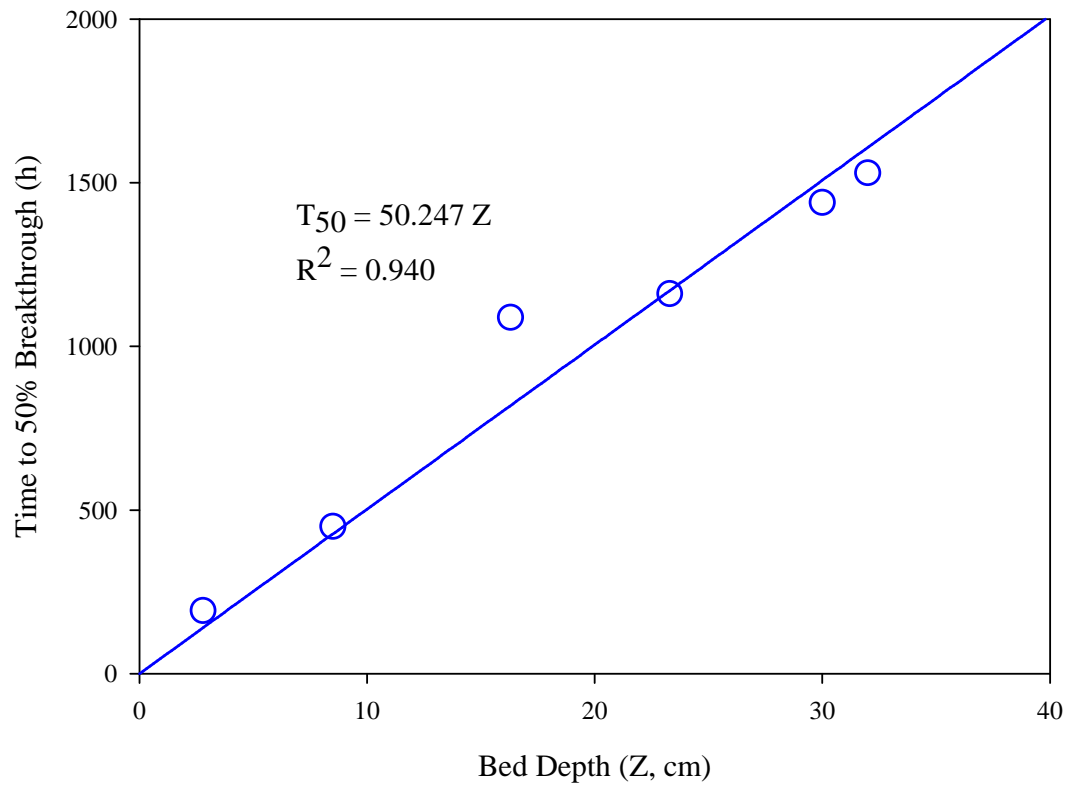


Figure 6.10. Bed depth service time (BDST) at 50% breakthrough for the decolorization of 1000 mg/L RB4 with salt and base by the ZVI column B as a function of column bed depth.

capacity of the ZVI column (N_0) was calculated to be 167.0 mg dye/cm³. Based on a total column bed depth of 32 cm and a pore volume of 270.5 cm³, column B can be operated with 1.0 mL/min for 67 days with a decolorization efficiency up to 50% and be able to treat a total volume of RB4 solution equal to 100 L without any regeneration.

6.4 Summary

Key parameters of the ZVI/sand column, such as porosity, pore volume, uniformity coefficient, hydraulic conductivity, and intrinsic permeability were evaluated. Based on KI and KBr tracer tests conducted at the flow rate 10 mL/min, asymmetric shapes and extended tailing of the breakthrough curves were observed, indicating non-ideal transport. Curve fitting of the data based on the convection-dispersion equation and using the CXTFIT 2.0 program correctly described the extended tailing, but failed to describe the asymmetric tracer concentration peak and underestimated the pore water velocity. Such non-ideal transport characteristics can be explained by (1) high dispersion coefficients due to the relatively large size grain of the iron/sand mixture, (2) non-homogeneous iron/sand mixture packing, and (3) sorption- and dye aggregation-related non-equilibrium transport.

The decolorization of RB4 was performed with a continuous-flow, ZVI column at typical reactive dyebath conditions (1 g/L dye, 4 g/L base and 100 g/L salt) in order to determine the feasibility of a long-term, continuous-flow, dyebath decolorization process. Based on the observed RB4 effluent concentration, 80% decolorization of RB4 was achieved for the first 110 pore volumes (21 days or 30 L of a 1000 mg/L RB4 solution). Porosity losses were observed after 300 pore volumes due to formation of iron

precipitates and/or dye aggregation, which resulted in an increase of pore water velocity and a shift of reaction kinetics from pseudo first-order to zero-order, which in turn may be attributed to saturation of reactive ZVI surface sites during the long-term operation of the column. The 50% decolorization capacity of the column, estimated from a bed depth service time plot, was equal to 6350 mg dye/cm³, which amounts to treatment of a total volume of dye solution equal to 100 L without any column regeneration. This information, based on the BDST model, can be used to scale up and design ZVI columns for the continuous-flow decolorization of anthraquinone-bearing reactive dyebaths.

CHAPTER 7

BIODEGRADATION ASSESSMENT OF RB4 DECOLORIZATION PRODUCTS IN A MIXED, AEROBIC HALOPHILIC CULTURE

7.1 Introduction

Although some research has been conducted on the reductive ZVI decolorization of azo dyes, followed by biomineralization of their decolorization products (Tan et al., 1999; Perey et al., 2002;), limited information exists on the reductive transformation (decolorization and mineralization) of reactive anthraquinone dyes and their decolorization products. Additionally, very limited research has been conducted on the decolorization of spent reactive dyebaths containing high concentrations of both dye and salt, typically present in spent reactive dyebaths (Lee, 2003; Epolito, 2004; Lee et al., 2005). This is mainly because typical anaerobic microbial communities (e.g., methanogens) cannot function at relatively high salt conditions (Fontenot et al., 2003). Lee (2003) investigated the decolorization of a spent Reactive Blue 19 (RB19) dyebath by a mixed halophilic culture under various conditions. The spent RB19 dyebath was not decolorized under aerobic conditions, whereas decolorization up to 87% was achieved under anoxic conditions. The research presented in this chapter was based on the hypothesis that ZVI reductive transformation of anthraquinone dyes may result in the formation dye decolorization products that are more amendable to biodegradation/biomineralization by a mixed, aerobic halophilic culture. RB4 decolorization products were prepared using a ZVI column with recycle, and then were

fed to a batch halophilic culture in order to assess the biodegradation/mineralization potential of the RB4 decolorization products.

The objectives of the work reported in this chapter were as follows: (1) evaluation of RB4 decolorization kinetics and regeneration of a ZVI column; (2) assessment of potential inhibitory effects of RB4 decolorization products on the halophilic culture; (3) assessment of possible biodegradation and biomineralization of the RB4 decolorization products under aerobic conditions using the halophilic culture.

7.2 Materials and Methods

7.2.1 ZVI Column

In order to generate RB4 decolorization products for the biodegradation assessment, a continuous-flow ZVI column (50 cm long \times 1.9 cm I.D.; Plexiglas) was constructed (Figure 7.1). Column valves and tubings were made of polypropylene and a variable speed (1 to 100 rpm) peristaltic pump (MasterFlex; Model 7523-30; Cole-Parmer) was used to pump the RB4 stock solution through the column in an up-flow mode to prevent gas entrainment. The column was packed with only sonicated/methanol treated iron filings (Connelly-GPM Inc., Chicago, IL) and operated with recycle to produce and collect a relatively large volume of decolorization products. The first 10 cm section of the column was packed with iron filings which passed through an ASTM 12-mesh stainless-steel sieve to obtain uniform flow and to prevent tubing clogging. Larger filings retained on the ASTM 12-mesh sieve were used to pack a 40-cm column section. The top 10 cm section of the column was then packed with smaller filings. The total weight of iron filings was 318.3 g. A 5-L dye stock solution was prepared at 1000 mg/L

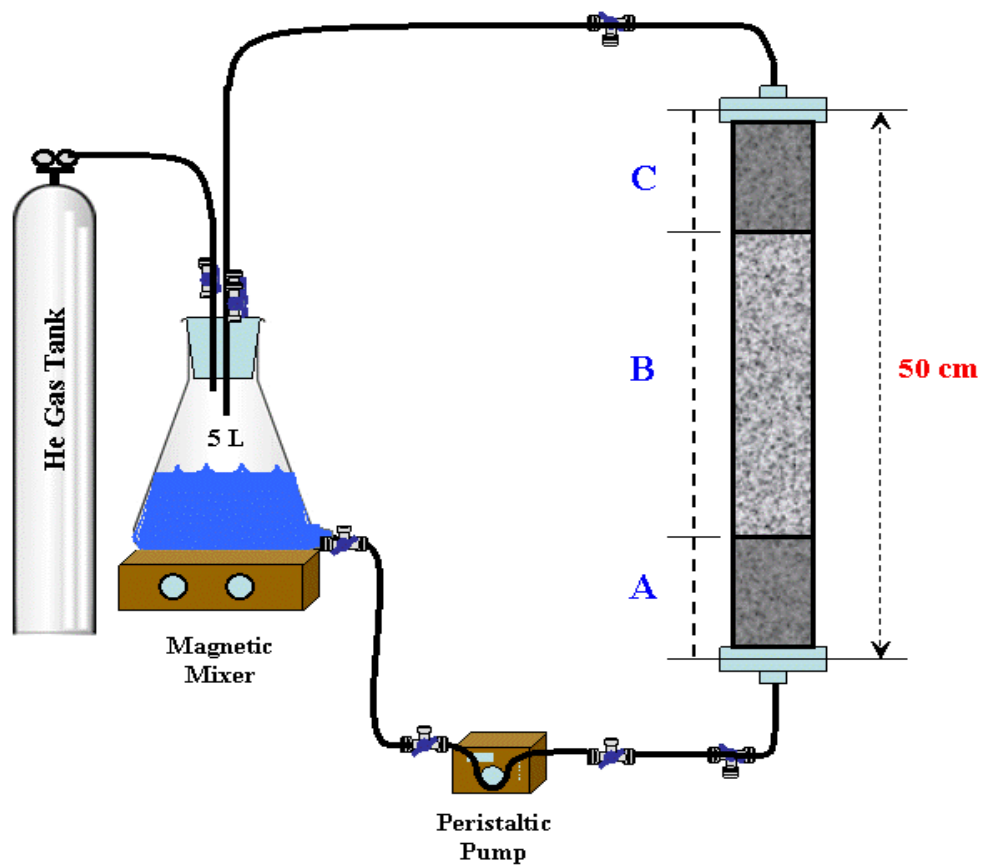


Figure 7.1. Schematic of the ZVI column used for the preparation of the RB4 decolorization products for the biodegradation assays [section A (10 cm), iron filings passed through the 12-mesh sieve; section B (30 cm), iron filings retained on the 12-mesh sieve; and section C (10 cm), iron filings passed through the 12-mesh sieve].

of reacted RB4 which represents typical dyebath conditions and was added to a glass dye reservoir. The dye stock solution reservoir was kept under a He gas atmosphere wrapped with a black plastic sheet to prevent any light exposure. The column pore volume was determined by pumping a known volume of the dye stock solution through the dry column at a very low flow rate and collecting the effluent; the difference in volume was taken to be the total column pore volume.

The ZVI column was operated under two different conditions (two runs). The first column run was conducted with a flow rate of 1.0 mL/min for the first 8 days, and then changed to a flow rate of 5.0 mL/min. UV/Visible absorbance and pH of the column influent and effluent were periodically measured. Column operation was stopped after 14 days. After regeneration of the column (see below), a second column run was conducted with a flow rate of 1.0 mL/min and was stopped after 3 days in order to achieve a relatively high concentration of RB4 decolorization products (based on absorbance at 485 nm). UV/Visible absorbance, dissolved organic carbon (DOC), and pH were measured at each sampling time. Samples used for absorbance measurements were first centrifuged at 14,000 rpm for 5 min. The RB4 decolorization products obtained with the two column runs were kept under a He gas atmosphere at 4°C until they were used for the biodegradation assay.

After each column decolorization run, column regeneration was used in order to reactivate the ZVI column, as follows. The column was first flushed with 6-L of deoxygenated D.I. water, and then flushed with 6-L of deoxygenated sulfuric acid (0.01 N H₂SO₄) at various flow rates (10~20 mL/min). The column was also tapped gently, if needed, during the regeneration. The column effluent during regeneration was collected

and a DOC mass balance was performed for the second regeneration. The column regeneration efficiency was assessed by comparing the dye decolorization kinetics before and after column regeneration.

7.2.2 Halophilic Stock Culture

A suspended-growth, halophilic, aerobic mixed culture was used in the present study. This culture was previously enriched from an anoxic sediment sample obtained from Mono Lake, California (Beydilli, 2001; Lee, 2003; Matthews, 2003). Mono Lake is alkaline and hypersaline with an average pH of 9.8 and salinity ranging from 75 to 90 g/L of NaCl (Oremland et al., 2000). Other researchers have isolated halophiles from the anoxic sediments of Mono Lake (Bum et al., 2001; Litchfield and Gillevet, 2002). The culture was maintained at 22°C under fully aerobic conditions and separately fed with glucose and a medium containing yeast extract, mineral salts, trace metals, vitamins as well as NaCl at 100 g/L. The composition of the stock halophilic culture media used in the development and maintenance of the culture is shown in Table 7.1 and the metal and vitamin stock composition can be found in Tables 7.2 and 7.3, respectively. The stock halophilic culture media did not contain any chemical reducing agent to avoid any abiotic dye reduction and color removal. The feeding media used for this culture contained 100 g/L NaCl, 0.02 g/L yeast extract, 6.6 g/L NaHCO₃ and 62.6 mL/L of the concentrated stock media.

The culture was transferred to a 9-L reactor (6-L liquid volume) where it was maintained on a 6-hour feeding cycle and aerated with compressed air delivered by a pressure/vacuum pump (Welch) passed through a water trap (to achieve air

Table 7.1. Composition of the halophilic stock culture media

Component	Concentration	Feeding Solution (16 × diluted)	Influent Concentration ^c
1. K ₂ HPO ₄	12.00 g/L	750 mg/L	600 mg/L
2. KH ₂ PO ₄	6.70 g/L	418.75 mg/L	335 mg/L
3. NH ₄ Cl	58.06 g/L	3628.75 mg/L	2900 mg/L
4. CaCl ₂ ·2H ₂ O	1.35 g/L	84.38 mg/L	67.5 mg/L
5. MgCl ₂ ·6H ₂ O	2.70 g/L	168.75 mg/L	135 mg/L
6. MgSO ₄ ·7H ₂ O	5.35 g/L	334.38 mg/L	267.5 mg/L
7. FeCl ₂ ·4H ₂ O	1.35 g/L	84.38 mg/L	67.5 mg/L
8. Tracer metals stock ^a	13.40 mL/L	837.5 mL/L	0.67 mL/L
9. Vitamin stock ^b	13.40 mL/L	837.5 mL/L	0.67 mL/L

^a Composition given in Table 7.2

^b Composition given in Table 7.3

^c Based on the total feed volume (i.e., glucose + media) per feeding

Table 7.2. Composition of the trace metal stock solution used in the preparation of the halophilic culture media^a

Component	Concentration (g/L)	Feeding Solution (16 × diluted) (mg/L)	Influent Concentration (mg/L) ^b
ZnCl ₂	0.50	31.25	25
MnCl ₂ ·4H ₂ O	0.30	18.75	15
H ₃ BO ₃	3.00	187.5	150
CoCl ₂ ·6H ₂ O	2.00	125	100
CuCl ₂ ·2H ₂ O	0.10	6.25	5
NiSO ₄ ·6H ₂ O	0.20	12.5	10
Na ₂ MoO ₄ ·2H ₂ O	0.30	18.75	15

^a Adopted from Wolin et al. (1963)

^b Based on the total feed volume (i.e., glucose + media) per feeding

Table 7.3. Composition of the vitamin stock solution used in the preparation of the halophilic culture media^a

Component	Concentration (g/L)	Feeding Solution (16 × diluted) (mg/L)	Influent ^b Concentration (mg/L)
Biotin	0.20	12.5	10
Folic Acid	0.20	12.5	10
Pyridoxine Hydrochloride	1.00	62.5	50
Riboflavin	0.50	31.25	25
Thiamine	0.50	31.25	25
Nicotinic Acid	0.50	31.25	25
Pantothenic Acid	0.50	31.25	25
Vitamin B12	0.01	0.625	0.5
p-Aminobenzoic Acid	0.50	31.25	25
Thioctic Acid	0.50	31.25	25

^a Adopted from Wolin et al. (1963), and Mah and Smith (1981)

^b Based on the total feed volume (i.e., glucose + media) per feeding

humidification) and a fine pore diffuser. The glucose feed solution and media were added separately via two peristaltic pumps (MasterFlex; Model 7523-30; Cole-Parmer) with the ON time controlled by a timer. The glucose feed solution (75 g/L glucose) was kept at 4°C to prevent spoilage due to microbial growth and added to the culture once every 6 hours at a rate of 30 mL/feeding (2.25 g glucose/feeding) resulting in a glucose organic loading rate of 1500 mg glucose/L-d. The culture media solution was added to the culture once every 6 hours at a rate of 120 mL/feeding. The culture was maintained with a 10-day hydraulic (and solids) retention time and liquid volume between 6 and 7.2 L by removing 1.2 L of culture every two days. This culture was maintained under this feeding protocol for 10 months. Routine stock culture monitoring included pH, dissolved oxygen (DO), volatile suspended solids (VSS), and dissolved organic carbon (DOC).

In order to determine the biological activity and specific decay rate constant (b , day^{-1}) of the culture, oxygen uptake rate (OUR) measurements were performed. Culture aliquots of 1 L were transferred to a 2-L glass reactor at the end of the 6-hour feeding cycle (i.e., just before culture feeding). The culture was aerated with pre-humidified compressed air passed through a fine-pore stone diffuser and was maintained without any feeding (i.e., under starvation). A magnetic stirrer provided continuous mixing of the culture. The OUR measurement was started a day later after transferred from the main reactor in order to confirm starvation conditions of the culture. After one day aeration, culture samples were then transferred from the 2-L reactor to a 300-mL BOD bottle. Then, an oxygen probe (YSI, model 5750; Yellow Springs, Ohio) was immediately inserted into the BOD bottle which contained a magnetic stirring bar. After the meter reading had stabilized, the initial DO was recorded and then monitored over time. The

OUR was determined from the slope of a plot of observed DO readings (mg/L) versus time (min) using linear regression. Several OUR measurements were conducted with the same culture under starvation over a period of 5 days. Each OUR measurement was carried out at 22°C. The VSS and DOC were also monitored in order to determine the specific oxygen uptake rate [SOUR, mg DO/g VSS - h]. The SOUR was calculated as follows:

$$\text{SOUR} = \frac{\text{OUR}}{\text{VSS}} \times \frac{60 \text{ min}}{\text{h}} \quad (7-1)$$

where: OUR = oxygen uptake rate (mg/L - min); VSS = volatile suspended solids (g/L). Under starvation conditions (i.e., substrate concentration ≈ 0), the net biomass growth can be described by the following equation:

$$\frac{dX_a}{dt} = -b X_a \quad (7-2)$$

where, X_a = active biomass concentration (mg VSS/L); b = specific death rate constant (d^{-1}). Due to the fact that OUR is proportional to X_a , equation 7.2 can be written as:

$$\frac{d(\text{OUR})}{dt} = -b(\text{OUR}) \quad (7-3)$$

Integration of equation 7-3 yields

$$\ln \left[\frac{\text{OUR}}{\text{OUR}_0} \right] = -b t \quad (7-4)$$

The specific decay rate constant (b , day^{-1}) was determined by linear regression from the slope value of a plot of $\ln[(\text{OUR})/(\text{OUR}_0)]$ versus time (days).

7.2.3 Batch Aerobic Biodegradation Assay

In order to assess for any possible inhibitory effects and further biodegradation and/or biomineralization of the RB4 decolorization products, an aerobic batch assay was performed with the mixed, aerobic halophilic culture. Aliquots of 3-L of the halophilic stock culture were concentrated by centrifugation at 3500 rpm for 25 min in order to obtain a 5-fold concentrated biomass. Four sub-cultures were prepared using 2-L glass reactors (1.0 L total liquid volume) as follows (see Table 7.4). One sub-culture was amended with reacted RB4 (culture A), two sub-cultures were amended with RB4 decolorization products generated with the first and second ZVI column run (culture B and C, respectively), and one sub-culture without any dye (control culture). In addition, one 2-L reactor was prepared with RB4 decolorization products generated with the second ZVI column run and served as an abiotic control. The control culture without any dye or dye decolorization products was set up in order to assess any inhibitory effect of RB4 and/or its decolorization products on the halophilic culture. The abiotic control reactor was used in order to determine any effect of aeration on the decolorization products. An aliquot of 50 mL of the concentrated stock media was transferred to each sub-culture, and then adjusted to pH 7.0 with 1.0 N HCl. An aliquot of 200 mL of concentrated halophilic stock culture was then transferred to each reactor except the abiotic control. The total liquid volume was 1 L, resulting in 25% dilution of the RB4 dye and its decolorization products. The NaCl concentration was adjusted to the same level as in the stock culture (100 g/L), and then 2 mL of 250 g/L glucose solution was added to each active sub-culture. The initial biomass and glucose concentrations were 1500 mg VSS/L and 500 mg glucose/L, respectively. Aeration of each culture was provided by

Table 7.4. Batch biodegradation assay set-up

Component	Control culture	Abiotic Control	Sub-culture A (RB4)	Sub-culture B (RB4-products 1)	Sub-culture C (RB4-products 2)
Salt and base solution (mL) ^a	750	250	-	-	-
RB4 dye stock solution (mL) ^b	-	-	750	-	-
RB4 decolorization products (mL) ^c	-	750	-	750	750
Stock media (mL)	50	-	50	50	50
Concentrated culture (mL) ^d	200	-	200	200	200
Glucose stock solution (mL) ^e	2	-	2	2	2
Total volume (mL)	1000	1000	1000	1000	1000

^a Salt, 100 g/L NaCl; base, 3 g/L Na₂CO₃ and 1 g/L NaOH

^b 500 mg/L reacted RB4 stock solution with salt and base

^c RB4 decolorization products (RB4-products 1 and RB4-products 2) were prepared with ZVI column run 1 and 2, respectively.

^d 3-L of the halophilic stock culture was 5-fold concentrated by centrifugation at 3500 rpm for 25 min.

^e 250 g glucose/L

pre-humidified compressed air passed through a fine-pore stone diffuser. A magnetic stirrer provided continuous culture mixing. The batch assay lasted for 28 days. A second phase of the batch assay began with another addition of glucose at the same concentration (500 mg glucose/L) and lasted for 13 days. UV/Visible absorbance, VSS, DOC, and pH were periodically measured during each phase. Samples used for absorbance measurements and DOC were first centrifuged at 14,000 rpm for 5 min. All assays were conducted at 22°C.

7.3 Results and Discussion

7.3.1 RB4 Decolorization by a Continuous-flow ZVI Column

The continuous-flow, ZVI column decolorization kinetics and regeneration efficiency of the column were investigated with an influent RB4 concentration of 1,000 mg/L at high salt and base conditions typically used in reactive textile dyebaths. The porosity and pore volume of the ZVI column were determined to be 0.663 and 94.0 mL, respectively. As explained in the Materials and Methods section above, two column runs were performed. As a result, two different solutions of RB4 decolorization products were generated and were kept at 4°C under a He gas atmosphere (RB4-products 1 and RB4-products 2, respectively). Dye concentrations based on UV/Visible absorbance measurements were used to determine decolorization rates based on the pseudo first-order rate equation (equation 5-1) by non-linear regression. RB4 profiles during the first column run and non-linear regression fits to the pseudo first-order rate equation are shown in Figure 7.2. All regression fits resulted in R^2 values greater than 0.994. As the flow rate increased the observed overall, decolorization constant increased. During the

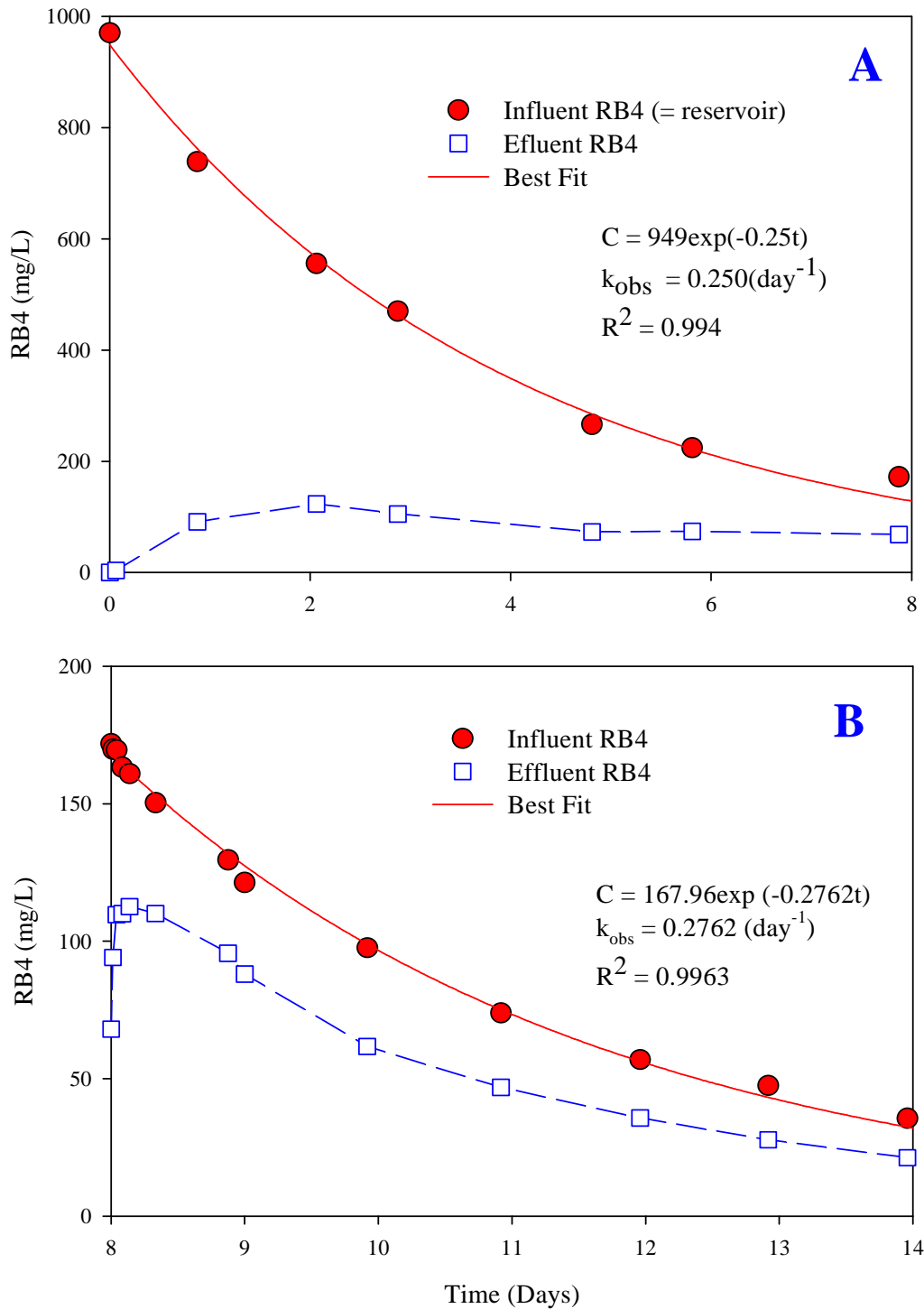


Figure 7.2. Influent and effluent concentration of RB4 during the first column run with recycle: (A) RB4 concentration profiles over the first 8 days at a flow rate of 1.0 mL/min; (B) RB4 concentration profiles after the increase of the flow rate to 5.0 mL/min (closed system with recycle of the column effluent to the dye reservoir).

column operation, about 40 and 50% of the initial dye solution DOC was not accounted for in the column influent and effluent, respectively (Figure 7.3), which is attributed to either adsorption of decolorization products and/or dye aggregation in the ZVI column. Figure 7.4 shows the UV/Visible spectra during the continuous-flow ZVI decolorization of RB4 at an initial concentration of 1,000 mg/L. As dye decolorization proceeded, the absorbance at 598 nm gradually decreased and the absorbance at 485 nm increased as expected due to the formation of RB4 decolorization products. A lower absorbance at 485 nm was observed for the RB4 decolorization products obtained in the first column run after 14 days of column operation compared to the absorbance of the decolorization products obtained in the second column run after 3 days of column operation. As explained in the Materials and Methods section above, the goal of the second column run was to achieve a significant degree of RB4 decolorization, but also a relatively high concentration of decolorization products.

The regeneration efficiency of the column was evaluated using D.I. water and a sulfuric acid solution after the first and second column run. Due to the fact that 40 to 50% of the dye stock solution DOC was not accounted for by DOC measurements of the column influent and effluent, a DOC mass recovery was investigated by trapezoidal integration of the area under the column effluent DOC concentration curve. Based on the DOC value of the RB4 decolorization solution and the DOC recovered during column regeneration, a DOC balance of 92 and 86% was achieved for the first and second column run, respectively. As mentioned in previous chapters, loss of column reactivity may be attributed to (1) aggregation and adsorption of RB4 and its decolorization products; and/or (2) ZVI surface coverage by iron corrosion products. During column

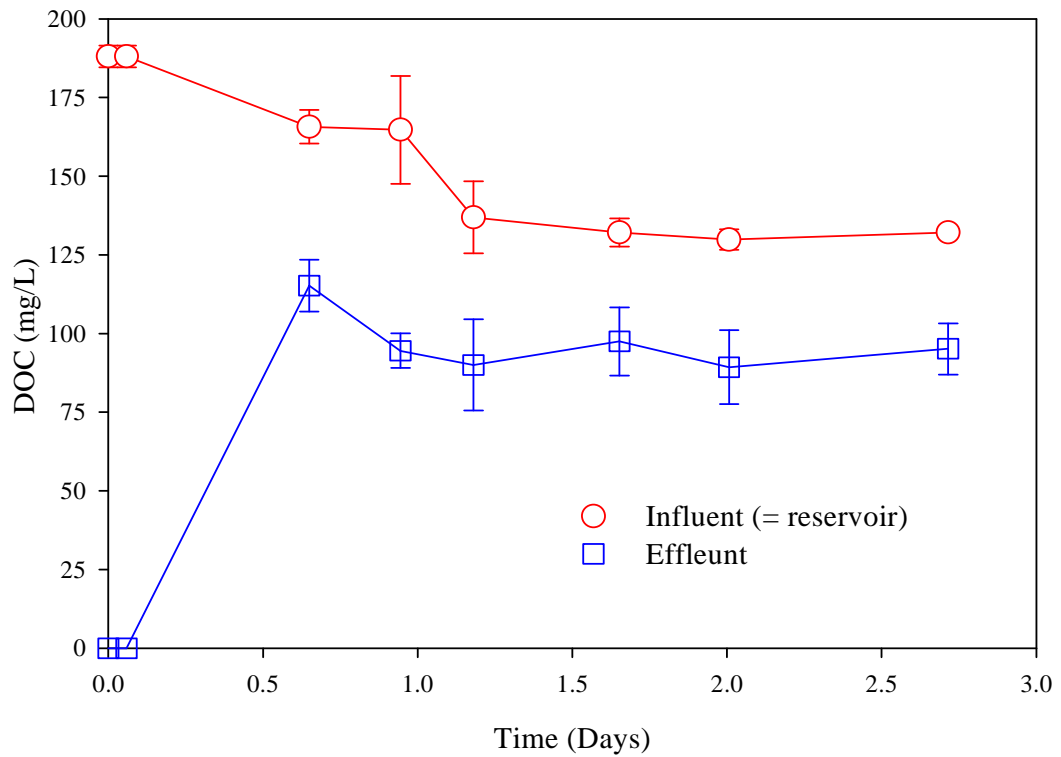


Figure 7.3. DOC profiles during the second ZVI column run with recycle of the column effluent to the dye reservoir (Influent RB4 equal to 1,000 mg/L) (Error bars represent \pm standard error of the mean).

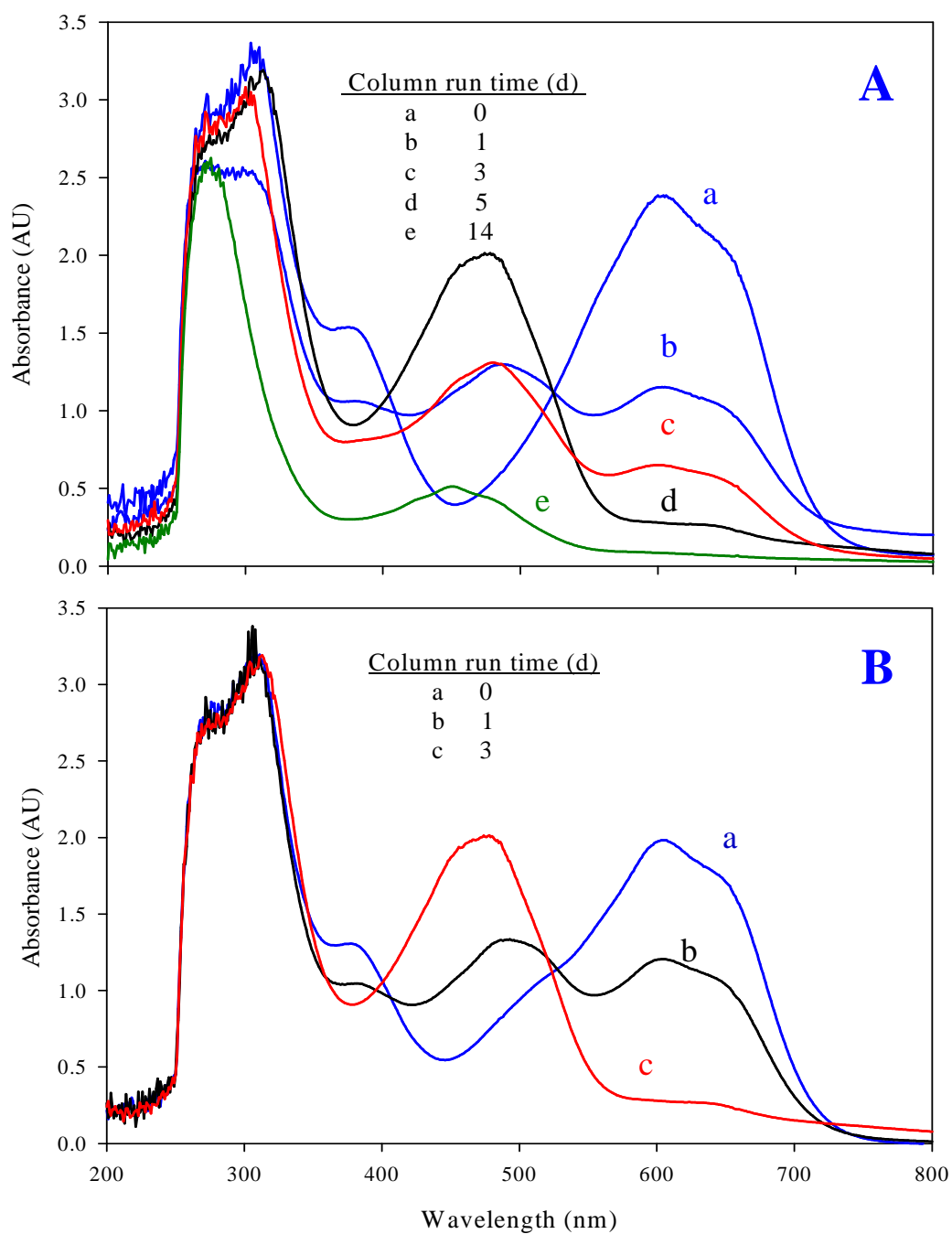


Figure 7.4. UV/Visible spectra during the continuous-flow decolorization of reacted RB4 using a ZVI column with effluent recycle to the dye reservoir (Initial dye concentration 1,000 mg/L; 100 g/L NaCl, 3 g/L Na₂CO₃, and 1 g/L NaOH): (A) first column run (14 days); (B) second column run (3 days).

regeneration, the acid solution dissolved and removed corrosion products which covered the ZVI surface. After the first column regeneration, the RB4 decolorization kinetics under the same column operational conditions were compared to those obtained during the first column run and results are shown in Figure 7.5. Based on these results, very similar RB4 decolorization kinetics were obtained after column regeneration. However, the operation time was relatively short (less than 14 days) and the column was operated with recycle of the column effluent back to the influent reservoir. Thus, it is expected that long-term column operation may result in slower decolorization kinetics due to the change in column porosity and accumulation of iron corrosion and dye decolorization products. Lai and co-workers (2000) showed that a dilute sulfuric acid was the most effective in restoring the Ni/Fe activity in continuous-flow columns, although a decrease in reaction kinetics was observed with long-term column operation and multiple column regenerations.

7.3.2 Halophilic Culture Performance

The halophilic culture was maintained under fully aerobic conditions (4.0 mg O₂/L) for 10 months at 22°C. The organic loading rate was 1500 mg glucose/L-d. The steady-state biomass concentration and pH were 2500 mg/L ± 150 mg VSS/L and 8.0 ± 0.3 (mean ± standard deviation). Several OUR measurements were performed with a subset of the halophilic culture which was maintained under starvation conditions in order to estimate the specific death rate constant (b , day⁻¹). The results of OUR measurements along with DOC and VSS data are shown in Table 7.5. Figure 7.6 shows the DO profiles and the OUR plot for the estimation of the specific death rate constant of

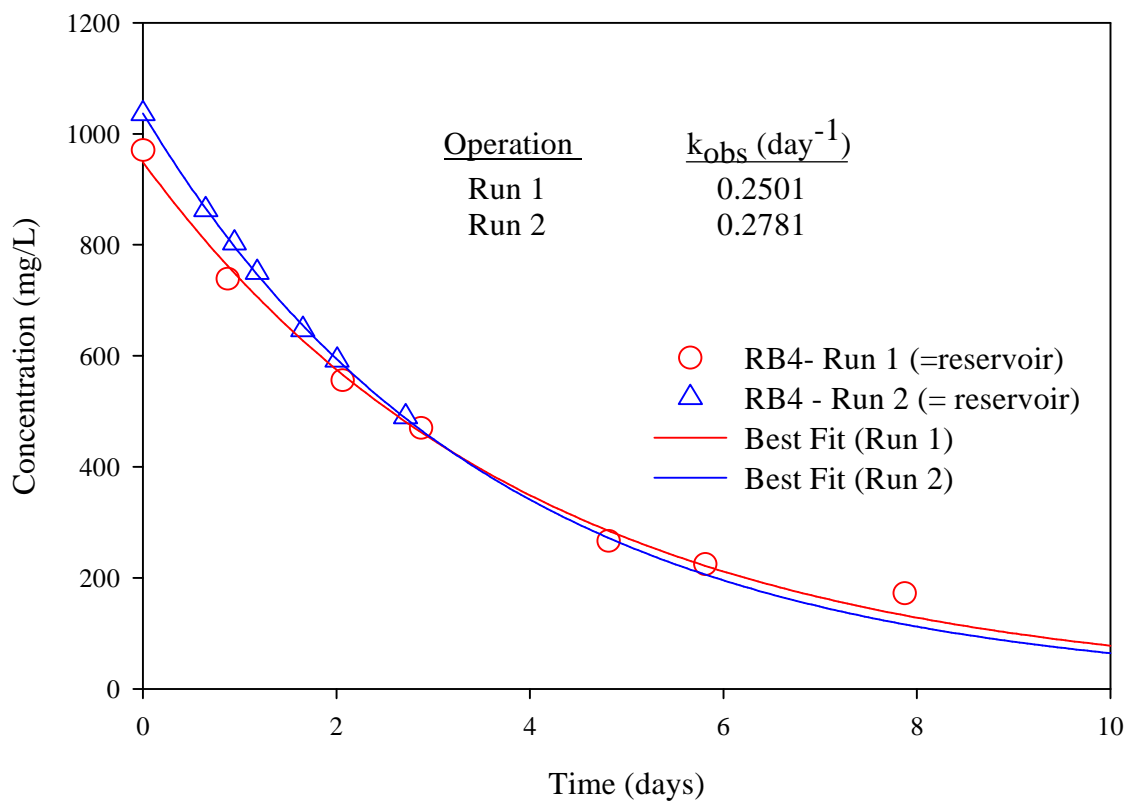


Figure 7.5. Comparison of RB4 decolorization kinetics by the ZVI continuous-flow column (with recycle of the column effluent to the dye reservoir) before and after regeneration (Initial dye concentration 1,000 mg/L; flow rate 1.0 mL/min).

Table 7.5. Results of the OUR measurements with the halophilic culture kept under starvation conditions

Time (day)	OUR (mg O ₂ /L-min) ^b	VSS (mg/L) ^b	SOUR (mg O ₂ /g VSS-h)	DOC (mg/L) ^b
0 ^a	0.118 ± 0.002 (0.999; 6) ^c	747 ± 32	9.478	58.3 ± 19.8
1	0.078 ± 0.001 (0.999; 6)	718 ± 39	6.476	40.6 ± 4.3
2	0.058 ± 0.001 (0.999; 6)	704 ± 29	4.960	45.3 ± 4.6
3	0.045 ± 0.001 (0.999; 6)	624 ± 35	4.288	51.8 ± 4.5
4	0.034 ± 0.001 (0.997; 6)	636 ± 12	3.245	51.7 ± 2.1
5	0.024 ± 0.001 (0.996; 6)	609 ± 15	2.335	56.1 ± 0.3

^a Initial OUR was measured a day after the culture was removed from the main reactor.

^b Mean ± standard deviation

^c R²; number of data points (*n*)

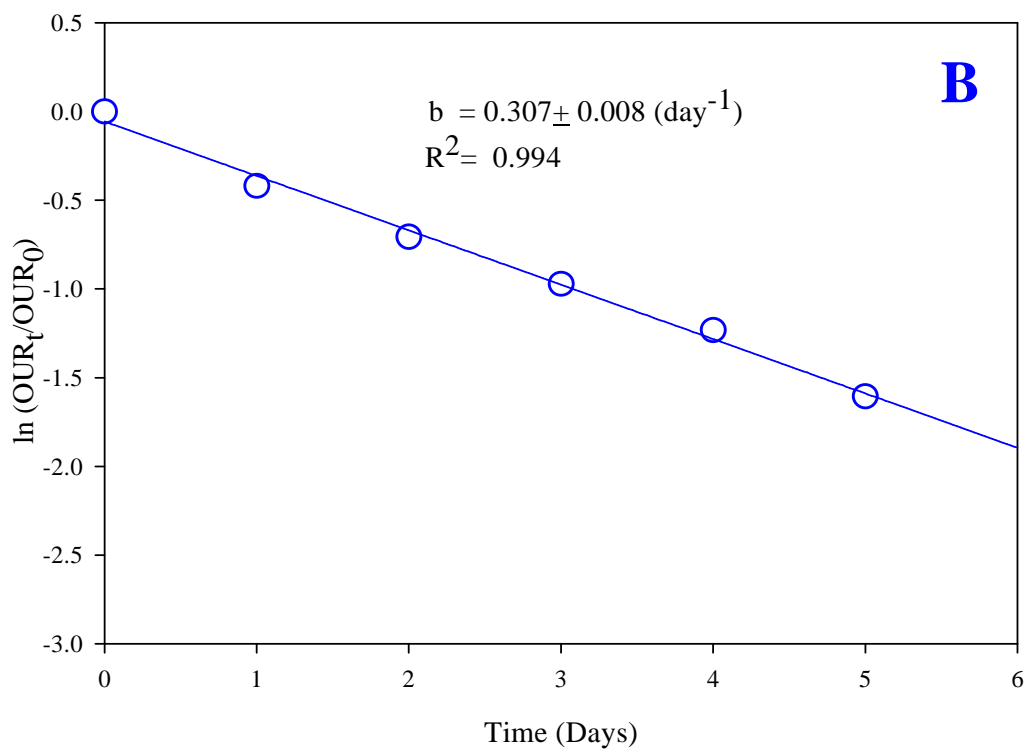
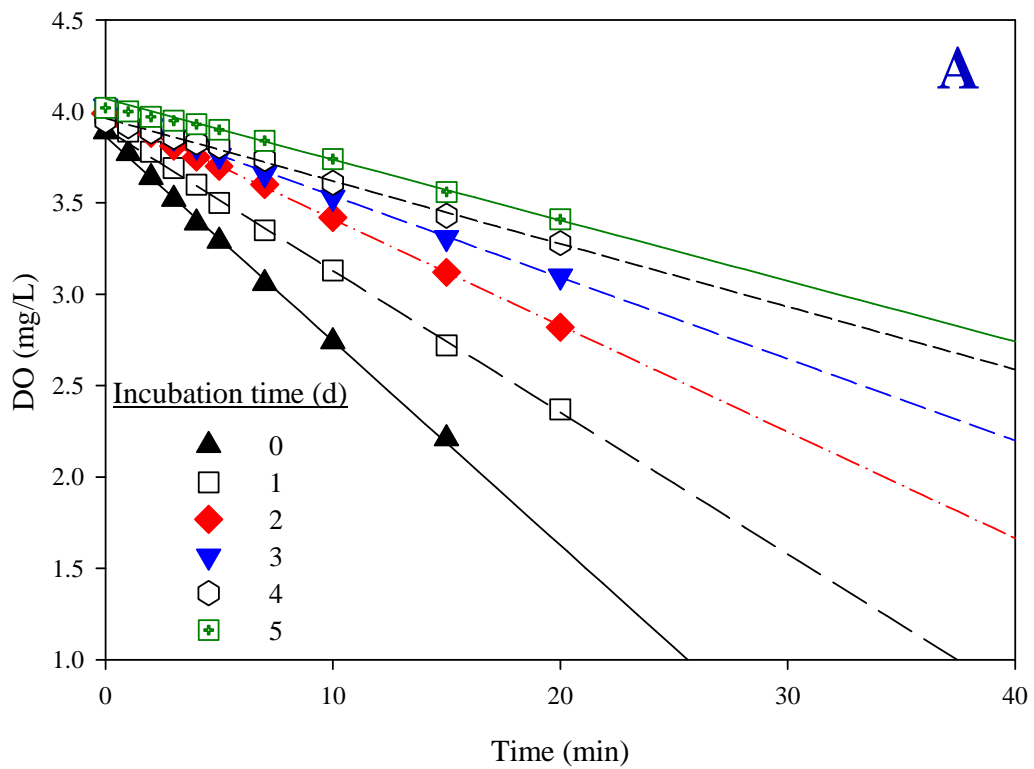


Figure 7.6. DO profiles (A) and OUR plots for the estimation of the specific death constant (B) of the halophilic culture incubated under starvation conditions.

the halophilic culture based on OUR measurements based on a linear regression of the OUR data according to equation 7-4. The following estimate was obtained from the OUR measurements: $b = 0.307 \pm 0.008 \text{ d}^{-1}$ (mean \pm standard error; $R^2 = 0.994$; $n = 7$). Overall, a relatively high specific death rate constant value was observed for this culture. Figure 7.7 and Table 7.5 show DOC, VSS, OUR and SOUR data for the halophilic culture during the OUR measurements. Under starvation conditions, the biomass concentration and OUR decreased over time as expected. An initial decrease in DOC was also observed, but then after the first day of culture incubation under starvation conditions, the DOC concentration gradually increased until the last measurement (day 5). The increase in DOC is attributed to the very high value of culture death rate constant. A similar increase in DOC was observed in a previous study using the same halophilic culture (Lee, 2003; Matthews, 2003).

7.3.3 Biodegradation Assessment of RB4 Decolorization Products

This part of the research examined the potential biodegradation of the RB4 decolorization products with the halophilic, mixed culture as well as their potential inhibitory effects on the culture. All assays were conducted under aerobic conditions and lasted for 41 days. The initial biomass concentration of each culture was $1,520 \pm 210 \text{ mg VSS/L}$ (mean \pm standard deviation). During these assays, the pH in all four cultures remained between 6.5 and 8.0. After 28 days of incubation, the cultures pH was adjusted to 7.0 and all cultures were amended with glucose at the same initial concentration (500 mg/L) in order to examine possible aerobic biodegradation of RB4 decolorization products with prolonged culture incubation.

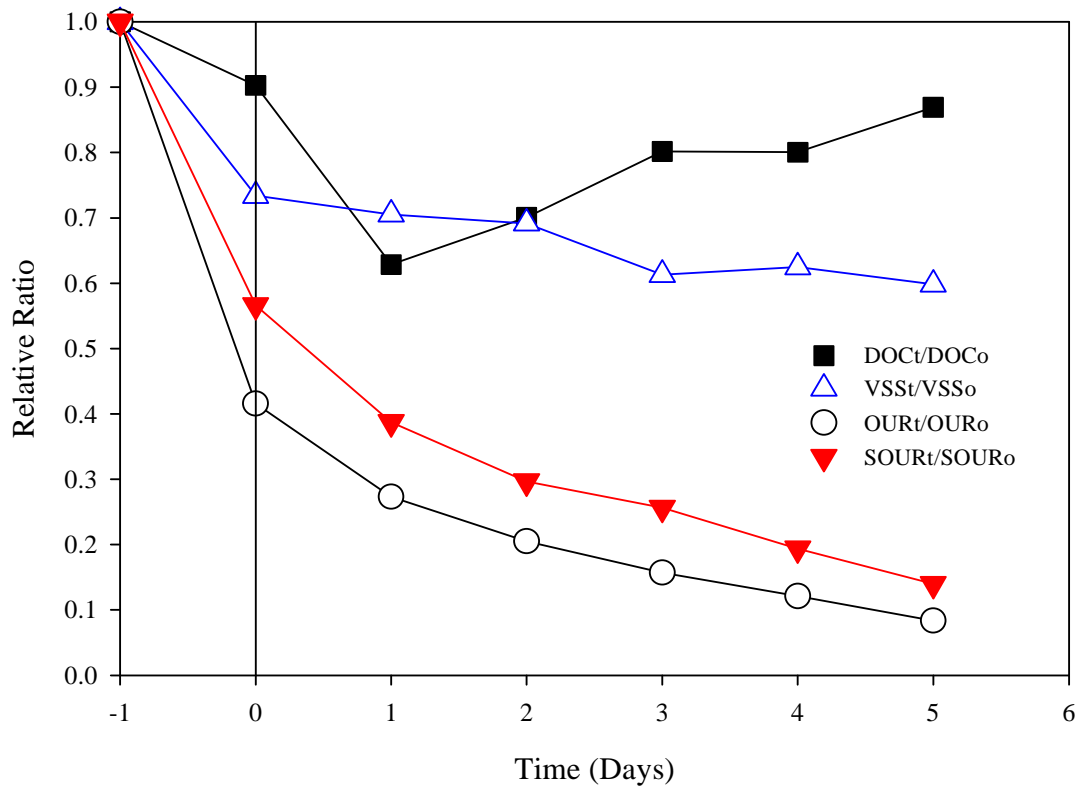


Figure 7.7. Relative ratio of the DOC, VSS, OUR and SOUR profiles in the halophilic culture under starvation conditions.

The DOC profiles in all cultures over the entire biodegradation assay period are shown in Figure 7.8A and B. The initial DOC concentration in the cultures amended with either RB4 or its decolorization products was relatively higher than in the control culture due to presence of the dye or its decolorization products. After the first glucose addition, the DOC concentration decreased rapidly in all cultures. However, after the second glucose addition, relatively lower rates of glucose consumption (inferred from the DOC values) were observed in all cultures, as shown in Figure 7.8C, especially in the two cultures amended with RB4 decolorization products. The relatively lower glucose consumption rates may be attributed to the lower biomass concentrations remaining in these cultures after 28 days of incubation under starvation and high death rate (see below). It is noteworthy, that after the glucose consumption was complete, the residual DOC concentration in all cultures, including the control culture, remained relatively unchanged, which indicates that the dye- and dye products-derived DOC did not degrade under the conditions of the halophilic culture even with prolonged incubation. The VSS profiles in all cultures over the entire biodegradation assay period are shown in Figure 7.9. Each culture showed a similar trend of the VSS profile. While the VSS of the control and RB4-amended culture rapidly decreased by 50% within the first 5 days of incubation, a significant decrease of the VSS concentration in the two cultures amended with the RB4 decolorization products was not observed within 5 days of incubation. This difference in VSS concentration during the first 5 days of incubation may be attributed to a possible utilization of a low concentration of degradable components of RB4 decolorization products. After a prolonged incubation, the VSS concentration in these two cultures decreased and matched that of the control and RB4-amended cultures (Figure 7.9). Based

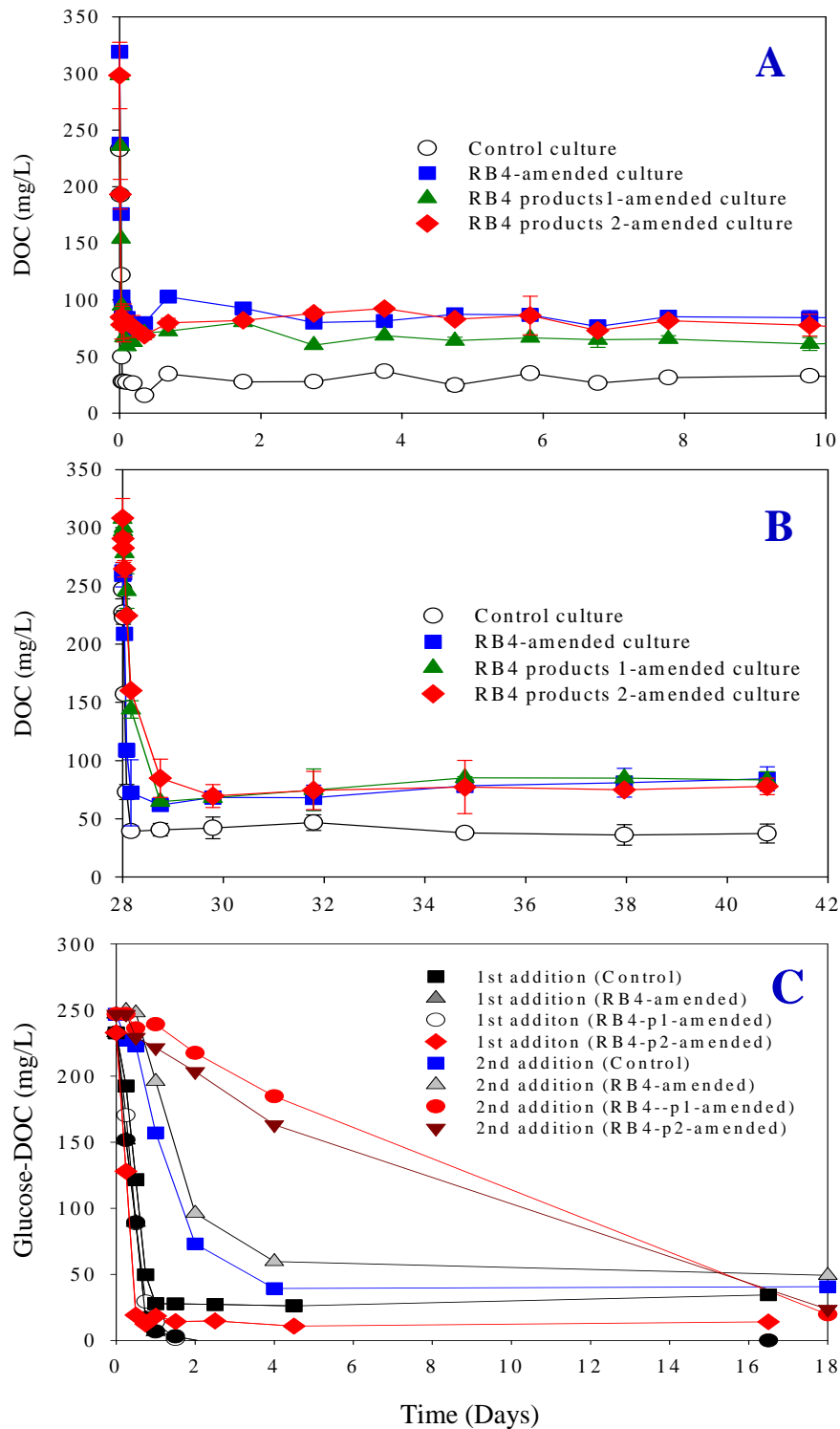


Figure 7.8. DOC profiles in the batch halophilic cultures: (A) phase I – after first glucose addition; (B) phase II – after second glucose addition; (C) glucose-DOC profiles after each glucose addition.

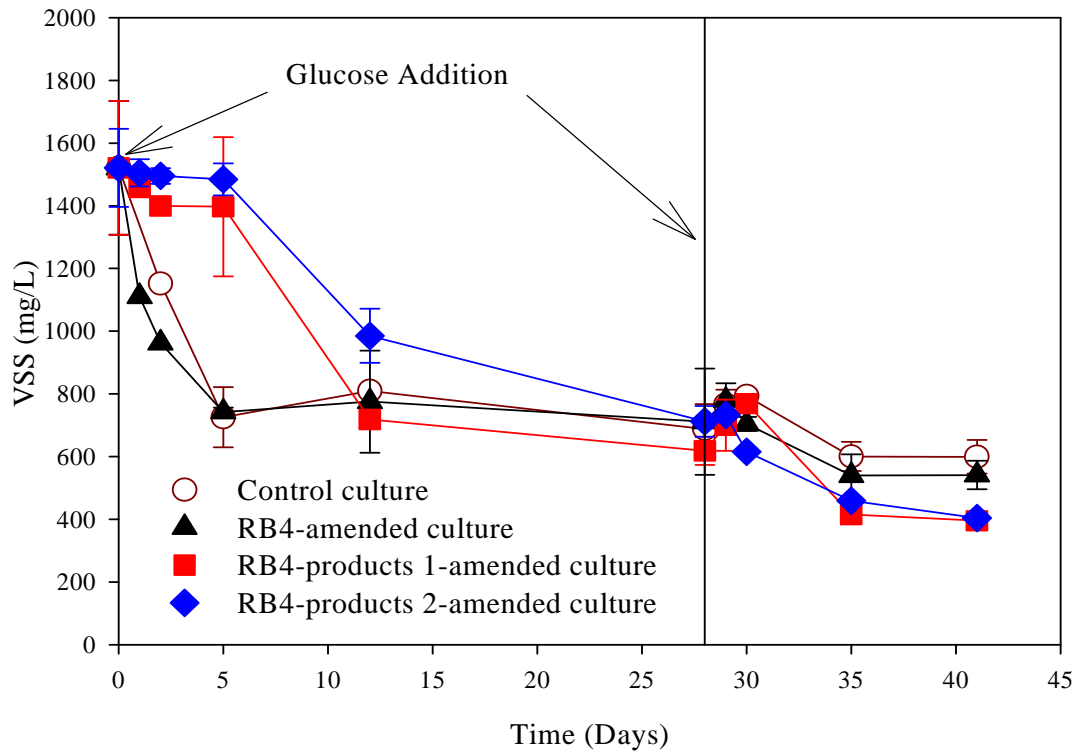


Figure 7.9. VSS profiles in the batch halophilic cultures.

on glucose consumption and VSS data, RB4 and its decolorization products did not have any significant inhibitory effect on the halophilic culture. Similar results have been reported for three spent azo dye baths and their decolorization products tested with the same halophilic culture under various conditions (Lee and Pavlostathis, 2003).

The consumption rate of biodegradable DOC in the batch biodegradation assays was described by the Monod model:

$$\frac{d(\text{DOC})}{dt} = \frac{k' \text{ DOC}}{K_s + \text{DOC}} \quad (7-5)$$

where, DOC = biodegradable dissolved organic carbon (mg/L); k' = maximum biodegradable DOC utilization rate for a constant biomass concentration (mg DOC/L-h); K_s = half-velocity coefficient (mg/L)

Integration of equation 7-5 yields

$$\text{DOC} = \text{DOC}_0 - K_s \ln\left(\frac{\text{DOC}}{\text{DOC}_0}\right) - k't \quad (7-6)$$

Based on non-linear regression of the biodegradable DOC data as shown in Figure 7.10 according to the above equation, the following estimates were obtained. Control culture: $K_s = 5.8 \pm 4.7$ mg/L and $k' = 260.1 \pm 36.7$ mg/L-h (mean \pm standard error; $R^2 = 0.986$; $n = 6$); RB4-amended culture: $K_s = 20.5 \pm 4.5$ mg/L and $k' = 323.1 \pm 4.0$ mg/L-h (mean \pm standard error; $R^2 = 0.976$; $n = 6$); culture amended with RB4 decolorization products 1 (first column run): $K_s = 18.8 \pm 4.8$ mg/L and $k' = 289.6 \pm 37.0$ mg/L-h (mean \pm standard error; $R^2 = 0.974$; $n = 6$); and culture amended with RB4 decolorization products 2 (second column run): $K_s = 19.5 \pm 7.7$ mg/L and $k' = 547.2 \pm 101.4$ mg/L-h (mean \pm standard error; $R^2 = 0.988$; $n = 5$).

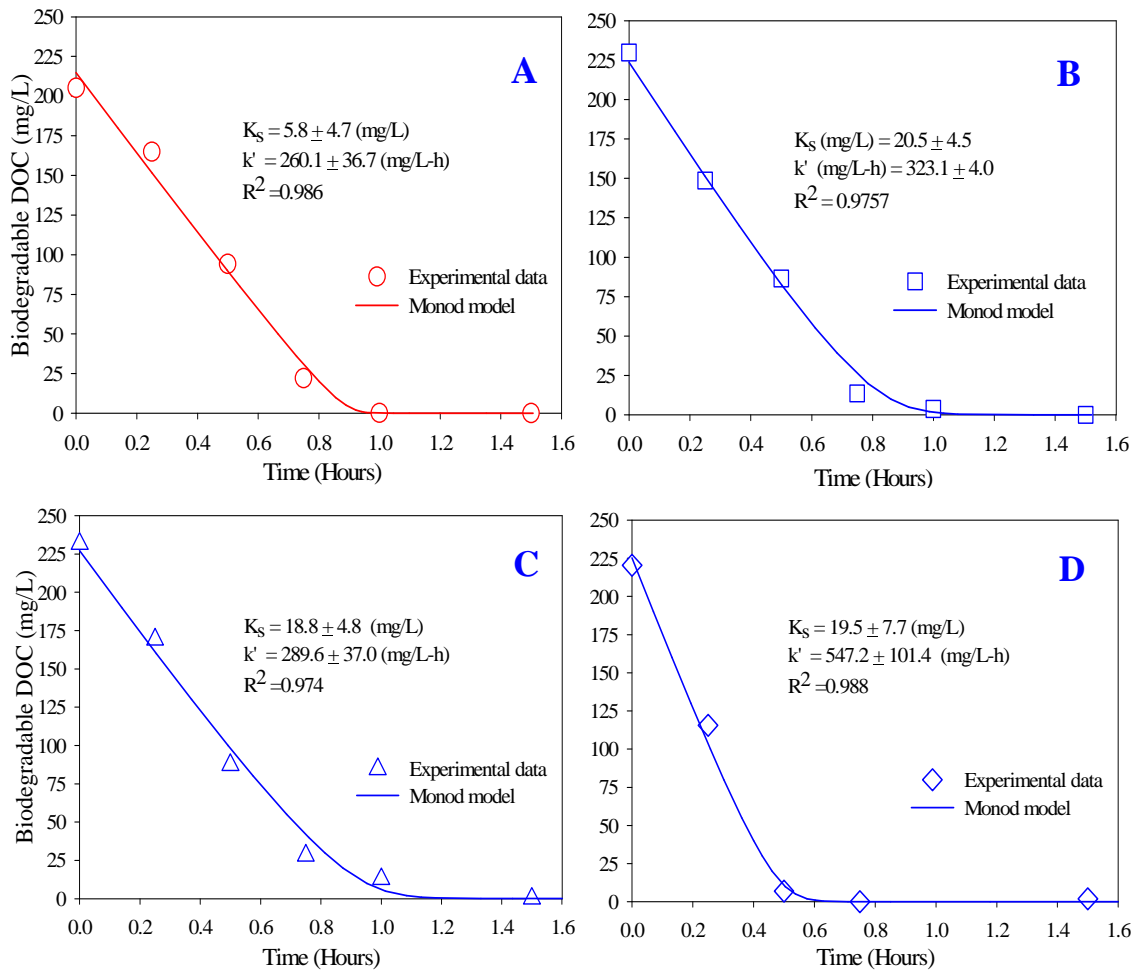


Figure 7.10. Non-linear fit of the Monod model to the biodegradable DOC (glucose) concentration profiles (A) control culture without any dye amendment; (B) RB4-amended culture; (C) and (D) cultures amended with RB4 decolorization products generated during ZVI column run 1 and 2, respectively.

The UV/visible spectra and absorbance profiles at both 485 and 598 nm for the cultures amended with RB4, its decolorization products and the abiotic control are shown in Figures 7.11 and 7.12. A significant increase of the absorbance at the characteristic wavelength of RB4 (i.e., at 598 nm) was not observed during this assay and any significant change of the absorbance at both 485 nm and 598 nm was not observed in the culture amended with RB4. However, a significant decrease of the absorbance at the wavelength of the RB4 decolorization products (i.e., at 485 nm) was observed in both cultures amended with RB4 products and the abiotic control. This observation is contrary to a previous report which attributed the decrease in the absorbance of RB4 decolorization products to aggregation enhancement of decolorization products upon re-aeration (Lee, 2003). In the case of the abiotic control, aeration may have resulted in a low extent of chemical oxidation of RB4 decolorization products. However, it is noteworthy that a decrease of the absorbance at 485 nm in the cultures amended with the RB4 decolorization products did not result in an increase of absorbance at the 598 nm. Thus, it is possible that in the case of cultures amended with RB4 decolorization products, either chemical oxidation took place at a lower extent and/or re-oxidized decolorization products may have aggregated on the biomass and removed during the centrifugation step of sample preparation before absorbance measurements.

7.4 Summary

The continuous-flow, decolorization kinetics and regeneration efficiency of a ZVI column were investigated in order to prepare RB4 decolorization products for the biodegradation assay under spent textile reactive dyebath conditions. During column

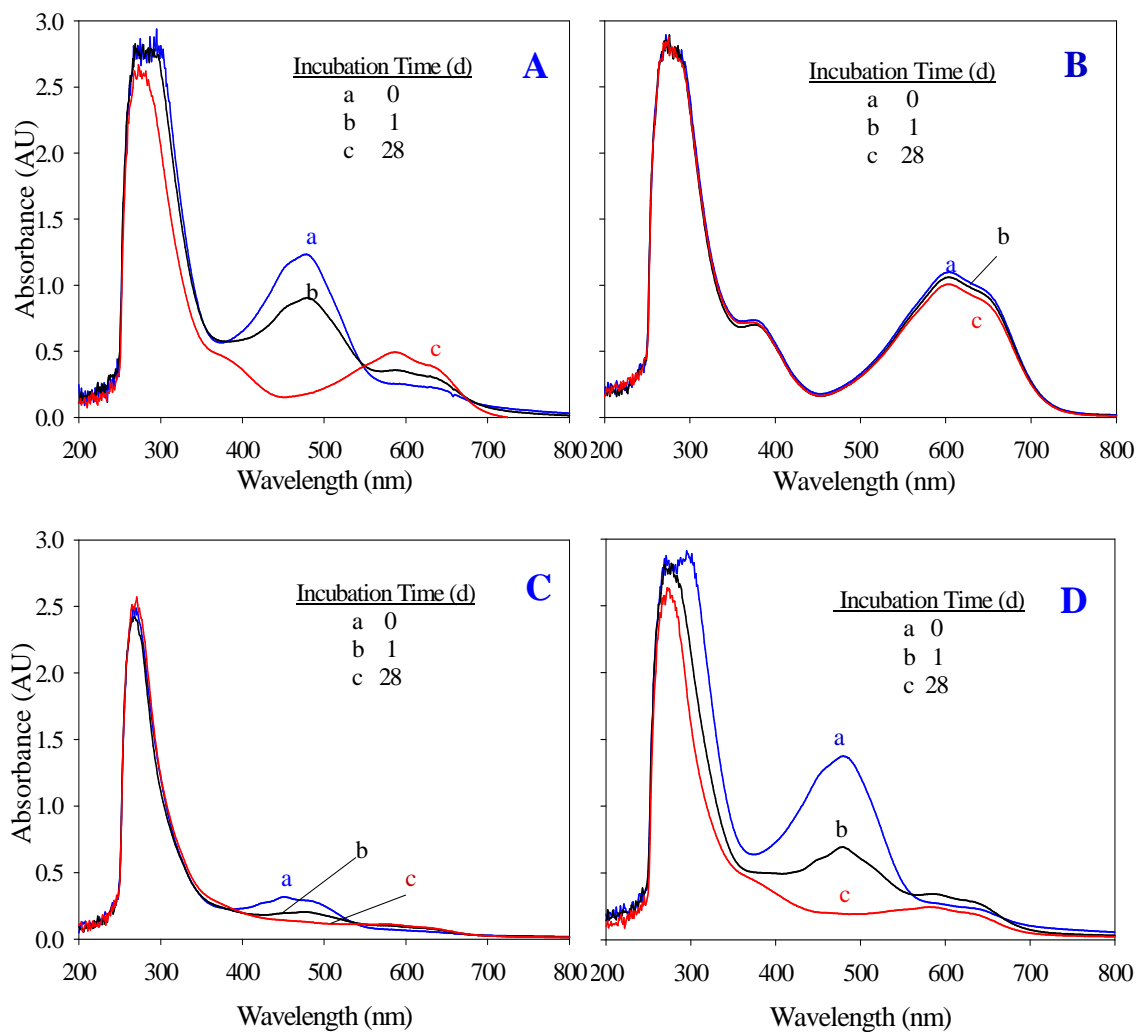


Figure 7.11. UV/Visible spectra during the biodegradation assay in the halophilic culture as a function of incubation time: (A) abiotic control with RB4 products 1 (run 1); (B) RB4-amended culture; (C) culture amended with RB4 decolorization products 1; (D) culture amended with RB4 decolorization products 2.

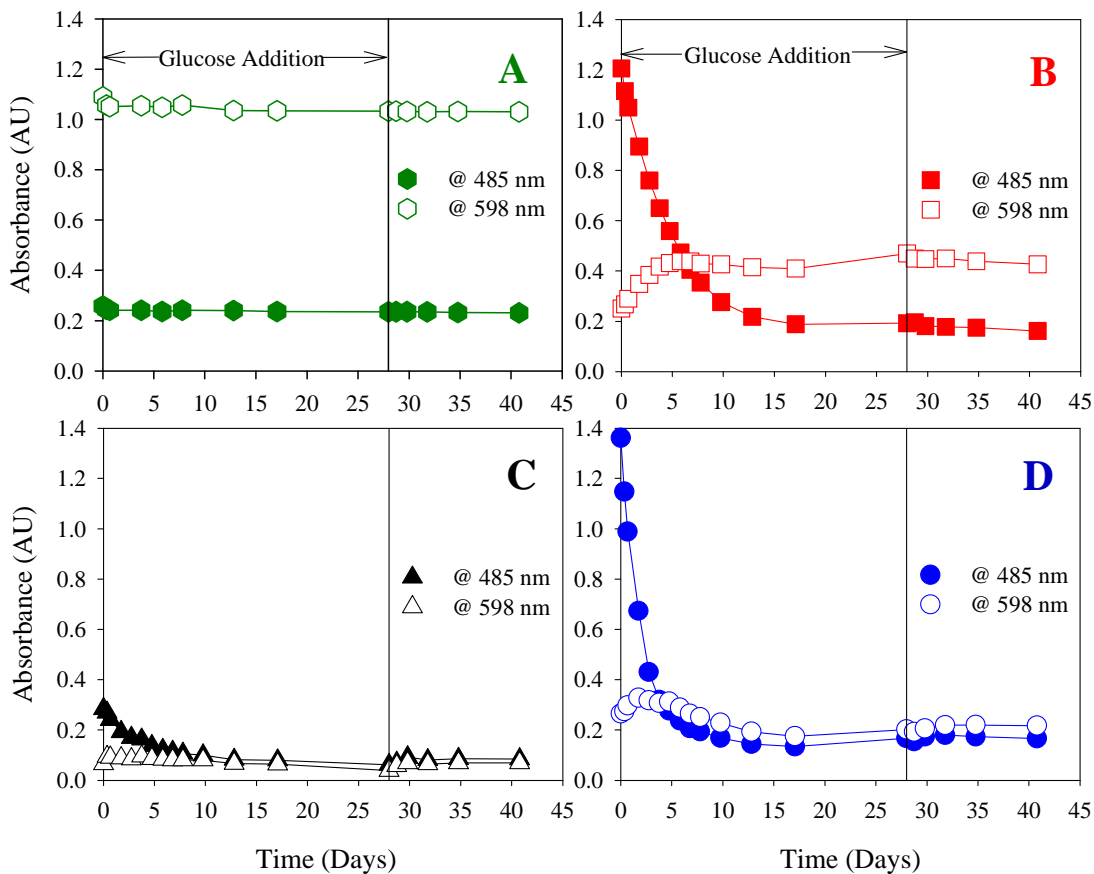


Figure 7.12. Absorbance profiles during the biodegradation assay: (A) culture amended with RB4; (B) abiotic control with RB4 product 1 (column run 1); (C) culture amended with RB4 products 1; (D) culture amended with RB4 products 2 (characteristic wavelength of RB4 is 598 nm and RB4 products is 485 nm).

operation, between 40 and 50% of the initial dye DOC was not accounted for in the column effluent, and was retained within the column as shown by a DOC balance performed based on the DOC values of the collected RB4 decolorization products and the column effluent during column regeneration. Column regeneration using D.I. water and a sulfuric acid solution resulted in column reactivation and similar RB4 decolorization kinetics to these of the original column run.

In order to assess possible inhibitory effects and biodegradation of the RB4 decolorization products, an aerobic batch biodegradation assay was performed with a mixed, aerobic halophilic culture. Based on OUR measurements, a relatively high specific death rate constant was estimated for this culture. Both the carbon source (i.e., glucose) utilization and biomass levels were not affected by the addition of RB4 or its decolorization products. However, significant biodegradation and/or mineralization of RB4 decolorization products was not observed in these cultures maintained under aerobic conditions. Partial absorbance decrease at the characteristic wavelength of the RB4 decolorization products during aeration may be attributed to either a low extent of chemical oxidation and/or products aggregation and association with the biomass.

CHAPTER 8

CONCLUSIONS AND RECOMMENDATIONS

One of the most commercially significant anthraquinone reactive dyes, Reactive Blue 4 (RB4), was chosen for the assessment of zero-valent iron (ZVI) reductive decolorization and the biodegradation of its decolorization products. Significant research was performed in order to evaluate the key operational parameters of ZVI batch decolorization and continuous-flow ZVI decolorization kinetics under anoxic conditions, as well as the potential for the biodegradation of RB4 decolorization products in a halophilic culture under aerobic conditions.

In this study it was found that ZVI decolorization of RB4 is mass transfer limited based on two operational parameters (mixing intensity and initial dye concentration). The high salt and base concentrations typical of spent reactive dyebath conditions enhanced the rate of RB4 decolorization. It was also found that continuous-flow ZVI decolorization is feasible, but porosity losses and a shift of reaction kinetics can occur in long-term column operation. ZVI decolorization of RB4 in this research was successfully described with a pseudo first-order or a site saturation model. The decolorization products had no inhibitory effect on the halophilic, aerobic culture, but were not further mineralized.

Based on the results of the present study, the following specific conclusions can be drawn:

1. The ZVI decolorization process is a surface-catalyzed, mass transfer-limited process. As the mixing speed increased, the observed decolorization rate constant (k_{obs}) increased. As the initial dye concentration increased, a decrease of the dye

decolorization rate was also observed. RB4 was decolorized faster under hypersaline conditions than RB4 in D.I. water.

2. Non-ideal transport characteristics were observed in a continuous-flow ZVI column. Based on KI and KBr tracer tests, asymmetric shapes and extended tailing of the breakthrough curves were observed. The CXTFIT 2.0 program based on the 1D advection-dispersion equation correctly described the extended tailing, but failed to describe the asymmetric tracer concentration peak and underestimated the column pore water velocity.
3. Up to 80% decolorization of 1,000 mg/L RB4 was achieved in the continuous-flow ZVI column for the first 110 pore volumes (21 days or 30 L). Therefore, continuous-flow ZVI decolorization of anthraquinone reactive dyes is feasible. However, porosity losses and a shift of reaction kinetics occurred after a long-term column operation. Porosity losses were observed after 56 days of continuous operation due to formation of iron precipitates and/or dye aggregation, which resulted in an increase of pore water velocity and a shift of reaction kinetics from pseudo first-order to zero-order.
4. Both carbon source (i.e., glucose) utilization and microbial growth were not affected by the addition of RB4 or its decolorization products generated using a continuous-flow ZVI column with effluent recycle. However, biodegradation and/or mineralization of RB4 decolorization products was not observed after a long-term incubation of a halophilic, aerobic culture. Partial absorbance decrease at the characteristic wavelength of the RB4 decolorization products (i.e., 485 nm)

may be attributed to either a low extent of chemical oxidation and/or products aggregation and association with the biomass.

This research demonstrated the feasibility of ZVI decolorization of reactive anthraquinone dyes which will help in the development of a continuous-flow, dyebath decolorization process and the possible reuse of the renovated dyebath in the dyeing operation. Such system could lead to substantial reduction of water usage as well as a decrease of salt and dye discharges.

One of the limitations for the research presented here was the lack of advanced techniques for the identification of the RB4 decolorization products due to time constraints. Liquid Chromatography/Mass Spectrometry (LC/MS) analysis was not conducted at the time this research ended. Such analyses will lead to better understanding of decolorization pathways and identification of decolorization products will provide useful means to investigate the potential for possible biomineralization of RB4 decolorization products in future studies.

APPENDIX A
CALIBRATION CURVES

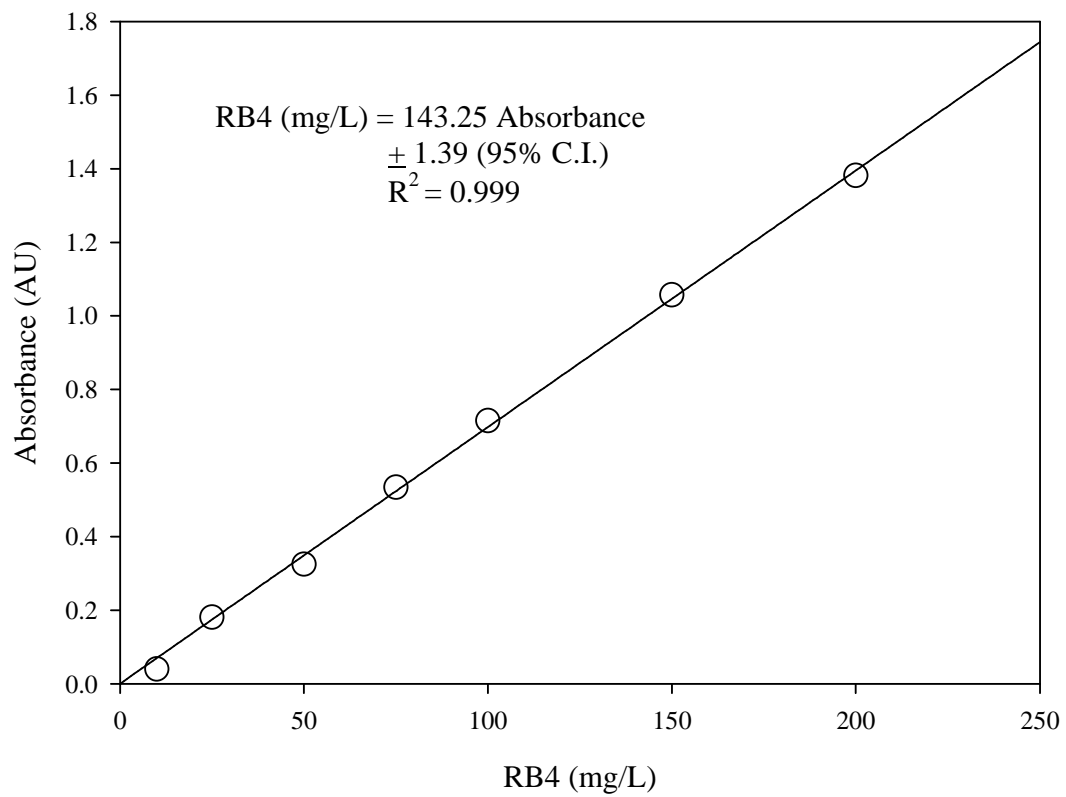


Figure A.1. Calibration curve for reacted RB4 in D.I. water (Absorbance at 598 nm).

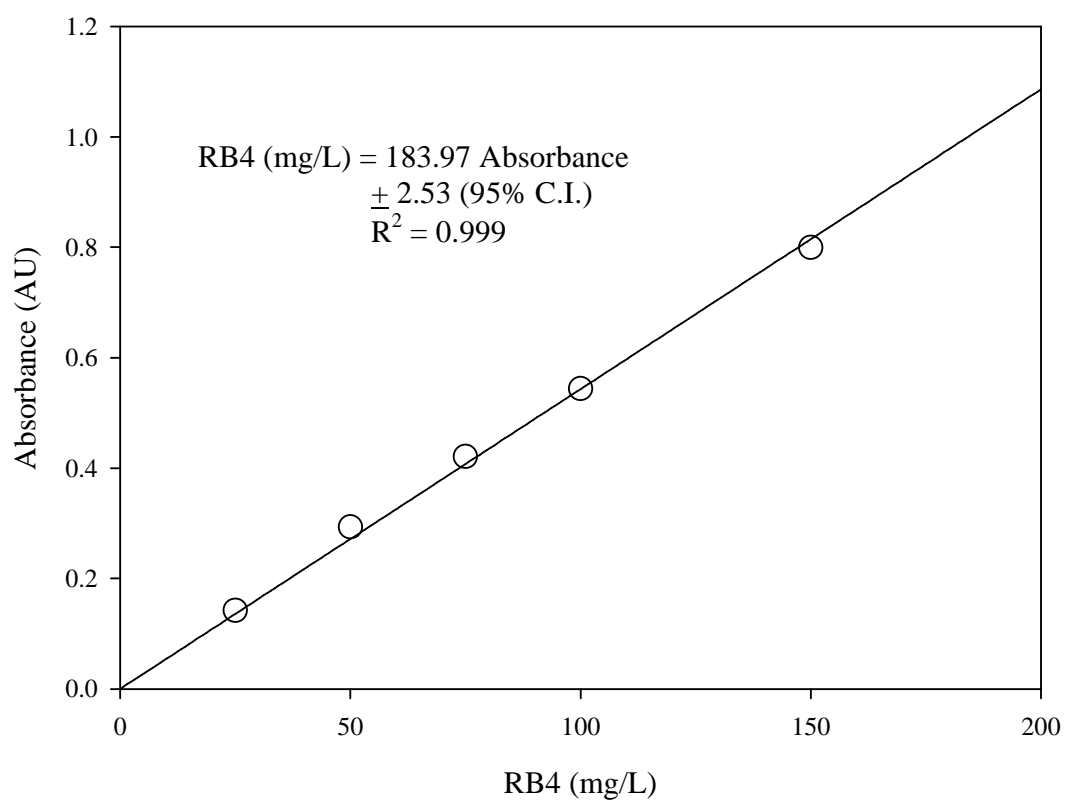


Figure A.2. Calibration curve for reacted RB4 in salt and base solution (Absorbance at 598 nm; 100 g NaCl/L; 3 g Na₂CO₃/L; 1g NaOH/L).

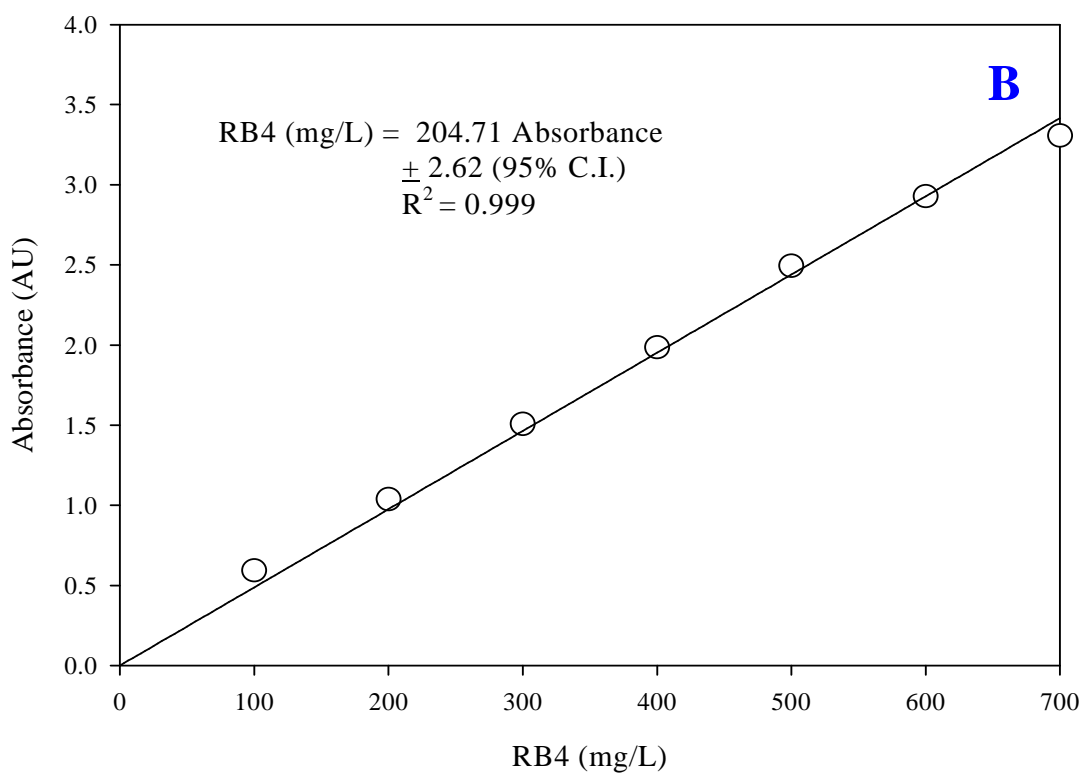
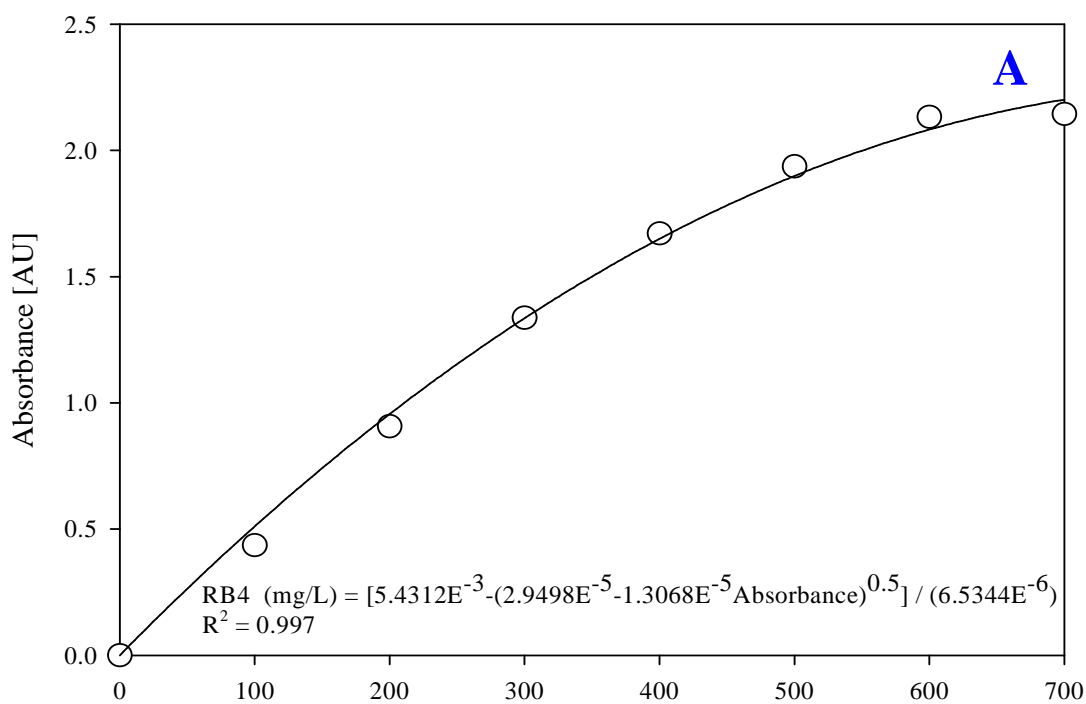


Figure A.3. Calibration curves for high concentration reacted RB4 in salt and base solution using 1.5 mL cuvettes (A) and 2.0 mL cuvettes (B) (Absorbance at 598 nm; 100 g NaCl/L; 3 g Na₂CO₃/L; 1g NaOH/L).

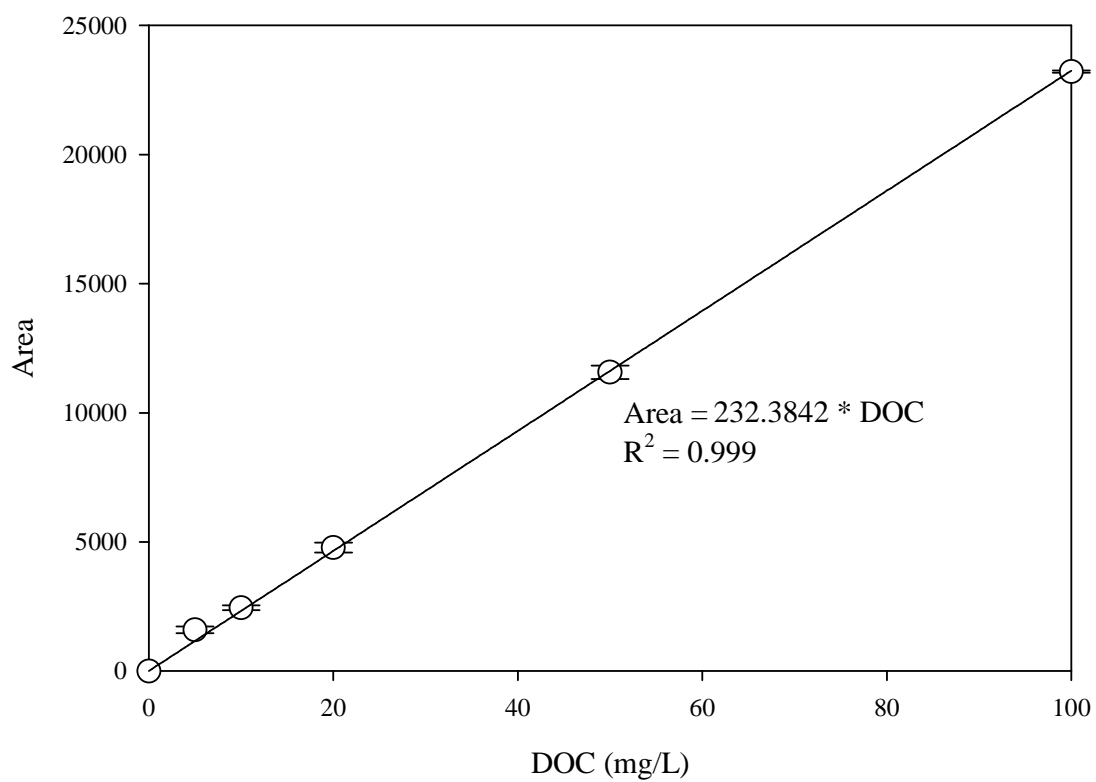


Figure A.4. Calibration curve for dissolved organic carbon (DOC) (Error bars represent \pm one standard error of the mean).

REFERENCES

- Agrawal, A., Ferguson, W. J., Gardner, B. O., Christ, J. A., Bandstra, J. Z., Tratnyek, P. G. (2002) Effects of carbonate species on the kinetics of dechlorination of 1,1,1-trichloroethane by zero-valent iron. *Environmental Science & Technology*, **36**(20): 4326-4333.
- Agrawal, A. and Tratnyek, P. G. (1996) Reduction of nitro aromatic compounds by zero-valent iron metal. *Environmental Science & Technology*, **30**(1): 153-160.
- Aksu, Z. (2001) Biosorption of reactive dyes by dried activated sludge: equilibrium and kinetic modelling. *Biochemical Engineering Journal*, **7**(1): 79-84.
- Aspland, J. R. (1997) *Textile Dyeing and Coloration*. Research Triangle Park, NC, USA, American Association of Textile Chemists and Colorists.
- Banat, I. M., Nigam, P., Singh, D and Marchant, R. (1996) Microbial decolorization of textile-dye-containing effluents: a review. *Bioresource Technology*, **58**(3): 217-227.
- Baughman, G. L. and E. J. Weber (1994) Transformation of Dyes and Related-Compounds in Anoxic Sediment - Kinetics and Products. *Environmental Science & Technology* **28**(2): 267-276.
- Beigel, C. and Pietro, L. D. (1999) Transport of triticonazole in homogeneous soil columns: influent of nonequilibrium sorption. *Soil Science Society of America Journal*, **63**: 1077-1086.
- Beydilli, M. I. (2001) *Reductive Biotransformation and Decolorization of Reactive Azo Dyes*. School of Civil and Environmental Engineering. Atlanta, Georgia Institute of Technology.
- Beydilli, M. I., Pavlostathis, S. G. and Tincher, W. C. (2000) Biological decolorization of the azo dye reactive red 2 under various oxidation-reduction conditions. *Water Environment Research*, **72**(6): 698-705.
- Bhattacharyya, A., Kawi, S. and Ray M. B. (2004) Photocatalytic degradation of orange II by TiO₂ catalysts supported on adsorbents. *Catalysis Today*, **98**: 431-439.
- Bigg, T. and Judd, S. J. (2000) Zero-valent iron for water treatment. *Environmental Technology*, **21**(6): 661-670.
- Bigg, T. and Judd, S. J. (2001) Kinetics of reductive degradation of azo dye by zero-valent iron. *Process Safety and Environmental Protection*, **79**(B5): 297-303.

- Blum, J. S., Stolz, J. F., Oren, A. and Oremland, R. S. (2001) Selenihalanaerobacter shriftii gen. nov., sp nov., a halophilic anaerobe from Dead Sea sediments that respire selenate. *Archives of Microbiology*, **175**(3): 208-219.
- Bowers, D. F. (1986) Corrosion considerations for alkaline papermaking. *Tappi Journal*, **69**(1): 62-66.
- Buabuna, F. G., Orhon, D., Cokgor, E. U., Insel, G. and Yaprakli, B. (1998) Modeling of activated sludge for textile wastewaters. *Water Science and Technology*, **38**(4/5): 9-17.
- Buitron, G., Quezada, M. and Moreno, G. (2004) Aerobic degradation of the azo dye acid red 151 in a sequencing batch biofilter. *Bioresource Technology*, **92**: 143-149.
- C. O'neil, F. R. H., Hawkes, D. L., Esteves, S. and Wilcox, S. J. (1999) Anaerobic-aerobic biotreatment of stimulated textile effluent containing varied ratios of starch and azo dye. *Water Research*, **34**(8): 2355-2361.
- Cao, J., Wei, L., Huang, Q., Wang, L. and Han, S. (1999) Reducing degradation of azo dye by zero-valent iron in aqueous solution. *Chemosphere*, **38**(3): 565-571.
- Carliell, C. M., Barclay, S. J., Shaw, C., Wheatley, A. D. and Buckley, C. A. (1998) The effect of salts used in textile dyeing on microbial decolourisation of a reactive azo dye. *Environmental Technology*, **19**(11): 1133-1137.
- Chen, G., Chai, X., Yue, P. L. and Mi, Y. (1997) Treatment of textile desizing wastewater by pilot scale nanofiltration membrane separation. *Journal of Membrane Science*, **127**(1): 93-99.
- Chen, J. L., Al-Abed, S. R., Ryan, J. A. and Li, Z. (2001) Effects of pH on dechlorination of trichloroethylene by zero-valent iron. *Journal of Hazardous Materials*, **83**(3): 243-254.
- Churchley, J. H., Greaves, A. J. Hutchings, M. G., James, A. E., Phillips, D. A. S. (2000) The development of a laboratory method for quantifying the bioelimination of anionic, water soluble dyes by a biomass. *Water Research*, **34**(5): 1673-1679.
- Delee, W., O'Neill, C., Hawkes, F. R. and Pinheiro, H. M. (1998) Anaerobic treatment of textile effluents: a review. *Journal of Chemical Technology and Biotechnology*, **73**(4): 323-335.
- Schreiber, D. C. and Pavlostathis, S.G. (1998) Biological oxidation of thiosulfate in mixed heterotrophic/autotrophic cultures. *Water Research*, **32**(5): 1363-1372.
- Doong, R.-A. and Wu, S.-C. (1992) Reductive dechlorination of chlorinated hydrocarbons in aqueous solutions containing ferrous and sulfide ions. *Chemosphere*, **24**(8): 1063-1075.

- Epolito, W. J. (2004). *Characterization of the Textile Anthraquinone Dye, Reactive Blue 4*. Georgia Institute of Technology. Atlanta, Georgia Institute of Technology.
- Epolito, W. J., Lee, Y. H.; Bottomley, L. A. and Pavlostathis, S. G. (2005a) Characterization of the textile anthraquinone dye Reactive Blue 4. *Dyes and Pigments*, **67**(1): 35-46.
- Epolito, W. J. et al, (2005b) Decolorization kinetics of the textile anthraquinone dye Reactive Blue 4 (*In preparation*).
- Epolito, W. J. et al, (2005c) Characterization of decolorization products of the textile anthraquinone dye Reactive Blue 4 (*In preparation*).
- Faust, S. D. and Aly, O. M. (1987) *Adsorption Process for Water Treatment*. Boston, Butterworths.
- Fontenot, E. J. (1998) *Decolorization of Selected Reactive Blue Dyes under Methanogenic Conditions*. School of civil and Environmental Engineering. Atlanta, Georgia Institute of Technology.
- Fontenot, E. J., Lee, Y. H., Matthews, R. D., Zhu, G. and Pavlostathis, S. G. (2003) Reductive decolorization of a textile reactive dye bath under methanogenic conditions. *Applied Biochemistry and Biotechnology*, **109**(1-3): 207-225.
- Fu, Y. and Viraraghavan, T. (2001) Fungal decolorization of dye wastewaters: a review. *Bioresource Technology*, **79**: 251-262.
- Gaber, H. M., Inskip, W. P., Comfort, S. D. and Wraith, J. M. (1995) Nonequilibrium transport of atrazine through intact soil cores. *Soil Science Society of America Journal*, **59**: 60-67.
- Gillham, R. W. and Ohannesin, S. F. (1994) Enhanced degradation of halogenated aliphatics by zero-valent iron. *Ground Water*, **32**(6): 958-967.
- Glenn, H. J. and Gold, M. H. (1983) Decolorization of several polymeric dyes by the lignin-degrading basidiomycete *Phanerochaete chrysosporium*. *Applied and Environmental Microbiology*, **45**(6): 1741-1747.
- Gould, J. P. (1982) The kinetics of hexavalent chromium reduction by metabolic iron. *Water Research*, **16**: 871-877.
- Gu, B. P., Phelps, T. J., Liang, L., Dickey, M. J., Roh, Y., Kinsall, B. L., Palumbo, A. V. and Jacobs, G. K. (1999) Biogeochemical dynamics in zero-valent iron columns: implications for permeable reactive barriers. *Environmental Science and Technology*, **33**: 2170-2177.

- Gui, L., Gillham, R. W. and Odziemkowski, M. S. (2000) Reduction of N-nitrosodimethylamine with granular iron and nickel-enhanced iron. 1. Pathways and kinetics. *Environmental Science and Technology*, **34**: 3489-3494.
- Hamlin, J. D., Phillips, D. A. S. and Whiting, A. (1999) UV/Visible spectroscopic studies of the effects of common salt and urea upon reactive dye solutions. *Dyes and Pigments*, **41**(1-2): 137-142.
- Hao, O. J., Kim, H and Chiang, P. C. (2000) Decolorization of wastewater (Critical review). *Environmental Science and Technology*, **30**: 449-505.
- Helland, B. R., Alvarez, P. J. J. and Schnoor, J. L. (1995) Reductive Dechlorination of Carbon-Tetrachloride with Elemental Iron. *Journal of Hazardous Materials*, **41**(2-3): 205-216.
- House, H. O. (1972) *Modern synthetic reactions*. Menlo Park, Calif., Benjamin/Cummings.
- Hu, Q. and Brusseau, M. L. (1995) Effect of solute size on transport in structured porous media. *Water Resource Research*, **31**(7): 1637-1646.
- Hutchins, R. A. (1973) New method simplifiers design of activated carbon systems. *Chem. Eng.*, **80**(19): 133.
- Ingamells, W. (1993) *Colour for Textiles: A User's Handbook*. West Yorkshire, England, Society of Dyers and Colourists.
- Jiang, H. and Bishop, P. L. (1994) Aerobic biodegradation of azo dyes in biofilms. *Water Science and Technology*, **29**(10/11): 525-530.
- Isik, M., Sponza, D. T. (2004) Monitoring of toxicity and intermediates of C.I. direct black 38 azo dye through decolorization in an anaerobic/aerobic sequential reactor system. *Journal of Hazardous Materials*, **B114**: 29-39.
- Johnson, T. L., Fish, W., Gorby, Y. A. and Tratnyek, P. G. (1998) Degradation of carbon tetrachloride by iron metal: complexation effects on the oxide surface. *Journal of Contaminant Hydrology*, **29**(4): 379-398.
- Johnson, T. L., Scherer, M. M. and Tratnyek, P. G. (1996) Kinetics of halogenated organic compound degradation by iron metal. *Environmental Science & Technology*, **30**(8): 2634-2640.
- Klecka, G. M. and Gonsior, S. J. (1984) Reductive dechlorination of chlorinated methanes and ethanes by reduced iron (II) porphyrins. *Chemosphere*, **13**(3): 391-402.

- Krupa, N. E. and Cannon, F. S. (1996) GAC: pore structure versus dye sorption. *Journal of American Water Works Association*, **88**(6): 94-109.
- Lall, R., Mutharasan, R., Shah, Y. T. and Dhurjati, P. (2003) Decolorization of the dye, Reactive Blue 19, using ozonation, ultrasound, and ultrasound-enhanced ozonation. *Water Environment Research*, **75**(2): 171-179.
- Laszlo, J. A. (1995) Electrolyte effects on hydrolyzed reactive dye binding to quaternized cellulose. *Textile Chemist and Colorist*, **27**(4): 25-27.
- Lavine, B. K., Auslander, G. and Ritter, J. (2001) Polarographic studies of zero valent iron as a reductant for remediation of nitroaromatics in the environment. *Microchemical Journal*, **70**(2): 69-83.
- Lee, L. S., Rao, P. S. C., Brusseau, M. L. and Ogwada, R. A. (1988) Nonequilibrium sorption of organic contaminants during flow through columns of aquifer materials. *Environmental Toxicology and Chemistry*, **7**: 779-793.
- Lee, Y. H. (2003) *Reductive Biotransformation and Decolorization of Reactive Anthraquinone Dyes*. School of Civil and Environmental Engineering. Atlanta, Georgia Institute of Technology: 346.
- Lee, Y. H. and Pavlostathis, S. G. (2004) Decolorization and toxicity of reactive anthraquinone textile dyes under methanogenic conditions. *Water Research*, **38**: 1838-1852.
- Lee, Y. H., Matthews, R. D. and Pavlostathis, S. G. (2005) Biological Decolorization of Reactive Anthraquinone and Phthalocyanine Dyes under Various Oxidation-Reduction Conditions. *Water Environment Research*.
- Libra, J. A., Borchert, M., Vigelahn, L. and Storm T. (2004) Two stage biological treatment of a diazo reactive textile dye and the fate of the dye metabolites. *Chemosphere*, **56**: 167-180.
- Litchfield, C. D. and Gillevet, P. M. (2002) Microbial diversity and complexity in hypersaline environments: a preliminary assessment. *Journal of Industrial Microbiology & Biotechnology*, **28**(1): 48-55.
- Loraine, G. A., Burris, D. R., Li, L. and Schoolfield, J. (2002) Mass transfer effects on kinetics of dibromoethane reduction by zero-valent iron in packed-bed reactors. *Journal of Environmental Engineering-ASCE*, **128**(1): 85-93.
- Lubenow, B., Perey, J., Chiu, P. C. and Cha, D. K. (2002) Enhancing biodegradation of azo- and nitro-aromatic compounds through reductive pretreatment with elemental iron. *224th ACS National Meeting*, Boston, MA, United States.

- Mackenzie, P. D., Horney, D. P. and Sivavec, T. M (1999) Mineral precipitation and porosity losses in granular iron columns. *Journal of Hazardous Materials*, **68**: 1-17.
- Mah, A. R., and Smith, M. R. (1981) The methogenic bacteria. *In The Prokaryotes: A Handbook of Habitats, Isolation and Identification of Bacteria*. New York, Springer-Verlag.
- Markovska, L., Meshko, V. and Noveski, V. (2001) Adsorption of basic dyes in a fixed bed column. *Korean Journal of Chemical Engineering*, **18**(2): 190-195.
- Matheson, L. J. and Tratnyek, P. G. (1994) Reductive dehalogenation of chlorinated methanes by iron metal. *Environmental Science & Technology*, **28**(12): 2045-2053.
- Matthews, R. D. (2003) *Transformation and Decolorization of Reactive Phthalocyanine Dyes*. School of Civil and Environmental Engineering. Atlanta, Georgia Institute of Technology: 394.
- McKay, G. (1979) Waste Color Removal from Textile Effluents. *American Dyestuff Reporter*, **68**(4): 29.
- McKay, G., Blair, H. S. and Gardner, J. R. (1984) The sorption of dyes onto chitin in fixed bed columns and batch adsorbers. *Journal of Applied Polymer Science*, **29**: 1499.
- McMullan, G., Meehan, C., Conneely, A., Kirby, N., Robinson, T., Nigam, P. Banat, I. M., Marchant, R. and Smyth, W. F. (2001) Microbial decolourisation and degradation of textile dyes. *Applied Microbiology and Biotechnology*, **56**(1-2): 81-87.
- Melitas, N. and J. Farrell (2002) Understanding chromate reaction kinetics with corroding iron media using tafel analysis and electrochemical impedance spectroscopy. *Environmental Science & Technology*, **36**(24): 5476-5482.
- Miehr, R., Tratnyek, P. G., Bandstra, J. Z., Scherer, M. M., Alowitz, M. J. and Bylaska, E. J. (2004) Diversity of contaminant reduction reactions by zero-valent iron: role of reductate. *Environmental Science and Technology*, **38**: 139-147.
- Mojid, M. A., Rose, D. A. and Wyseure, G. C. L. (2004) A transfer-function method for analysing breakthrough data in the time domain of the transport process. *European Journal of Soil Science*, **55**(4): 699-711.
- Muruganandham, M. and Swaminathan, M. (2004) Decolourisation of reactive orange 4 by photo-fenton oxidation technology. *Dyes and Pigments*, **63**: 315-321.
- Naim, M. M., Abd, Yehia M. E. (2002) Removal and recovery of dyestuffs from dyeing wastewaters. *Separation and Purification Methods*, **31**(1): 177-228.

- Nam, S. and Tratnyek, P. G. (2000) Reduction of azo dyes with zero-valent iron. *Water Research*, **34**(6): 1837-1845.
- Nassar, M. S. and El-Geundi, M. S. (1991) Comparative cost of color removal from textile effluents using natural adsorbents. *Journal of Chemical Technology and Biotechnology*, **50**(2): 257-264.
- Netpradit, S., Thiravetyan, P. and Towprayoon, S. (2004) Evaluation of metal hydroxide sludge for reactive dye adsorption in a fixed-bed column system. *Water Research*, **38**: 71-78.
- Nigam, P., Armour, G., Banat, I. M., Singh, D., Marchant, R., McHale, A. P. and McMullan, G. (2000) Physical removal of textile dyes from effluents and solid-state fermentation of dye-adsorbed agricultural residues. *Bioresource Technology*, **74**(2): 179.
- Nurmi, J. T., Tratnyek, P. G., Sarathy, V., Baer, D. R., Amonette, J. E., Pecher, K., Wang, C., Linehan, J. C., Matson, D. W., Penn, R. L. and Driessen, M. D. (2004) Characterization and properties of metallic iron nanoparticles: spectroscopy, electrochemistry, and kinetics. *Environmental Science and Technology*, **39**(5): 1221-1230.
- Oh, B. T. and Alvarez, P. J. (2004) Removal of explosives using an integrated iron-microbial treatment in flow-through columns. *Bulletin of Environmental Contamination and Toxicology*, **73**(1): 1-8.
- Oh, S. Y., Cha, D. K., Chiu, P. C. and Kim, B. J. (2003) Enhancing oxidation of TNT and RDX in wastewater: pre-treatment with elemental iron. *Water science and technology*, **47**(10): 93-99.
- Oremland, R. S., Dowdle, P. R., Hoelt, S., Sharp, J. O., Schaefer, J. K., Miller, L. G., Blum, J. S., Smith, R. L., Bloom, N. S. and Wallschlaeger, D. (2000) Bacterial dissimilatory reduction of arsenate and sulfate in meromictic Mono Lake, California. *Geochimica. et Cosmochimica Acta*, **64**(18): 3073-3084.
- Pagga, U. and K. Taeger (1994) Development of a Method for Adsorption of Dyestuffs on Activated-Sludge. *Water Research*, **28**(5): 1051-1057.
- Panswad, T. and Luangdilok, W. (2000) Decolorization of reactive dyes with different molecular structures under different environmental conditions. *Water Research*, **34**(17): 4177-4184.
- Perey, J. R., Chiu, P. C., Haung, C. P. and Cha, D. K. (2002) Zero-valent iron pretreatment for enhancing the biodegradability of azo dyes. *Water Environment Research*, **74**(3): 221-225.

- Phillips, D. (1996) Environmentally friendly, productive and reliable: Priorities for cotton dyes and dyeing processes. *Journal of the Society of Dyers and Colourists*, **112**(7-8): 183-186.
- Pinheiro, H. M., Touraud, E. and Thomas, O. (2004) Aromatic amines from azo dye reduction: status review with emphasis on direct UV spectrophotometric detection in textile industry wastewaters. *Dyes and Pigments*, **61**(121-139).
- Poots, V. J. P., McKay, G. and Healy, J. J. (1976) Removal of acid dye from effluent using natural adsorbents 2 wood. *Water Research*, **10**(12): 1067-1070.
- Qamar, M., Saquib, M. and Muneer, M. (2004) Semiconductor-mediated photocatalytic degradation of an azo dye, chrysoidine Y in aqueous suspensions. *Desalination*, **171**: 185-193.
- Raghavacharya, C. (1997) Colour removal from industrial effluents - a comparative review of available technologies. *Chemical Engineering World*, **32**: 53-54.
- Robison, T. M., McMullan, G., Marchant, R. and Nigam, P. (2001) Remediation of dyes in textile effluent: a critical review on current treatment technologies with a proposed alternative. *Bioresource Technology*, **77**: 247-255.
- Rozzi, A., Malpei, F., Bonomo, L. and Bianchi, R. (1999) Textile wastewater reuse in Northern Italy (COMO). *Water Science and Technology*, **39**(5): 122-128.
- Rys, P. and H. Zollinger (1989) Reactive dye-fiber systems. The theory of coloration of Textiles. A. Johnson. West Yorkshire, England, *Society of Dyers and Colorists*, 552.
- Santos, A. B., Bisschops, I. A. E., Cervantes, F. J. and Liera, J. B. (2005) The transformation and toxicity of anthraquinone dyes during thermophilic (55 °C) and mesophilic (30 °C) anaerobic treatments. *Journal of Biotechnology*, **115**: 345 - 353.
- Santos, A. Z., Netro, J. M., Tavares, C. R. G., and Costa, S. M. G. (2004) Screening of filamentous fungi for the decolorization of a commercial reactive dye. *Journal of Basic Microbiology*, **44**(4): 288-295.
- Scherer, M. M., Westall, J. C., Ziomek-Moroz, M. and Tratnyek, P. G. (1997) Kinetics of carbon tetrachloride reduction at an oxide-free iron electrode. *Environmental Science & Technology*, **31**(8): 2385-2391.
- Selvam, K., Dwaminathan, K. and Chae, K-S. (2003) Decolourization of azo dyes and a dye industry effluent by a white rot fungus *Thelephora sp.* *Bioresource Technology*, **2003**(88): 115-119.
- Shirakashi, T., Kakii, K. and Kuriyama, M. (1993) Removal of mercury from laboratory wastewater. *Mizu Kankyo Gakkaishi*, **16**(7): 488-496.

- Siantar, D. P., Schreier, C. G., Chou, S-S. and Reinhard, M. (1996) Treatment of 1,2-dibromo-3-chloropropane and nitrate- contaminated water with zero-valent iron or hydrogen/palladium catalysts. *Water Research*, **30**(10): 2315-2322.
- Snoeyink, V. L. and Jenkins., D. (1980). *Water Chemistry*. New York, John Wiley & Sons, Inc.
- Stapleton, J. M. and J. R. Mihelcic (2001) Darcy's law and hydraulic conductivity. *AEESP Environmental Engineering Processes Laboratory Manual*. Champaign, IL, Association of Environmental Engineering and Science Professors. **CD**.
- Steenkeen-Richter, I. and W. D. Kermer (1992) Decolorizing Textile Effluents. *Journal of the Society of Dyers and Colourists*, **108**(4): 182-186.
- Stolz, A. (2001) Basic and applied aspects in the microbial degradation of azo dyes. *Applied Microbiology and Biotechnology*, **56**(1-2): 69-80.
- Su, C. M. and Puls, R. W. (1999) Kinetics of trichloroethene reduction by zerovalent iron and tin: Pretreatment effect, apparent activation energy, and intermediate products. *Environmental Science & Technology*, **33**(1): 163-168.
- Tan, N. C. G., Prenafeta-Boldu, F. X., Opsteeg, J. L., Lettinga, G. and Field, J. A. (1999) Biodegradation of azo dyes in cocultures of anaerobic granular sludge with aerobic aromatic amine degrading enrichment cultures. *Applied Microbiology and Biotechnology*, **51**(6): 865-871.
- Tatarko, M. and Bumpus, J. A. (1998) Biodegradation of congo red by phanerochaete chrysosporium. *Water Research*, **32**(5): 1713-1717.
- Tincher, W. C. and Robertson, J. R. (1982) Analysis of dyes in textile dyeing wastewater. *Textile Chemist and Colorist*, **14**(12): 41-47.
- Toride, N., Leij, T. and van Genuchten, M. T. (1995) *The CXTFIT code for estimation transport parameters from laboratory or field tracer experiments (version 2.0)*. Research Report No 137. Riverside, CA, US Salinity laboratory.
- Tratnyek, P. G. (2001) Visualizing redox chemistry: probing environmental oxidation-reduction reactions with indicator dyes. *Chemical Educator*, **6**: 172-179.
- Van der Zee, F. P., Lettinga, G. and Field, J. A. (2001) Azo dye decolorisation by anaerobic granular sludge. *Chemosphere*, **44**(5): 1169-1176.
- Van der Zee, F. P., Bisschops, I. A. E., Blanchard, V. G., Bouwman, R. H. M., Lettinga, G. and Field, J. A. (2003) The contribution of biotic and abiotic processes during azo dye reduction in anaerobic sludge. *Water Research*, **37**: 3098-3109.

- Vandevivere, P. C., Bianchi, R. and Verstraete, W. (1998) Treatment and reuse of wastewater from the textile wet-processing industry: review of emerging technologies. *Journal of Chemical Technology and Biotechnology*, **72**: 289-302.
- Van't Hul, J. P., Racz, I. G. and Reith, T. (1997) The application of membrane technology for reuse of process water and minimization of wastewater in textile washing range. *Journal of Society Dyers Colourists*, **113**(10): 287-295.
- Walker, G. M. and Wearherley, L. R. (1997) Adsorption of acid dyes onto granular activated carbon in fixed beds. *Water Research*, **31**(8): 2093.
- Wang, Y. and Yu, J. (1998) Adsorption and degradation of synthetic dyes on the mycelium of *trametes versicolor*. *Water Science and Technology*, **38**(4/5): 233-238.
- Weber, E. J. (1996) Iron-mediated reductive transformations: investigation of reaction mechanism. *Environmental Science & Technology*, **30**(2): 716-719.
- Wesenberg, D., Kyriakides, I. and Agathos, S. N. (2003) White-rot fungi and their enzymes for the treatment of industrial dye effluents. *Biotechnology Advances*, **47**: 161-187.
- Westerhoff, P. and J. James (2003) Nitrate removal in zero-valent iron packed columns. *Water Research*, **37**(8): 1818-1830.
- Westerhoff, P. and P. Johnson (2001) A zero-valent iron (Fe⁰) packed-bed treatment process. Denver, CO, *AWWA Research Foundation and American Water Works Association*.
- Wolin, E. A., Wolin, M. J. and Wolfe, R. S. (1963) Formation of methane by bacterial extracts. *Journal of Biological Chemistry*, **238**: 2882-2886.
- Wragg, A. A. and de Nahui, F. N. B. (1992) Copper recovery from aqueous waste streams using packed and fluidized bed cementation; influence of process parameters. *Institution of Chemical Engineers Symposium Series*, **127**(Electrochem. Eng. Environ. 92): 141-152.
- Wu, J., Eiteman, M. A. and Law, S. E. (1998) Evaluation of membrane filtration and ozonation processes for treatment of reactive-dye wastewater. *Journal of Environmental Engineering-ASCE*, **124**(3): 272-277.
- Yabusaki, S., Cantrell, K., Sass, B. and Steefel, C. (2001) Multicomponent reactive transport in an in situ zero-valent iron cell. *Environmental Science & Technology*, **35**: 1493-1503.
- Zhang, P., Simunek, J. and Bowman, R. S. (2004) Nonideal transport of solute and colloidal tracers through reactive zeolite/iron pellets. *Water Resources Research*, **40**(4).

Zhang, P. F., Tao, X., Li, Z. and Bowman, R. S. (2002) Enhanced perchloroethylene reduction in column systems using surfactant-modified zeolite/zero-valent iron pellets. *Environmental Science & Technology*, **36**(16): 3597-3603.

Zollinger, H. (2003) *Color Chemistry: Syntheses, Properties, and Applications of Organic Dyes and Pigments*. Weinheim, New York.